frontiers | Frontiers in Medicine

REVIEW
published: 30 June 2022
doi: 10.3389/fmed.2022.891369

The Development and Clinical Application of Innovative Optical Ophthalmic Imaging Techniques

*Palaiologos Alexopoulos[1], Chisom Madu[1], Gadi Wollstein[1,2,3] and Joel S. Schuman[1,2,3,4,5]**

[1] Department of Ophthalmology, NYU Langone Health, NYU Grossman School of Medicine, New York, NY, United States, [2] Department of Biomedical Engineering, NYU Tandon School of Engineering, Brooklyn, NY, United States, [3] Center for Neural Science, College of Arts & Science, New York University, New York, NY, United States, [4] Department of Electrical and Computer Engineering, NYU Tandon School of Engineering, Brooklyn, NY, United States, [5] Department of Neuroscience & Physiology, NYU Langone Health, NYU Grossman School of Medicine, New York, NY, United States

The field of ophthalmic imaging has grown substantially over the last years. Massive improvements in image processing and computer hardware have allowed the emergence of multiple imaging techniques of the eye that can transform patient care. The purpose of this review is to describe the most recent advances in eye imaging and explain how new technologies and imaging methods can be utilized in a clinical setting. The introduction of optical coherence tomography (OCT) was a revolution in eye imaging and has since become the standard of care for a plethora of conditions. Its most recent iterations, OCT angiography, and visible light OCT, as well as imaging modalities, such as fluorescent lifetime imaging ophthalmoscopy, would allow a more thorough evaluation of patients and provide additional information on disease processes. Toward that goal, the application of adaptive optics (AO) and full-field scanning to a variety of eye imaging techniques has further allowed the histologic study of single cells in the retina and anterior segment. Toward the goal of remote eye care and more accessible eye imaging, methods such as handheld OCT devices and imaging through smartphones, have emerged. Finally, incorporating artificial intelligence (AI) in eye images has the potential to become a new milestone for eye imaging while also contributing in social aspects of eye care.

Keywords: optical coherence tomography, optical coherence tomography (angiography) (OCTA), adaptive optics, visible light OCT, full field OCT, artificial intelligence – AI

OPEN ACCESS

Edited by:
Peng Xiao,
Sun Yat-sen University, China

Reviewed by:
Tanyatuth Padungkiatsagul,
Mahidol University, Thailand
Weiye Song,
Shandong University, China
Eduardo Normando,
Imperial College London,
United Kingdom

***Correspondence:**
Joel S. Schuman
joel.schuman@nyu.edu

Specialty section:
This article was submitted to Ophthalmology, a section of the journal Frontiers in Medicine

Received: *07 March 2022*
Accepted: *23 May 2022*
Published: *30 June 2022*

Citation:
Alexopoulos P, Madu C, Wollstein G and Schuman JS (2022) The Development and Clinical Application of Innovative Optical Ophthalmic Imaging Techniques. Front. Med. 9:891369. doi: 10.3389/fmed.2022.891369

Abbreviations: AI, artificial intelligence; AMD, age-related macular degeneration; AO, adaptive optics; AUC, area under the receiver-operator characteristic curve; CNV, choroidal neovascularization; CSR, central serous retinopathy; DALK, deep anterior lamellar keratoplasty; DED, dry eye disease; DL, deep learning; DR, diabetic retinopathy; FA, fluorescein angiography; FAF, fundus autofluorescence; FD-OCT, fourier-domain optical coherence tomography; FFNN, feed forward neural network; ILM, internal limiting membrane; IPL, inner plexiform layer; GA, geographic atrophy; GCL, ganglion cell layer; INL, inner nuclear layer; IOP, intraocular pressure; IPL, inner plexiform layer; LDH, laser doppler holography; ML, machine learning; NIR-OCT, near-infrared optical coherence tomography; NN, neural network; ONH, optic nerve head; OCT, optical coherence tomography; OCT-A, optical coherence tomography angiography; ORG, optoretinogram; POAG, primary open angle glaucoma; RGC, retinal ganglion cell(s); RNFL, retinal nerve fiber layer; ROP, retinopathy of prematurity; RP, retinitis pigmentosa; RPE, retinal pigment epithelium; SD-OCT, spectral-domain optical coherence tomography; SNR, signal-to-noise ratio; SS-OCT, swept-source optical coherence tomography; TD-OCT, time-domain optical coherence tomography; VF, visual field(s); Vis-OCT, visible light optical coherence tomography.

INTRODUCTION

No more than four decades ago, images of the eyes were limited to just slit-lamp photographs, fundus photographs, fluorescein angiography (FA), and ultrasounds. Since then, a tremendous growth in technology has given birth to a plethora of techniques to image the eye and has drastically transformed patient care. The invention of optical coherence tomography (OCT) in 1991 was a breakthrough in the field of ophthalmology and has shifted the way patients are managed. Several iterations of OCT are currently utilized, and more are being investigated that would allow researchers and clinicians to obtain a much more in-depth insight into ocular diseases. More recently, evolutions in the field of artificial intelligence (AI) and machine learning (ML), termed by many the "fourth industrial revolution," have been proved to outperform human evaluations in several aspects, thus providing potential as powerful supplementary tools to help physicians in all aspects of ophthalmic care. The goal of this review is to summarize major advances in the most important aspects of eye imaging, describe novel emerging imaging techniques, and evaluate their use in clinical settings. Hence, imaging modalities widely used in clinical practice (OCT, fundus imaging) and promising imaging techniques (AO) and analysis tools (AI) were selected to be described in more detail.

OPTICAL COHERENCE TOMOGRAPHY

Optical coherence tomography was introduced in 1991 (1). It is a non-contact and non-invasive technology that uses low-coherence interferometry, in which a beam from a low coherence interferometer is scanned by moving a reference arm that serves as a reference for depth in the axial direction. In the eye, backscattered light from retinal layers is detected sequentially pixel by pixel to form a depth profile (A-scan) (2). Scanning this beam in the transverse plane creates a B-scan, combining all the acquired A-scans. This provides high resolution two-dimensional images of tissue depth structure and can be applied to the entire anatomy of the eye (retina, optic nerve, cornea, and angle). By collecting a sequential series of B-scans, a three-dimensional image can be produced, with volumetric information on the tissue interrogated.

The first iteration of OCT was time-domain OCT (TD-OCT), which interprets the location of the backscattered light as described above. The image acquisition speed of TD-OCT is constrained by the mechanics of the device; in the first TD-OCT systems, a cross sectional image was acquired in roughly 190 s (3). To address this limitation, high-sensitivity interferometric receivers, optical fiber, and galvanometric beam steering devices were implemented that resulted in an increase in scanning speed (up to 100 A-scans/s), producing the first commercial OCT device, launched in 1996 (4). Further developments in TD-OCT allowed for a maximum speed of 400 A-scans/s (third-generation TD-OCT) (3).

Ten years after the introduction of TD-OCT (2001), new methods of signal acquisition were presented. Fourier-domain OCT (FD-OCT) was the next generation of OCT imaging, with the major changes being that the reference mirror remained fixed, and the frequency spectrum of the reflected light was measured simultaneously and transformed from the frequency to the time domain using Fourier transform. These systems are divided into spectral-domain OCT (SD-OCT) and swept-source OCT (SS-OCT): for SD-OCT, the signals are separated by a grating into different wavelengths, whereas, for SS-OCT (introduced in 2012), the light emitted from the laser source sweeps through frequencies in sequence (3). The center wavelength of these two techniques also differs: most commercial SD-OCT devices use a center wavelength of 850-nm versus 1,050 nm of SS-OCT; the longer wavelengths enable for better penetration and thus improved imaging of deeper structures (5). These implementations allowed for a tremendous increase in scan acquisition speed of commercial devices, from 400 A-scans/s to roughly 100,000 A-scans/s for SD-OCT and more than 200,000 A-scans/s for SS-OCT (5–7). Apart from the scanning speed, these techniques also resulted in improved sensitivity and a signal-to-noise ratio, overall better scan quality, and the ability to perform 3-D imaging.

Optical coherence tomography has become standard in ophthalmology, with multiple applications in diagnosis, monitoring, and management of eye conditions across the board (8). Major advances and implementations in OCT are discussed in the following section, which provide novel and exciting applications in the field of ophthalmic imaging.

Optical Coherence Tomography Angiography

Optical coherence tomography angiography (OCT-A) utilizes the motion of red blood cells within blood vessels to image vessels and vascular flow. Commercially available devices developed in 2015 use different algorithms of signal decorrelation from 2 or more repeated B-scans of the same region to display areas of motion: AngioVue (OptoVue, Fremont, CA, United States) uses split-spectrum amplitude-decorrelation angiography (SSADA), whereas Cirrus AngioPlex and PLEX Elite (Zeiss, Dublin, CA, United States) use an OCT-microangiography complex algorithm that is a full-spectrum, complex number-based algorithm (9). The benefits of OCT-A versus other vascular imaging modalities (fluorescent angiography, indocyanine green angiography) are the lack of extrinsic dye injection, leading to adverse effects, and the ability to image vascular networks in different depths (**Figure 1**). While dye-based angiography can reveal vessel leakage, OCT-A cannot.

Scans acquired with OCT-A can be processed to improve the signal-to-noise ratio (SNR) and display very small vessels more accurately. Denoising methods, such as Gaussian filter (10), compressive sensing (11–20), and Bayesian estimation (11, 21), can suppress noise while maintaining vasculature information. Filters that focus on the specific structure of vessels are also applied, such as Frangi filter (22, 23), Gabor wavelets, and Fuzzy-C-Means Classification (24). Quality limiting factors with OCT-A imaging are the presence of artifacts (projection, motion), visibility of vessels dependent on the rate of blood flow and scan speed, and low output image contrast (25, 26).

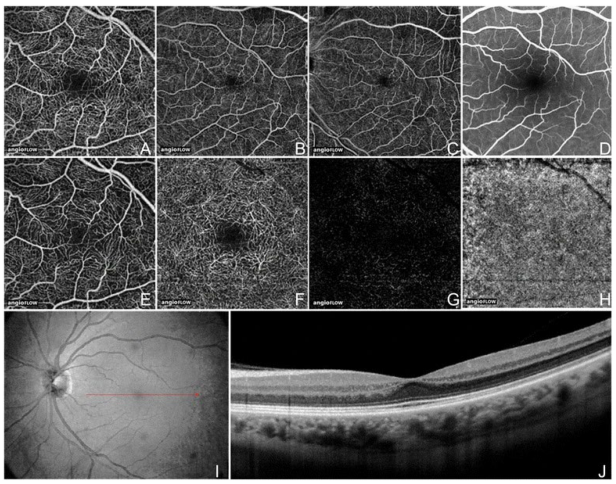

FIGURE 1 | Optical coherence tomography angiography (OCT-A) fields of view and segmentation layers (Angiovue). The normal left eye of a 56-year-old Caucasian man using the Angiovue optical coherence tomography angiography (OCTA) software of the RTVue XR Avanti (Optovue, Inc., Fremont, CA, United States). **(A)** Full-thickness (internal limiting membrane to Bruch's membrane) 3 mm × 3 mm OCT angiogram. **(B)** Full-thickness 6 mm × 6 mm OCT angiogram. **(C)** Full-thickness 8 mm × 8 mm OCT angiogram. **(D)** Fluorescein angiography cropped to approximately 8 mm × 8 mm or 30 degrees demonstrates a less capillary detail than **(A–C)**. **(E)** 3 mm × 3 mm OCT angiogram of the "Superficial" inner retina. **(F)** 3 mm × 3 mm OCT angiogram of the "Deep" inner retina. **(G)** 3 mm × 3 mm OCT angiogram of the outer retina shows absence of vasculature. The white represents noise. **(H)** 3 mm × 3 mm OCT angiogram of the choriocapillaris is generally homogenous. There is black shadowing from retinal vessels. **(I)** Enface intensity OCT image. **(J)** Highly sampled OCT b-scan image. This figure was reprinted from de Carlo et al. (507) with permission.

The OCT-A can be utilized for conditions involving vascular damage or choroidal neovascularization (CNV) (25). Apart from allowing the subjective identification of vascular abnormalities, OCT-A can also provide quantitative data (vessel density, blood flow, and foveal avascular zone size) that could be employed as vascular biomarkers (27–32).

Diabetic retinopathy (DR) is a disease affecting, among other tissues, the retinal microvasculature (33, 34). It is the leading cause of blindness in the middle-aged and elderly population (35). Early in the disease process, deeper retinal capillary plexuses are primarily affected (36–40). OCT-A can detect both microaneurysms (the hallmark of early DR) and neovascularization (in proliferative disease) in various depths (25, 38, 41–44). Being non-invasive and high resolution, OCT-A can be used for early diagnosis and possible screening of DR when compared to fluorescein angiography (FA) (3, 45). Ong et al. and Russell et al. have proposed new models for DR staging and progression based on OCT-A findings (46, 47).

In the setting of age-related macular degeneration (AMD), OCT-A can detect impaired blood flow at sites of drusen or pseudodrusen (48, 49) and geographic atrophy (GA) (50–52) with high reproducibility when compared to SD-OCT (53). It can also identify CNV (sensitivity, 81% and specificity, ≥93%) with more detail and better contrast than FA (54–64).

In glaucoma, various studies have demonstrated reduced blood flow and blood vessel density at the level of the optic nerve head (ONH) and peripapillary area (65–72). OCT-A scans from macular and ONH scans in glaucoma have been shown to display good reproducibility, which supports the use of OCT-A longitudinally as well (73). Vessel density parameters have also been associated with visual field progression (74, 75).

For other conditions, Zhu et al. have recently proposed that OCT-A metrics can be used to assess and detect myopia development in adolescents (76).

A limitation of OCT-A compared to other vessel imaging techniques is the limited area visualized. Kawai et al. have proposed the introduction of a front prism that would generate ultra-wide field panoramic images and allow imaging of the peripheral chorioretinal vessels, while applying image averaging to correct for the drop-off in image quality (77, 78). Miao et al. also introduced the use of megahertz-rate OCT-A as a faster imaging technique that also yields better contrast images (79). Post-processing methods (angiogram subtraction, distortion correction) and eye tracking during scan acquisition have also significantly improved the scan quality and reduced artifacts (80–86). Furthermore, new types of software have been developed to automate the analysis of OCT-A images; Viekash et al. have also established software to automatically quantify the foveal avascular zone, a region affected by various ocular diseases (87), while tools have been constructed to automatically process, segment, and quantitatively analyze the blood vessels (88–90).

Visible Light Optical Coherence Tomography

Vis-OCT, first reported by Povazay and coauthors in 2002 (91), has been developed most intensively in the last decade. It relies on light sources from the visible spectrum (555–800 nm), which provides a better axial resolution than typical OCT devices that use near-infrared (NIR) illumination (1.2–1.4 μm versus 1.7–7.5 μm, respectively) (92–96). Other benefits of Vis-OCT include a smaller bandwidth to achieve the same resolution, leading to easier dispersion compensation, and higher image contrast due to higher scattering coefficients (97). One of the advantages of Vis-OCT is the ability to measure oximetry in blood vessels. Blood, which contains oxyhemoglobin (HbO_2) or deoxyhemoglobin (Hb), exhibits more contrast at the isosbestic point in the wavelengths of Vis-OCT than in the NIR. Combining this property with simultaneous measurement of the blood flow rate using Doppler OCT methods, many metabolic parameters of retinal circulation can be extracted, such as O_2 saturation (sO_2), O_2 extraction fraction, total retinal O_2 delivery, and the metabolic rate; Vis-OCT has been validated and is superior to NIR-OCT for these parameters (97–103).

Vis-OCT has been widely studied in disease models in animals and is now transitioning to clinical practice. Rodents with DR and retinopathy of prematurity (ROP) have been studied using Vis-OCT, and metabolic changes in both conditions were apparent before structural changes (103–105). The first use on humans was performed by Yi et al. on a single healthy subject, with Vis-OCT displaying increased contrast of the inner (the retinal nerve fiber

layer – RNFL) and outer (a photoreceptor inner/outer segment, a retinal pigment epithelial layer, Bruch's membrane) retinal layers compared to NIR-OCT (106). Vis-OCT has since been used for calculating metabolic parameters with upgraded light sources, decreased noise, and great axial resolution (96). Shu et al. also developed a Vis-OCT platform than can be used for humans and demonstrated it successfully in conditions such as retinal occlusive diseases and DR (107). Given its ability to provide metabolic information about oxygenation and circulation, and its advantages of retinal layer imaging over NIR-OCT, Vis-OCT might be a better imaging candidate for conditions affecting these cell layers, for example, the RNFL, inner plexiform layer (IPL), and inner nuclear layer (INL) in glaucoma or the outer retinal layers and retinal pigment epithelium (RPE) in AMD. Its ability to provide metabolic information about oxygenation and circulation, contributors to retinal and optic nerve diseases, reinforces this point.

Vis-OCT has continued to develop. Registration and averaging of multiple volumes have allowed the visualization of single cells, and the concept of Vis-OCT fibergraphy (Vis-OCTF) of imaging-specific retinal ganglion cell (RGC) axon bundles has been introduced in animal models (108–110). Ultrahigh resolution Vis-OCT (UHR Vis-OCT) is capable of imaging sublayers within retinal layers, such as the IPL (**Figure 2**), and improvements in the axial resolution have also been made using rapid spectral shaping, axial tracking, and *in vivo* spatially dependent numerical dispersion compensation (111–113). Zhang et al. have also developed a circumlimbal scanning method to image the anterior segment, capable of visualizing the Schlemm canal and the limbal microvascular network (114). In addition, Wang et al. have recently devised a dual-channel system with both Vis-OCT and NIR-OCT-A capable of simultaneous retinal imaging and metabolic measurement acquisition; the use of a fiber-based dual channel Vis- and NIR-OCT to image the human retina was first reported by Song et al. (115, 116). In a clinical setting, this dual channel system was initially reported to quantify RNFL spectroscopic markers in glaucomatous subjects and glaucoma suspects, which were correlated with disease severity (117). A combination of both Vis-OCT and OCT-A (Vis-OCT-A) has also been reported by Song et al., with narrow bandwidth spectrometers, optimized image protocols, and improved acquisition speed (100,000 A-scans/s) (118).

Handheld Optical Coherence Tomography

In a typical OCT imaging session, the patient sits upright with the head stabilized with a chin rest and headrest. The use of portable or handheld OCT is indicated in cases where this positioning is not possible. Populations included in this category are bedridden or postoperative patients, the pediatric population and cases where access to health care is limited or difficult. Portable HH-OCT would potentially offer an easier-to-use and less-expensive alternative to current commercial OCT devices. Chen et al. displayed that measurements from HH-OCT have good repeatability and reproducibility of both axial and transverse measurements when compared to Heidelberg Spectralis (119).

The HH-OCT is widely used nowadays for pediatric ocular conditions. HH-OCT/OCT-A systems can reliably visualize and measure vitreous opacities and bands, perifoveal vessels, the macular shape, anterior chamber features, retinal tumors,

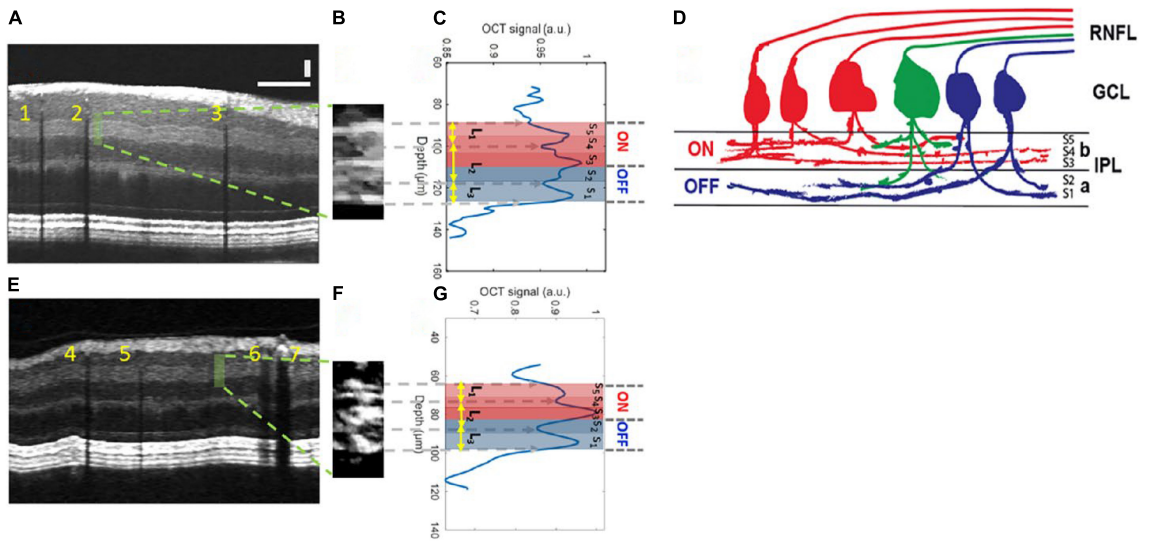

FIGURE 2 | Inner plexiform layer (IPL) sublayer visualization with Vis-OCT. **(A)** A speckle-reduced vis-OCT image from a healthy eye. A horizontal bar: 500 μ m; a vertical bar: 50 μ m. **(B)** A magnified view of the region highlighted by the dashed box in **(A)** (15 srA-lines segments). **(C)** A depth-resolved OCT amplitude profile of the IPL sublayers. We averaged 15 srA-lines, corresponding to approximately 88 μ m along the lateral direction within the highlighted region in **(A)**. **(D)** Illustration of the lamination of ganglion cells from RNFL to the IPL. The "red" ganglion cells (ON center) are laminating dendrites to the "b" sublamella of the IPL whereas "blue" cells (OFF center) laminate to the "a" sublamella. The "green" ganglion cell is bi-laminating. **(E)** A speckle-reduced vis-OCT image from a glaucoma eye. **(F)** A magnified view of the region highlighted by the dashed box in **(E)**. **(G)** A depth-resolved line profile of the glaucoma eye IPL sublayers. This figure was reprinted from Ghassabi et al. (113) with permission under a Creative Commons Attribution 4.0 International License.

and ganglion cell complex (GCC)/IPL/RNFL thickness in both premature and full-term infants (120–130). Hence, they are useful in conditions, such as congenital and pediatric glaucoma, macular edema, macular hole, epiretinal membrane, retinoschisis, retinal dystrophies, and other conditions (128, 129, 131–133). Some measurements obtained, mostly from the fovea, could potentially be used to screen for conditions like ROP (132). HH-OCT-A in specific is extremely useful in cases of CNV in children, such as ROP, retinal dystrophies, inflammatory disorders, trauma or cases of unexplained visual loss (134–136). Ocular measurements, specifically RNFL thickness, have been shown to be associated with systemic health conditions in infants (low birth weight, sepsis, and necrotizing enterocolitis) (137).

The approaches to making OCT devices more mobile are promising. HH-OCT probes have been developed and are currently used in animal experimental models (Leica, Heidelberg); this allows for transportation of the device, although the probes are tied to bulky mobile carts (138, 139). Smaller versions of OCT machines have also been achieved that offer comparable results to bench-top OCT devices, with some offering *en face* reflectance, OCT-A volumes, combination with SLO and supine imaging (140–148). Handheld SS-OCT devices have also been created, containing ultrahigh speed and averaging capabilities (Lu et al.) or capable of imaging both the anterior and posterior segments in quick succession (Nankivil et al.) (149, 150). Ni et al. have recently proposed models for high-speed scanning (the HH-SS-OCT model using a 400 kHz VCSEL light source, scanning speed, 1,720 MHz; volume acquisition time, 1.875 s) and an increased field of view scanning to 105 degrees (**Figure 3**) (151, 152).

Intraoperative Optical Coherence Tomography

Intraoperative OCT (I-OCT) can aid surgeons by providing a live imaging feedback during surgery. The devices currently used for I-OCT are either handheld or integrated in microscopes or probes (153). HH-OCT in this setting is best utilized when mounted onto the surgical microscope to improve stability and precise movement. The images obtained with that method are fast, accurate, and reproducible; drawbacks include pausing the surgery for image acquisition and potential requirement of technician assistance (154). I-OCT integrated within the surgical microscope partially resolves these issues, as it can be used without pausing the operation or additional specialized technical support; additionally, there are opportunities to enhance I-OCT with decision-making algorithms and high-tech instrumentation (e.g., heads-up display) (155). An advanced technique is implementation of OCT scanners in ophthalmic probes, creating an instrument for intraocular use, especially for vitreoretinal surgery (156).

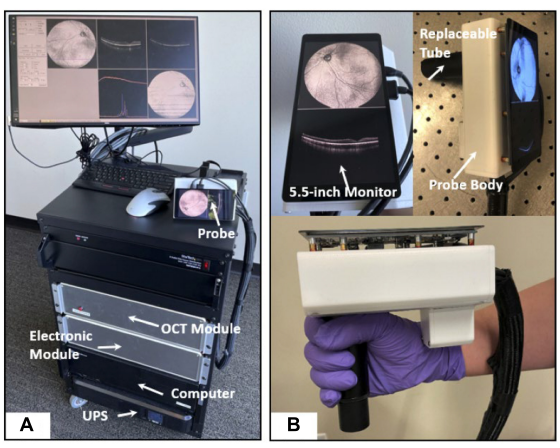

FIGURE 3 | High-speed and widefield handheld SS-OCT-A with a VCSEL light source. **(A)** A photograph of the front of fully assembled handheld OCTA system in a portable cart. **(B)** A photograph of the handheld probe. This figure was reprinted from Ni et al. (151) with permission.

The I-OCT can provide insight into diagnosis and surgical planning, optimal outcome confirmation, complication prevention and control, prognosis, and education. Ehlers et al. in two studies (PIONEER and DISCOVER) reported that I-OCT findings can affect surgical decision-making in 29–68% of select surgery types (154, 157). For epiretinal membrane peeling, I-OCT can precisely locate the margins of the membrane, dictate the best start and end points for peeling, and confirm successful peels without further complications (a point of disagreement between subjective observation and I-OCT) (154, 157–160). In macular hole repairs, I-OCT can confirm the release of traction, effectiveness of the tamponade or flap and hole closure; on the latter, Kumar et al. recognized residual tissue at the hole edge (a "hole-door" sign) as an imaging factor predicting the rate of hole closure (161–166). Recently, Cehajic-Kapetanovic et al. have reported to be the first group using I-OCT to guide a robot-assisted drug delivery during vitreoretinal surgery; in that context, I-OCT can be used to guide all kinds of retinal and subretinal treatments, including highly promising gene therapies for retinal conditions (167–169).

In surgeries of the anterior segment, the ease of imaging of the cornea makes it an attractive I-OCT target (153). For deep lamellar anterior keratoplasty (DALK), where the corneal stroma is dissected, I-OCT allows the surgeon to evaluate the depth of the dissection, make on-the-spot adjustments, and confirm layer separation and integrity of Descemet's membrane (153, 170–173). Implementations of I-OCT in DALK have been shown to lead to successful outcomes (171, 174, 175). Posterior corneal procedures like Descemet stripping (automated) endothelial keratoplasty (DSEK/DSAEK) and Descemet membrane endothelial keratoplasty (DMEK) can also benefit from the use of I-OCT. The handling, unfolding, and positioning of the graft can be performed more quickly and definitively with simultaneous I-OCT, which can also verify its correct orientation (176–181). Apart from this, fluid between the cornea and the graft (interface fluid) and areas of graft non-adherence or folds can be assessed and addressed (176, 182–184). In the setting of cataract extraction surgery, I-OCT could be beneficial for identifying and handling complications, confirming adequate placement of the lens and further improve the accuracy of refractive calculations and aid in the development of future lens designs (153, 185–187).

Whole-Eye Optical Coherence Tomography

Different parts of the eye require imaging configurations specific to the area examined (anterior segment versus retina), mainly due to different natural properties. For anterior segment, imaging light has to pass only through the air to the tissue of interest versus the refractive structures (cornea and lens) for retinal imaging. The scan depth using standard OCT is typically about 2 mm, well below the typical axial length of the eye (188). Whole-eye OCT offers the opportunity to acquire a view of the eye from anterior to posterior segments with a single scan.

Multiple approaches have been implemented for that goal. Commercial systems (Heidelberg Spectralis, OptovueiVue, Leica Bioptigen C-series) are able to scan 2 areas in sequence by changing the scan configurations, for example, the reference arm length. In addition, changing the imaging optics (by adding lenses or using an adjustable lens) or alternating the volume frames helps decrease the differences of the structures imaged (150, 189–191). The main drawback of switching scan configurations is the time gap for changing the settings. Recently, Luo et al. have demonstrated an SS-OCT prototype that utilizes a single source and a single detection channel for sequential imaging (192).

Newer approaches of whole-eye OCT aim to capture images of all structures at the same time and be true whole-eye scanners. Approaches include the use of 2 practically separate subsystems (the first for anterior segment and the second for retina) or a single system with either one or two different imaging depths (193–196). The latter is the most advanced method, with the dual-depth polarization system focusing on both structures at the same time, using either one or two interferometers (197, 198). Its big advantage is the focusing of each area while also achieving standard fields of view greater than 24 degrees to image both the macula and the ONH.

In clinical application, whole-eye OCT can provide biometric data for the entire eye (axial length and lens thickness); this, along with information about possible retinal comorbidities and/or microstructural lenticular changes (for example, posterior capsule integrity), can be useful in planning of refractive or cataract surgeries (199–202). Following cataract extraction surgery, it can also verify correct lens positioning and capsule integrity (202, 203). Moreover, visualization of the entire eye could be relevant to patients with high myopia and potentially provide insight into possible causes of pathologic myopia. In certain conditions involving multiple ocular structures, such as the anterior chamber angle and the RNFL in glaucoma, whole-eye OCT could provide data for multiple regions of interest (204).

Anterior Segment Optical Coherence Tomography

The interest of imaging the anterior segment became apparent soon after OCT's introduction in 1991. A decade and a half later, OCT systems designed specifically for that purpose were developed that utilized TD-OCT [Visante (Carl Zeiss Meditec, Dublin, CA, United States; 2005), Slit-Lamp OCT (Heidelberg Engineering GmbH, Heidelberg, Germany; 2006)] or SS-OCT [Casia SS OCT (Tomey, Nagoya, Japan); 2008] and were able to image the entire anterior segment.

The AS-OCT can be a tool in diagnosing conditions involving the anterior segment. A common condition is dry eye disease (DED), in which diagnosis can be a challenge due to poor association of corneal findings and actual symptoms (205). AS-OCT can measure the precorneal tear film thickness and individual tear film layers (lipid and aqueous) and the tear meniscus (area, height, depth, and radius) (**Figure 4**); these parameters correlate with objective corneal findings, subjective symptoms, and other tests used in DED (such as the Schirmer test) or can be used to evaluate treatment response and monitoring (206–214). For other corneal pathologies, AS-OCT can also be an aid in diagnosing various types of keratitides (fungal, viral, bacterial, and parasitic), ocular surface neoplasias, corneal edema, corneal dystrophies, differentiate pterygium from pseudopterygium and assessing keratoconus morphology (95, 215–223).

A special utilization of AS-OCT is in the setting of glaucoma research. Elevated intraocular pressure (IOP) in primary open angle glaucoma (POAG) is due to increased resistance in the aqueous outflow system, and AS-OCT can be used for evaluation and for better understanding of the pathophysiology. In POAG, the decreased Schlemm canal cross-sectional area has been reported compared to healthy subjects (224, 225). AS-OCT can also visualize the anterior chamber angle qualitatively and quantitatively (angle opening distance, angle recess area, and trabecular-iris space area), with these findings correlating well with ultrasound biomicroscopy (226, 227). Baskaran et al. reported the correlation of angle closure on AS-OCT and gonioscopic angle closure (228). Risk factors for angle closure can be identified using AS-OCT, such as iris thickness/area, anterior chamber width, lens vault, and anterior chamber area/volume (229–231). Further AS-OCT advances would allow better understanding of the inciting events of angle closure glaucoma. The response of the trabecular meshwork to elevated IOP can be visualized and quantified (232). In the laboratory, using automated software, a 3D reconstruction of the entire SC and collector channels is now possible; changes in these structures can help in guiding glaucoma surgeries and predict or monitor IOP-lowering treatment success (both medical and surgical) (233–237). Ruggeri et al. have recently combined AS-OCT with a wavefront-based aberrometer, which was capable of using the OCT beam to acquire refractive error measurements and allow for simultaneous imaging, autorefraction, and biometry (238).

Recent advances in the field of OCT have also been applied to modern AS-OCT, namely, increased scanning speeds (up to 2 million A-scans/s), greater depth, and improved axial resolution (up to 1 μm) (239–246). These have allowed the imaging of most structures of the anterior segment, including all the corneal layers and the precorneal tear film, the outflow system (trabecular meshwork, Schlemm canal, collector channels, and scleral veins), and the anterior chamber angle (247–250).

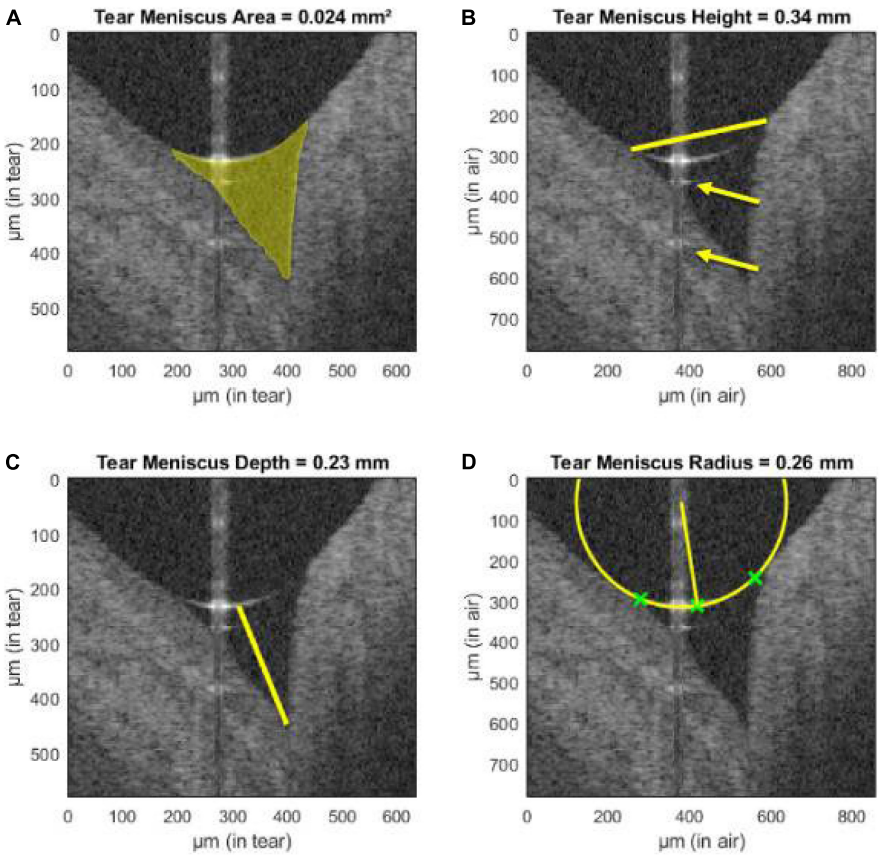

FIGURE 4 | Assessment of tear meniscus using UHR-OCT. Automatic segmentation of the lower tear meniscus in a healthy subject. Calculated parameters (represented in yellow) are **(A)** the tear meniscus area, **(B)** height, **(C)** depth, and **(D)** radius of curvature. Green crosses represent the points used for the estimation of the radius of curvature. The yellow arrows indicate mirror artifacts of the true upper meniscus boundary due to internal reflectors in the optical setup of the system. This figure was reprinted from Stegmann et al. (209) with permission.

Full-Field Optical Coherence Tomography

In FF-OCT, a light emitting diode is used to illuminate the entire scanning field simultaneously, which captures images orthogonal to the optical axis (en face) and avoids transverse scanning (251). Challenges to FF-OCT include eye movements and difficulties matching of the length of the optical path; cameras with high acquisition speeds and combinations with TD-OCT and FD-OCT aim to resolve these issues. Although time-domain FF-OCT (TD-FF-OCT) is possible, its slow volumetric capture capability limits is use (252). Fourier-domain FF-OCT (FD-FF-OCT), on the other hand, can capture 3D volumes of the cornea and retina with scanning speeds reaching 38.6 MHz (253). The single phase of FD-FF-OCT across the entire field does not introduce motion artifacts seen between A-scans in conventional OCT and allows for the use of higher scanning power, leading to fewer aberrations and less signal loss (252, 254).

The FF-OCT can be used to image and study structures of the anterior segment. Mazlin et al. presented the first FD-FF-OCT system capable of corneal imaging the corneal epithelium, stroma, and endothelium (255). The same team later created a system, combining FF-OCT with SD-OCT capable of cellular level imaging of the entire ocular surface (256). Using a common path (NIR light-emitting diode), the SD-OCT arm was used to track axial and lateral eye movements and adjust the optical arm lengths of the FF-OCT accordingly. This allowed for *in vivo* detailed imaging of all the corneal layers, sometimes even to the cellular level (superficial epithelium and stromal keratinocytes), including nerve plexuses. Apart from the cornea, quantitative parameters from structures, such as the tear film (tear flow velocity, amount of particulate matter, and evaporation time after blinking) and the corneal limbus (blood vessel morphology, blood flow velocity, and blood flow direction), were also measured. These can be useful for research studies of relevant anterior segment pathologies (DED, anterior chamber inflammation, and conditions leading to scarring). This approach is comparable to confocal microscopy, as it images the same corneal microscopic features much faster, in a non-contact manner and from a broader (nine times larger) field of view, with high axial resolution and without the requirement of fluorescein administration. These features make FF-OCT an excellent candidate for *in vivo* histological studies without sample preparation.

A similar approach with combination of FF-OCT and SD-OCT has been used for retinal imaging. A device using that principle was presented by Xiao et al., which was able to image the RNFL and photoreceptor layer in great detail (orientation of nerve fibers and cone photoreceptor mosaic, respectively) (257). These images were comparable to AO-OCT commercial devices (discussed below in greater detail), although the SNR was lower in the photoreceptor layer and not adequate to image other retinal layers, such as the ganglion cell layer and RPE; visualization of layers also required averaging of multiple images after acquisition. Other teams have also succeeded in imaging the photoreceptor layer with FF-OCT (258). For remote retinal scanning with FF-OCT, von der Burchard et al. have also proposed a low-cost device, which patients can use to examine themselves and monitor disease progression from their homes (259).

ADAPTIVE OPTICS

By using wavefront technology first utilized in astronomy and defense systems, adaptive optics (AO) systems have been implemented in ophthalmology with the goal of correcting for ocular anatomical and physiological higher order (optical/wavefront) aberrations (cornea, lens, and pupil), which cannot be corrected by glasses, contact lenses or refractive surgery (260). As a result, AO vastly improves the transverse (lateral) resolution as well as the speckle width and increases the SNR *via* imaging through a larger pupil, allowing more light to enter the eye. Further improvements in the lateral resolution have also been made by the addition of mirrors and error budget analyses (261–264). AO has so far been implemented in multiple imaging modalities, such as OCT (AO-OCT), scanning laser ophthalmoscopy (AO-SLO), and two-photon ophthalmoscopy (AO-TPO) (265, 266).

The improved lateral resolution of AO systems has enabled the visualization of single cells within the retina (**Figure 5**). By combining this feature with the high axial resolution of OCT, a resolution voxel smaller than most retinal cells is acquired: the lateral resolution achieved (2–3 μm) is about 5 times higher and overall resolution 36 times greater than commercial OCT (267–272). The big advantage, therefore, of AO is the ability to track cellular changes over time either for studying disease processes or monitoring treatment responses, both of which could be very useful clinical applications.

Cone photoreceptors are the cells most widely studied using both AO-OCT and AO-SLO. Anatomically, they have been shown to possess a wide range of reflectance properties, and their major components (inner segment, outer segment, somas, and axons) can be visualized, with results corresponding to histology. They can also be functionally distinguished by their light sensitivity in different types (short, medium, and long wavelengths). Photoreceptors are normally organized in a lattice hexagonal pattern in the retina, and their architecture can be extracted by semi-automated segmentation methods (273, 274). After identification, mapping the structure formation (Voronoi analysis) allows for descriptive quantitative measurements (cone density, cone spacing, and mosaic regularity), which can be utilized with good inter-device reproducibility (2.5–6.9%) as biomarkers or used to construct normative databases for research or clinical practice (**Figure 6**) (275–278). The calculation of functional biomarkers (cone reflectance) is also possible (279). Rods are more difficult to visualize than cones since they have a smaller diameter (especially peripherally), different refractive indices, and greater interference with the RPE (280). Despite these drawbacks, AO-SLO studies using improved AO systems have demonstrated visualization of rods in both normal and diseased subjects (281).

Imaging of several retinal cell types is possible with AO. These include individual RNFL bundles and sublayers of the ONL, which has been shown to consist of two distinct sublayers (somas and axons) (262, 269). These are mostly visible with AO-OCT, since the limited axial resolution of AO-SLO cannot easily image the transparent, multi-cell thick inner layers (280). Confocal AO-SLO, in which light is focused on a single spot and the backscattered light is refocused on a confocal aperture, is capable of imaging some of these structures (photoreceptor segments and nerve fibers), as well as blood vessels and the lamina cribrosa (282). AO-SLO-FA can also capture blood flow and detect vascular leaks. Other non-confocal detection modes (offset aperture, dark-field, split-detection, and offset pinhole) and the implementation of multi-volume averaging have also been implemented in order to visualize the ganglion cells and RPE (277, 283–285).

These features allow a detailed study of the retina and its cellular microstructure both in normal eyes and in ocular pathologies, making AO a useful adjunct to other OCT imaging technologies. In AMD, retinal layer and RPE changes can be monitored in areas of drusen/pseudodrusen or GA (286). Panorgias et al. have demonstrated both losses in reflectivity between the photoreceptor inner and outer segments in areas of GA (287). This could be extremely helpful in determining the progression of events in AMD and determining which tissues are affected first during the disease onset (277, 288).

Decreased cone density in areas of RNFL thinning was also displayed in glaucoma and other neuropathies (289, 290). Multiple groups have demonstrated that RNFL bundles are lost in areas of scotomas in glaucoma, and that the polarization properties change in the disease course (270, 271, 291). The increased transverse resolution of AO-OCT can also be utilized to better visualize the microstructure of the lamina cribrosa in glaucoma, a site of early damage, and, therefore, aid in earlier diagnosis (291).

The 3D representation of retinal microvasculature with AO-OCT can also make it a valuable tool in the assessment of DR, especially in combination with OCT-A, for study of microaneurysms, vessel tortuosity, and capillary dropout (270, 292–295). Decreased cone density has also been reported to be 10% lower in DR, which could suggest a method for earlier detection (296).

Finally, the cellular identification of either AO-OCT or AO-SLO can be used to study disease mechanisms of inherited color defects and monitor treatment response

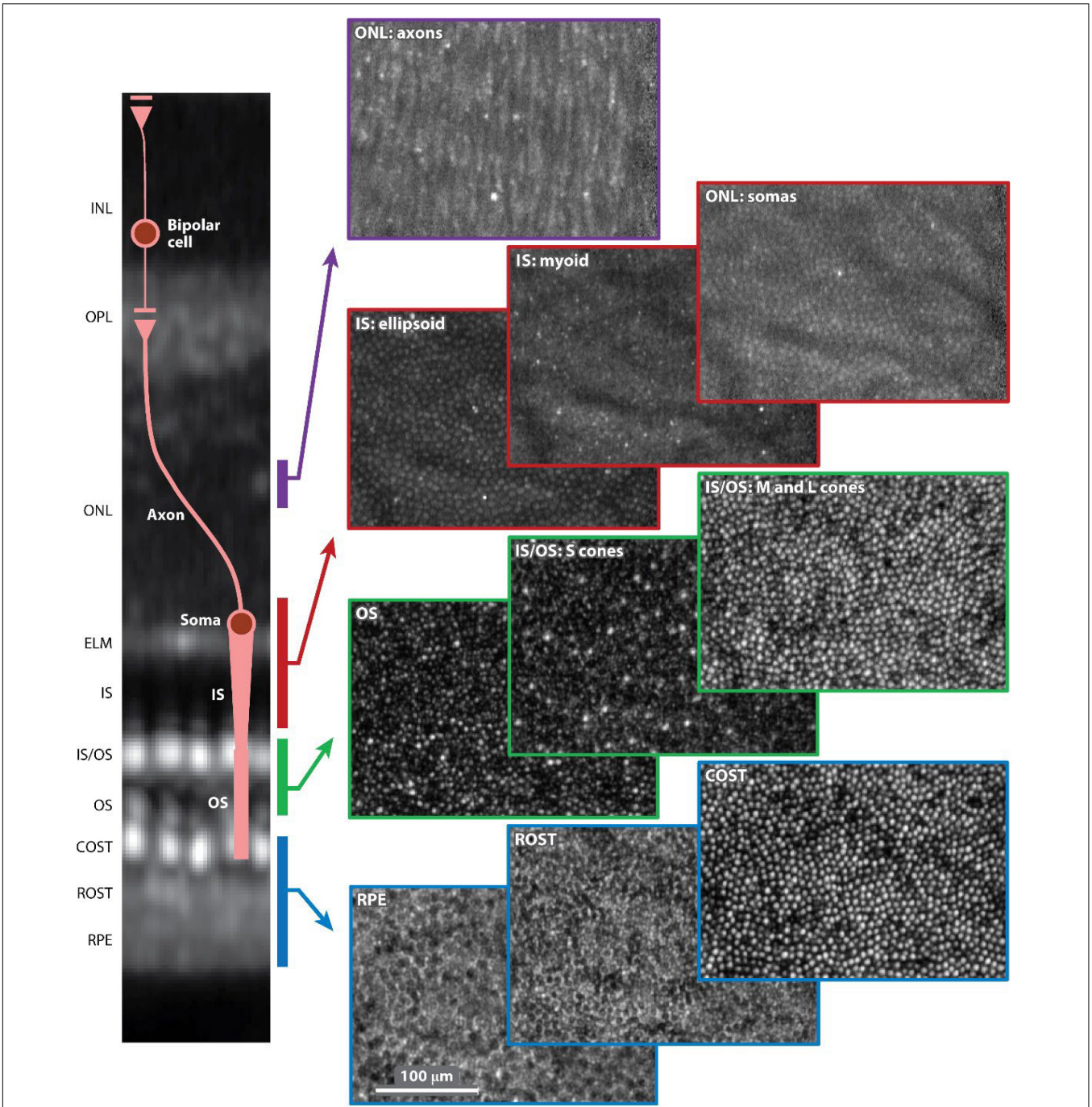

FIGURE 5 | Adaptive optics optical coherence tomography (AO-OCT) volume image of the outer retina of a 52-year-old normal subject. Ten en face (C-scan) images are shown selected from the volume and color-coded by depth in the outer retina, as denoted in the cross-sectional slice (B-scan) on the left. Each C-scan image is normalized to itself and presented on a log intensity scale. The AO-OCT volume image is an average of approximately 2,200 registered volumes that were acquired at 3.7° temporal to the fovea. AO-OCT, adaptive optics optical coherence tomography; COST, cone outer segment tip; ELM, external limiting membrane; INL, inner nuclear layer; IS, inner segment; IS/OS, inner segment/outer segment junction; ONL, outer nuclear layer; OPL, outer plexiform layer; OS, outer segment; ROST, rod outer segment tip; RPE, retinal pigment epithelium. This figure was reprinted from Miller et al. (262) with permission.

in stem cell transplantation therapies for said retinal diseases or central serous chorioretinopathy (280, 297, 298). For treatment of retinitis pigmentosa specifically, multiple AO modalities (AO-OCT and AO-SLO) can be used to stage the disease based on individual cell health, assess visual function from the cellular structure, and select candidates that could benefit from treatment (299, 300).

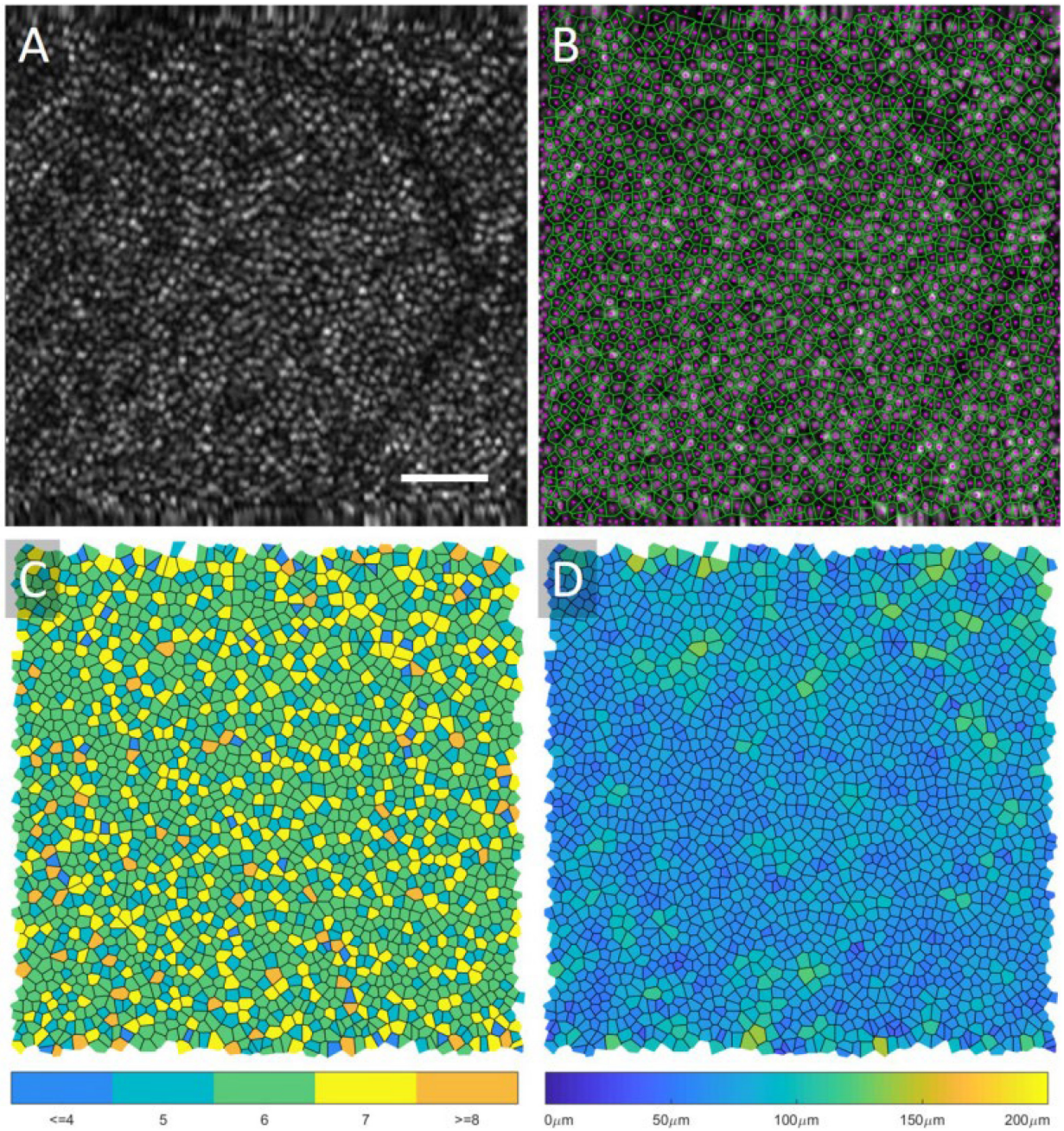

FIGURE 6 | Voronoi analysis of photoreceptors from AO-OCT. An original AO-OCT image taken at ∼6.5° retinal eccentricity is displayed in **(A)**, and the center of the cones (magenta) and the Voronoi map (green) is overlaid onto the image in **(B)**. In **(C)**, the Voronoi cells are shaded based on the number of neighbors, and, in **(D)**, the cells are shaded based on their area. A scale bar, 50 μ m. This figure was reprinted from Heisler et al. (508) with permission.

The application of AO-OCT in routine clinical settings is still challenging, mostly due to high cost, size, and complexity of the devices, time-consuming image acquisition and analysis, a limited scan area (generally no larger than 200 μm × 200 μm transversely), data size, and the lack of established normative databases (280). Some additional limitations are particularly present with specific populations who would benefit from AO applications, for example, unstable fixation in young children with inherited retinal dystrophies. For these reasons, AO-SLO and AO-OCT remain primarily research tools but are applicable to a number of ongoing clinical trials (301).

Despite these challenges, there have been developments over the last few years in the AO systems. Reumueller et al. have recently though developed AO-OCT prototypes that are promising and can be applied in patients with the aforementioned pathologies (302, 303). Improvements over

the standard AO-SD-OCT, such as point-scanning sensorless SD-OCT, computational AO, and line-scanning SD-OCT, are currently being investigated (277, 304, 305). The acquisition speed of images has been improved by various groups up to 1 million A-lines/s, the fastest retinal SD-OCT at the time, while the implementation of AO in SS-OCT systems allows for even higher speeds (262, 269, 291, 306–308). The increased scanning speeds have aided in resolving the issue of motion artifacts, an issue also addressed by means of active retinal tracking (integration of AO-SLO with wide field or tracking SLO) and registration of multiple scans (306, 309–314). The registration and image averaging of scans also allows for temporal tracing of cellular processes in time and improves the SNR and contrast, which make individual cells more apparent; examples include better visualization of the RPE, RGC somas, IPL bands, and hyalocytes on the internal limiting membrane (ILM) (262, 285, 315–319). These cellular parameters are attractive, as they can be used as biomarkers for screening or longitudinal follow-up. As an example, AO-SLO can detect cell destruction in retinal degenerations before the onset of symptoms, which would allow the formation of therapeutic clinical trials, while vision is still salvageable in these patients (280, 320). At the same time, improvements in the axial resolution of OCT devices *via* increasing the bandwidth of imaging sources (greater than 100 nm) have allowed the development of AO ultra-high-resolution OCT (AO-UHR-OCT) (267). Pandiyan et al. implement techniques (increased source bandwidth, improved Nyqyist sampling, increased illumination beam size at the pupil, spherical mirror-based telescopes instead of lens-based telescopes, optimized design software and tools) that improve the resolution of both structure and function, achieving visualization of both individual foveal rods/cones in *en face* projections and RGCs; this has also been achieved by other groups (321, 322).

Phase-Sensitive Optical Coherence Tomography and Optoretinogram

The AO has the potential to capture images of single cells from a snapshot in time. Assessment of the temporal function is also possible through the development of phase-sensitive OCT. It is known that the reflectivity of retinal cells, caused by photoisomerization of pigment chromophores, can vary after application of visual stimuli (optical phase changes) (323). Measurement of these changes is possible with either OCT, hence the term "phase-sensitive OCT" (324). This is the foundational basis of the optoretinogram (ORG), which allows recording of responses to visual stimulation. The ability to detect the function of individual photoreceptors would allow detection of retinal dysfunction in a microscopic scale. As opposed to OCT assessment, where the result is binarized (alive versus lost photoreceptors), ORGs provide a spectrum of function and identify cells that could be salvaged (280).

The implementation of ORG in a clinical setting still has some drawbacks. Studies, so far, have only focused on healthy individuals or patients without severe conditions, whose imaging might pose challenges, such as poor fixation, pathologies hindering image quality, and long periods of dark adaptation not easily tolerable. Furthermore, even after image acquisition, processing of these images is hours long. Despite these difficulties, ORG can potentially be implemented in other devices currently used (SLO and AO-SLO, OCT/OCT-A and AO-OCT) with minimal additions (a stimulus channel and appropriate software) to provide a functional component to structural measurements.

ARTIFICIAL INTELLIGENCE AND INTEGRATED MACHINE LEARNING

The implementation of AI in the field of ophthalmology has been a revelation. Ophthalmology offers a great basis for AI to grow and be utilized, owing to the combination of data availability for highly prevalent conditions (glaucoma, AMD, and DR), which are always rising as the population ages, developments in teleophthalmology, and the reliance of these conditions on low-cost, easily performed images (predominantly fundus images and OCT) (325). AI strives to solve some major obstacles in many aspects of eye care: It can provide valuable feedback for diagnosis, monitoring and follow-up, correct treatment decisions, and prediction of disease course. These benefits are especially relevant to conditions requiring highly specialized care by experts; its use by comprehensive ophthalmologists can provide a highly reliable solution to difficult specialist access, further hindered by the impact of the ongoing pandemic. These obstacles impact specific populations more than others, and broader access to eye care can help unveil true racial variations otherwise attributed to merely genetic differences. Improving medical decisions can also lead to lower eye care cost since the cost of specialist access, referrals, and treatment of advanced eye conditions is very high. As a result, apart from the medical benefits, the implementation of AI also has a strong social aspect, as it could provide solutions to health, clinical, racial, and financial equity.

The utilization of AI in ophthalmic imaging requires the cooperation of a variety of healthcare professionals, including but not limited to physicians, patients, researchers, government officials, and pharmaceutical and imaging device companies. With the collective goal of improving patient care and fostering equity as mentioned above, and with the potential of AI to substantially transform the management of patients, the Collaborative Community on Ophthalmic Imaging (CCOI) was founded in 2019. Experienced experts of the CCOI operate under the values of teamwork, transparency, innovation, and efficiency in a patient-centered approach, strive to resolve any potential issues in eye imaging, and establish the best strategies for the practical use of software in ophthalmology in a way that respects the basic principles of bioethics (325–328).

The Principles of Artificial Intelligence

The foundation of AI is the completion of tasks by computers through mimicking human (natural) intelligence and cognitive functions. Brain neurons receive signals (input), process that information, and generate results (outputs); these neurons are connected and form networks (neural networks – NNs) capable of complex calculations. These calculations are not static, as the brain can learn from previous data and experience. AI replicates

that approach using computer networks, a process referred to as machine learning (ML); inputs are provided to computer models that process them under sets of parameters and give outputs (329). The caveat in that process, which is the basis of supervised learning (SL), is that the real outputs are provided and, accordingly, the model learns to adjust these parameters (training) to calculate the outputs as accurately as possible. Over the past decade, the vast increase in data availability, computer hardware improvement (mostly graphics processing units – GPUs), and the theoretical improvements in NNs have led to an exponential growth of AI.

There are multiple approaches to AI network arrangements, and AI models range from very simple to highly complex. The most simple form of SL is linear regression, where multiple inputs are given to a model that then best adjusts the parameters of each input to provide the most accurate result (330). Logistic regression is an algorithm that adds a sigmoid function to linear regression and displays these results in a probabilistic format (values between 0 and 1) (330). Taking this approach a step further, whereas linear regression tests inputs independently of each other, non-linear regression has the ability to examine interactions between inputs and outputs in several layers (known as multilayer perceptrons), and this is the concept of feed forward neural networks (FFNNs) (330). As the algorithm processes many relationships in several layers, the NN can learn these associations, hence the name deep learning (DL) (331). The metrics of performance for these algorithms are the area under the curve (AUC) in the receiver-operator curve (ROC), sensitivity, specificity, and accuracy.

Specifically in ophthalmology and imaging, NNs have been fine-tuned to process imaging data and are called convolutional NNs (CNNs) (331). Convolution is a mathematical operation that applies filters to images (matrix of parameters) to produce image outputs with different channels (features), whose parameters are continuously tested; this process can be repeated in sequences and actually constructs an FFNN. Inputs can be images in either two- or three-dimensional slices, which is preferred as eye structures between slices are considered as a whole. The final outputs mostly fall into two categories: classification (categorical outputs) or segmentation (image outputs). These can provide both accurate staging of conditions and better-quality images through denoising for clinicians to interpret, since up to 46.3% of SD-OCT scans are prone to artifacts or segmentation errors (330, 332, 333).

Artificial Intelligence and Glaucoma

Glaucoma is a field that has recently attracted a lot of interest in the integration of AI to ophthalmology and imaging due its involvement of multiple eye structures (anterior chamber angle, iris, retina, and ONH), high prevalence, and reliance on multiple methods to establish a diagnosis. Current clinical assessment of glaucoma relies on a combination of various diagnostic tools to assess anatomy, structure, and function, such as gonioscopy, fundus examination of the ONH, tonometry, OCT scans, and perimetry (a visual field) testing, with none being totally sensitive or specific of its own (325, 334). The interpretation of these results also varies among clinicians (335).

The AI can significantly aid in differentiating glaucomatous from healthy eyes. On this matter, emphasis should be given on moderate glaucoma, where symptoms of early vision loss are apparent or very likely (327). DL algorithms can provide segmentation-free image analysis to quantify relevant structures and can even perform better than traditional segmentation approaches of retinal layers (332, 336). For structural assessment, algorithms could detect changes and signs of optic neuropathy from fundus pictures with greater sensitivity and specificity than clinicians (up to 96.2 and 97.7%, respectively); this can be advantageous, given the subjective and inconsistent interpretation by physicians (325, 337–340). AI can be used on fundus pictures to also differentiate glaucoma from other pathologies of the optic disc, such as papilledema, ischemic optic neuropathy, optic nerve atrophy, compressive optic neuropathy, hereditary optic neuropathy, hypoplasia, and toxic optic neuropathy (341–343). The standard modality of assessing structure, though, is OCT imaging; algorithms can provide assessment of the anterior chamber angle as well as segmentation of the RNFL adjusted for other parameters (age, gender, and eye biometry metrics) to improve the accuracy of the measurements (344–346). Studies have focused on many parameters of the retina and ONH (RNFL, prelaminar area, RPE, choroid, peripapillary sclera, Bruch membrane opening, and minimum rim width), and their performance was highly accurate in identifying glaucomatous eyes (>94%); AI analysis of OCT-A vascular abnormalities of the ONH also yields excellent results (347–354). When comparing various ML classifiers, Wu et al. showed that ganglion cell layer measurements were important in early glaucoma detection, whereas RNFL metrics were more useful during disease progression; in fact, Shin et al. showed that wide-field SS-OCT scans can even outperform the conventional parameter-based methods (355–357). In a recent meta-analysis, including data from numerous studies, Wu et al. reported remarkable overall performance in detecting glaucoma from both fundus pictures (AUC, 97%) and OCT (AUC, 96%), with similar outcomes in classifying glaucoma as well (358). Aside from layer segmentation, the analysis of raw unsegmented OCT volumes (feature agnostic approach) of the ONH has been shown to provide better results than classical ML techniques (AUC of 94% versus 89%) (359). The existing issues with AI applications to OCT, though, are the potentially poor image quality, limited generalizability of certain algorithms to multiple devices and patient-specific factors (anatomy and comorbidities) undermining OCT thickness values (325). To detect functional changes in the visual fields, CNN algorithms have been developed by various teams that mark visual field tests as either normal or glaucomatous with high precision (87.4–87.6%) (360, 361).

A very attractive approach is to use AI to combine structural information with functional outcomes. Glaucoma diagnosis is improved when using both ONH parameters and VF outcomes: algorithms capable of predicting 10-2 VF parameters from macular OCT scans, and 24-1 VF parameters from both macular and ONH OCT scans have been developed (362–365). Also, various teams (Lazaridis et al., Christopher et al., Datta et al., and Xiong et al.) have recently developed algorithms (RetiNerveNet and FusionNet) capable of using both OCT metrics (various

layer thickness values) and raw OCT or fundus images to predict VF changes with high accuracy (366–370). Overall, combination of structural and functional information has been shown to outperform structural or functional assessment alone.

These results are especially encouraging when it comes to screening for glaucoma; these imaging techniques are simple and inexpensive and would allow for identification of glaucoma at early stages. As opposed to diagnosis at a more advanced stage, early treatment initiation can both prevent irreversible vision loss and avoid expensive, invasive techniques used for later glaucoma stages, as the cost of management increases with glaucoma progression; its performance, however, still needs to be improved (327). The implementation of DL to AS-OCT is a field-attracting attention; Li et al. have very recently developed a novel 3D deep-learning-based digital gonioscopy system that identified angle closure suspects and that could be used as a screening method for primary angle closure glaucoma (371–376).

AI can also be a valuable tool in establishing the prognosis of glaucomatous progression. Functionally, Wen et al. reported that AI can estimate VF loss up to 5.5 years in the future with minimal error, given only a single test as a starting point (377). Algorithms are also capable of identifying slow disease progression consistently earlier than conventional methods, too (3.5 years versus >3.9 years) (378). Structurally, Christopher et al. reported that RNFL analysis can also predict glaucoma progression more accurately than VF testing (95% versus <86%), and with less error than standard linear regression models (325, 379). Sedai et al. have developed multimodal models using a combination of clinical, structural, and functional information to predict RNFL changes in healthy subjects, patients with glaucoma patients, glaucoma suspects with greater performance than standard linear trend-based estimation (380). These predictive algorithms, however, have not yet been implemented clinically.

Artificial Intelligence and Age-Related Macular Degeneration

With more than 200 million people affected worldwide, AMD constitutes the most common cause of blindness in developed countries (381). Although no AI device has yet been made commercially available for AMD yet, several algorithms to potentially aid physicians' decisions do exist.

Up to 25% of patients with AMD can remain undiagnosed by primary care providers, and the use of AI would not require an advanced skillset to operate or retinal expertise (328, 382). An ideal method of AMD screening should be able to efficiently detect AMD and distinguish it from other similar diseases, be cost-effective, and autonomous. Hence, the low cost and simplicity of fundus photographs make it a great candidate for wide AMD screening; models that can classify AMD based on the need for treatment have been developed, which function with great accuracy compared to professional graders (up to 92%) (383). This distinction is important when evaluating algorithms, as early treatment can significantly prevent vision loss in select cases of AMD (large drusen and intermediate AMD, CNV), and the cost of error is high for missing wet AMD; high sensitivity is, therefore, preferable (384). Macular OCT scans have the advantage of depicting the pathological findings of AMD in 3 dimensions and with high resolution; hence, they can be utilized as a next step, following the initial screening with fundus photographs to rule out false positive cases and further classify the true positives (385). De Fauw et al. have developed a screening algorithm capable of identifying multiple retinal conditions, which was able to outperform retinal specialists on both screening success and avoidance of severe and costly errors (386).

Models can also substantially assist physicians in establishing diagnosis of AMD. This can sometimes be challenging, as AMD findings can potentially go unnoticed or appear similar to other retinal conditions (polypoidal choroidal vasculopathy, macular dystrophies, CSR, and others) (328, 384). For this purpose, a variety of algorithms has been offered, focusing on different imaging modalities (fundus pictures, OCT and OCT-A, FA) to detect multiple pathological findings (drusen and pseudodrusen, intra- and subretinal fluid, GA); similar to DR, structural and vascular biomarkers are also utilized for AMD (387–392). As a representative example, Yan et al. were able to utilize a model for identification of drusen, inactive and active CNV with high precision (84.3–97.7%) and AUC (94.–99.%) (393). Keenan et al. also used SD-OCT data across 10 years from the AREDS2 study to construct a model capable of identifying retinal fluid with high accuracy, sensitivity, and specificity compared to retinal specialists (85.1%, 82.2%, 86.5% versus 80.5%, 46.8%, 97.%, respectively) (394).

Even though the use of AI tools in the context of AMD has not been fully optimized, tools capable of prognosis and monitoring the condition are starting to emerge. Algorithms can perform better than specialists in some cases, but their accuracy can be improved; classification accuracy has been reported to be up to 76% and 5-year prognosis accuracy up to 86% in recent studies (395, 396). For classification, Peng et al. developed a model (DeepSeeNet) that more accurately classified AMD, when compared to retina specialists (397). This is especially important in the setting of edema in wet AMD, where anti-VEGF injections are indicated; Potapenko et al. have recently trained a CNN identifying retinal edema with accuracy of 90.9% (398). Even more so when combined with HH-OCT, algorithms can be proved to be a powerful tool in self-monitoring of the condition and more easily identify patients in need of antiangiogenic treatment. As to predicting the disease course, algorithms will help tackle issues, such as predicting conversion to wet (neovascular) AMD, personalize anti-VEGF treatment and predict their response, and increase the use of supplements to decrease the rate of progression. Sarici et al. have recently reported a set of outer retinal biomarkers (ellipsoid zone and RPE attenuation and thickness) useful to predict evolution of dry AMD to subfoveal GA, while Abdelfattah et al. used drusen volume to predict development of wet AMD within 2 years (399, 400). Finally, tools that could be utilized in predicting response to anti-VEGF treatment have also been developed with accuracy comparable to retinal experts (65.4% vs. 53.8–76.9%) (401). A detailed review of tools for AMD progression prediction by fundus photographs or OCT has been constructed by Romond et al. (402).

The implementation of AI on AMD care still faces some challenges. The limitations of OCT (high cost, artifacts, low signal strength, and poor focus) still apply in this field. There is also a great need for dataset diversity in terms of age, race, and socioeconomic status in data analysis to provide broader and more accurate AI outputs, as baseline factors and phenotypes can vary among populations (389, 403).

In general, the impact of AI tools in the setting of AMD can be proved useful in screening, diagnosis, and differentiation of similar appearing conditions, prognosis, and disease monitoring. Whether or not they can benefit physicians and potentially influence clinical decisions remains to be seen.

Artificial Intelligence and Diabetic Retinopathy

Using AI in the setting of DR is one of the most promising applications in medicine. As opposed to general monitoring of diabetes, which can be performed easily (blood glucose testing, HbA1c levels and others), DR requires qualitative evaluation.

The modalities more commonly used for diagnosis and monitoring of DR are fundus pictures, OCT, and OCT-A scans (as mentioned above). AI has the potential to detect disease in early (even asymptomatic) stages, classify it, predict the disease course, and thus guide treatment in select eyes (404–406). Tools can match or even outperform physicians and can make access to screening broader and less expensive; algorithms and devices are already clinically available (IDx-DR by Digital Diagnostics, Coralville, IA, United States; SELENA+ by EyRIS, Singapore) and have been authorized for use in multiple fundus cameras (407–412). Training models for AI has been steadily increasing for diagnosing DR from fundus pictures, with accuracy, sensitivity, and specificity improving over time (reaching 95.7, 97.5, and 98%, respectively) (412–416).

Similar results are also seen when using CNNs for DR severity grading; Ryu et al. have recently developed a fully automated algorithm to classify DR stages with accuracy of 91–98%, sensitivity of 86–97%, and specificity of 94–99% (417, 418). Application of these models can also establish biomarkers useful for diagnosis and treatment response; these could be structural (retinal layer measurement, hyperreflective foci) or vascular (areas of non-perfusion, vascular leakage, microaneurysm count, and neovascularization) (387).

TELEOPHTHALMOLOGY AND SMARTPHONE FUNDUS IMAGING

Telemedicine is defined as "the use of electronic information and communications technologies to provide and support health care when distance separates the participants" (419). In response to its growing demand in recent years, further enhanced by the COVID-19 pandemic, ophthalmologists have begun to implement techniques and technologies more widely to better facilitate patient care in a remote setting. This would make access to eye care more accessible, easier and more convenient for patients, faster, and more cost-effective. In terms of ophthalmic care, teleophthalmology is mostly applicable to ophthalmic emergencies, screening, and monitoring of chronic conditions.

One such technique is imaging of the eye with a smartphone (smartphone imaging – SI). The use of smartphones for clinical imaging in ophthalmology was first introduced by Lord et al. in 2010 (420). It was demonstrated that an iPhone could be used to capture external photos of the orbit and surrounding structures, indirectly image the anterior segment and the fundus of the eye when used with a slit lamp fitted with a 78D lens or a handheld 20D lens (420).

Since its introduction, external attachments and phone applications that offer features, such as image storage and improved user-interface, have been developed with the aim of improving the image quality and utility of SI. Although many variations and distributors exist, a commonly used attachment is a macro lens that can be clipped over the camera of a smartphone to provide supplemental co-axial illumination, making imaged features of the eye more distinguishable (421). The ability for smartphones to be paired with additional attachments and other devices has given rise to techniques that make it applicable in a wider range of clinical scenarios than most other forms of imaging (421).

The current capability of SI in the observation of anterior segment features is promising. Refined techniques using either gonio or macro lens combinations make it possible to capture high-quality videos and standstill images of the iridocorneal angle (422, 423). A trial conducted by Pujari et al. found that inferior angle measurements acquired using the iPhone-macro lens combination demonstrate excellent correlation with measurements acquired using AS-OCT (424). SI can also be used for the analysis of globe torsion. Using a 360° protractor application, the axis of the eye can be compared between smartphone-macro lens images before and after surgical intervention to quantify torsion of the iris and retina (425, 426). It is possible to perform pupillometry using SI, giving smartphones additional utility in the management of neuro-ophthalmological disease (427, 428). McAnany et al. observed excellent agreement when comparing smartphone pupillometry with infrared camera pupillometry, and found significant correlations in pupillary light reflex and re-dilation size between both methods (429). Additionally, methods have been developed for smartphone photography to be used in measuring implantable contact lens vault and assessing the intraocular lens alignment of patients (430–432).

With respect to posterior segment features and pathology, SI can be used to assess and monitor the fundus of patients. While studies have outlined successful techniques for imaging of the optic disk with smartphones (**Figure 8**) (433–435), Pujari et al. document a strategy to evaluate the ONH using a macro lens phone attachment and 90D handheld lens (436). With a combination of a battery, an LED light source, a barrier, and an excitation filter fitted to an iPhone, Suto et al. also demonstrated for the first time that fundus FA can be captured with a smartphone, producing images comparable to those obtained by indirect ophthalmoscopy (437). More recently, Sivaraman et al. have come forward with a smartphone-coupled device capable of capturing widefield images of the retina beyond

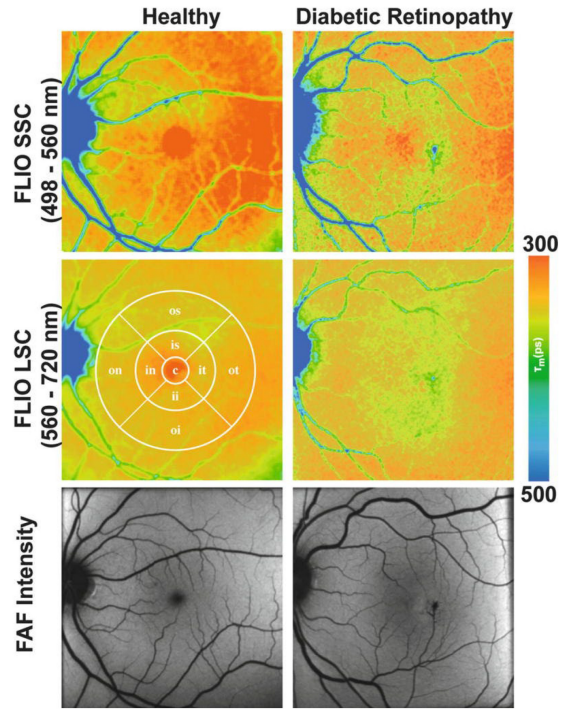

FIGURE 7 | Funds autofluorescence (FAF) lifetime images (FLIO) and FAF intensity images in diabetic retinopathy (DR). Mean funds autofluorescence (FAF) lifetime images (FLIO) from two spectral channels, as well as FAF intensity images from the retina of a healthy control **(Left)** and a diabetic retinopathy patient **(Right)**. The middle left panel comprises a standardized ETDRS grid. This figure was reprinted from Bernstein et al. (455) with permission.

the posterior pole, with a field of view of 65° with a single take (438).

The SI is suited for the screening of common diseases, such as glaucoma, AMD, and DR (439–441). SI-based screening for glaucoma, using frequency doubling technology and a head-mounted display, was found to be comparable to Humphrey VF testing with good agreement and correlation between both techniques (440). Photographs of the ONH can also be acquired with SI, with moderate agreement with in-person evaluation and respectable positive and negative predictive values (77.5 and 82.2%, respectively) (441–443). Home monitoring of IOP with rebound tonometers or contact lenses is also possible (441, 444, 445). Teleophthalmology in the setting of AMD screening mostly aims to detect conversion from dry to neovascular form; Li et al. were the first group to demonstrate similar wait times between remote screening in tertiary clinics and referral to retinal specialists, although with increased wait times for treatment initiation (446). Monitoring for AMD progression with Amsler grids or macular VF testing (for example, a ForeseeHome device by Notal Vision Ltd., Tel Aviv, Israel) is more promising and can be beneficial for high-risk patients (441, 447). For DR, screening can be accomplished with imaging modalities, such as non-mydriatic ultrawide-field and multifield fundus photographs, and has been proved to be reliable and cost-effective; Tan et al. compared smartphone ophthalmoscopy to standardized techniques and found that SI had an overall sensitivity of 87% and specificity of 94% (441, 448–450).

Like with many other current ophthalmic imaging modalities, the future of SI may lie in AI. Algorithms, such as AlexNet, EyeArt, and Medios, are accessible and can be coupled with SI for the screening for disease (451). Studies have demonstrated that SI analysis performed using AI is able to improve the sensitivity and specificity of SI in diagnosing retinal disease (452, 453).

FLUORESCENCE LIFETIME IMAGING OPHTHALMOSCOPY

The retina exhibits intrinsic autofluorescence: reactive to light stimulation, chemical compounds absorb photons, and promote electrons to a higher power state that subsequently return to their stable state, emitting red-shifted protons in the process. The intensity and patterns of fluorescence can be detected with high-sensitivity detectors in fundus cameras and ophthalmoscopes, mapped and used to diagnose and monitor many macular conditions (454). Since the majority of the signals originate from lipofuscin in the RPE, its high intensity predominates and shadows other retinal molecules that also emit fluorescence. The new technique of FLIO measures the decay lifetime of retinal fluorophores (FLIO lifetimes – FLTs), which are unique to molecules (Dysli et al. have described the lifetimes of each fluorophore in detail) and, therefore, more sensitive of weak fluorophores that are masked using fundus autofluorescence (FAF) (455–457). Hence, FLIO can reveal not only structural but also metabolic and biochemical changes in the retina.

In a clinical setting, the first FLIO device used was developed by Heidelberg Engineering in 2012 and has been shown to be highly reproducible (458–460). FLIO patterns have been identified for a variety of retinal diseases and can be valuable in early detection and detailed monitoring. In AMD, FLIO displays a characteristic pattern of ring-shaped prolongation of the FLTs around the fovea, which is present in the early stages of the disease even before the appearance of drusen and increases as the disease progresses (greater in advanced AMD) (461). Apart from this sign, areas of GA and drusen also display FLT prolongation, and this information could be proved useful in the understanding of their pathogenesis and metabolism as well as monitoring their development (461–463). Since AMD can appear similar to Stargardt disease, FLIO can be used to differentiate the two, since FLTs in Stargardt disease are not prolonged, and the typical ring pattern of AMD is not present. Most importantly, retinal flecks in Stargardt disease appear in FLIO about a year earlier than in other imaging methods like FAF (464). In the case of hydroxychloroquine toxicity, where early toxicity detection is challenging, FLIO could provide a better alternative to electroretinogram (ERG) or OCT, since it can detect prolonged FLTs before structural changes appear (465, 466). FLIO has also been used to identify changes in other retinal conditions as well, including DR (**Figure 7**), vascular occlusive diseases, CSR, choroideremia, RP, and macular holes, and is believed to be a promising diagnostic method (463, 467–473).

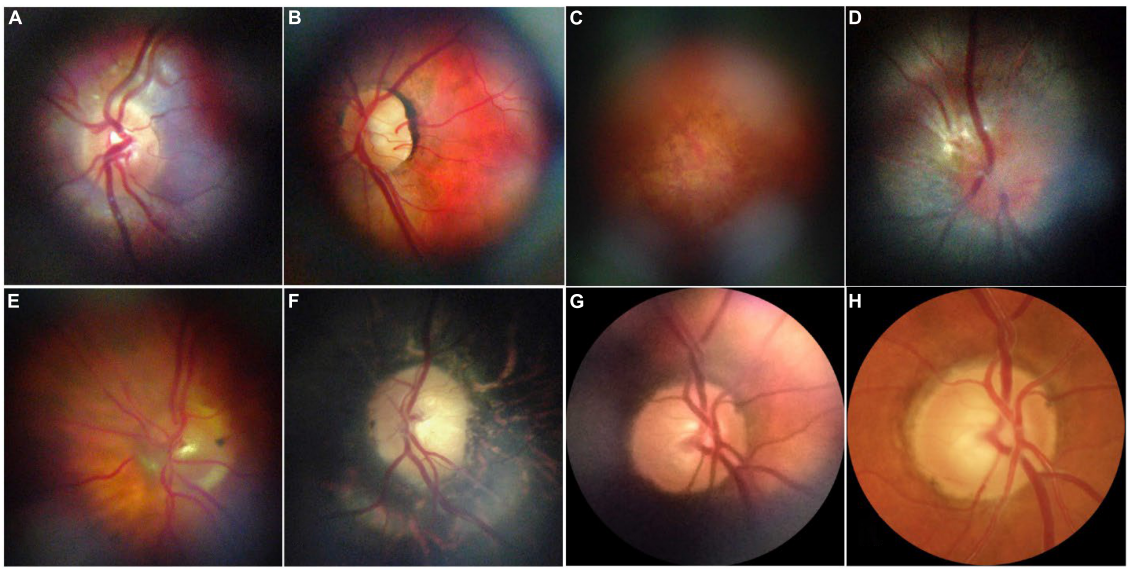

FIGURE 8 | Representative retinal images taken with D-eye. **(A)** A normal optic disk in an undilated child. **(B)** A normal posterior pole in a dilated 29-year-old woman. **(C)** Dry age-related maculopathy in an undilated 75-year-old man. **(D)** Optic nerve glioma in a 23-year-old undilated woman. **(E)** Posterior vitreous detachment in a dilated 72-year-old pseudophakic woman. **(F)** Waxy disk pallor and pigmentary changes in a 50-year-old man with retinitis pigmentosa **(G,H)**. Depiction of the same optic nerve head by D-Eye and Canon CR-2 Retinal Camera. This figure was reprinted from Russo et al. (434) with permission.

MULTIMODAL IMAGING

Multimodal imaging involves the incorporation of two or more imaging technologies for a single purpose. Combinations of imaging modalities make it possible to perform a more comprehensive examination of tissue by compensating for the individual limitations of a single device. Multimodal imaging is often used to improve the utility of commonly used OCT technologies.

The OCT-A is an example of a modality that greatly benefits from multimodal imaging. Although it provides significant clinical utility through its ability to capture the vasculature of the retina, limitations in the acquisition speed of OCT-A create prolonged susceptibility to motion artifacts, and other reductions

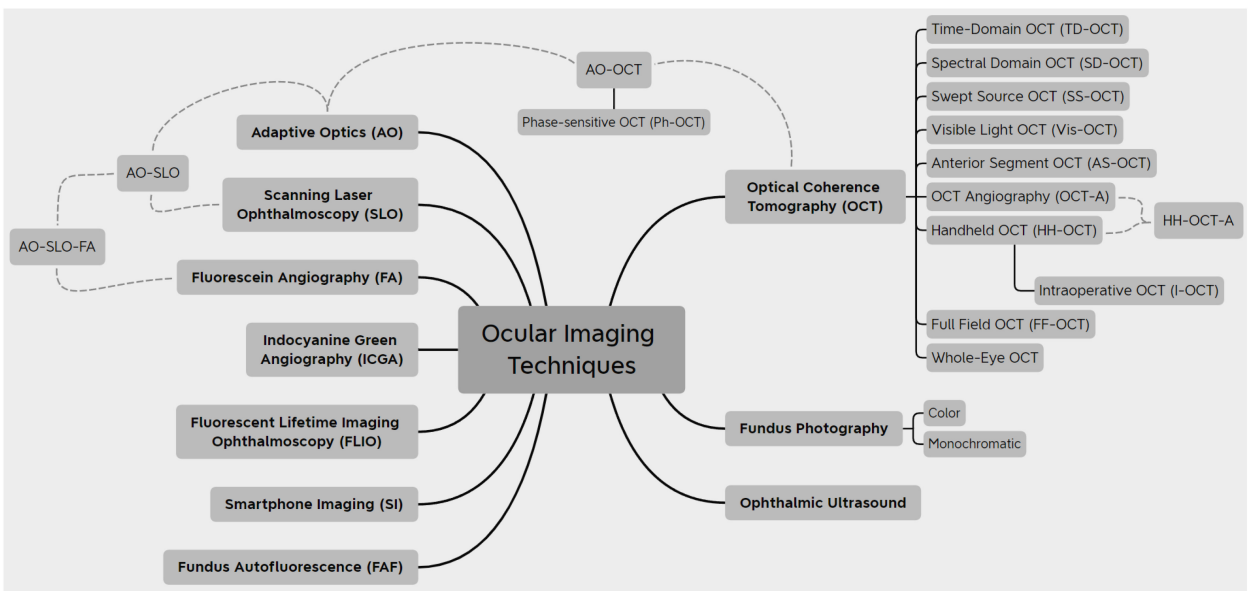

FIGURE 9 | A summary of the modern ocular imaging modalities.

TABLE 1 | Review and evolution of optical coherence tomography (OCT) imaging technologies in chronological order (3, 195, 196, 252, 255, 265, 308, 312, 499–506).

OCT technology	Year introduced	Commercial availability	Axial resolution in tissue (μm)	Lateral resolution in tissue (μm)	Maximum scanning rates (A-scans per second)	Major clinical application(s)	Advantages	Disadvantages
Time-domain OCT (TD-OCT)	1991	Yes	1.7–15	15–20	400	Most retinal pathologies.	Non-contact, non-invasive.	Low image acquisition speed. Poor spatial resolution.
Anterior segment OCT (AS-OCT)	1994	Yes	1.0	15	2,000,000	Anterior segment conditions (dry eye disease, corneal pathologies).	Detailed imaging of most structures of the anterior segment (corneal layers and precorneal tear film, outflow system, anterior chamber).	
Spectral domain OCT (SD-OCT)	2001	Yes	5–8	6–20	100,000 (clinical)	Most retinal pathologies.	Higher imaging speed and sensitivity than TD-OCT. Capture of 3D volumetric data *in vivo*. Retinal layer segmentation.	Imaging artifacts (projection, motion). Segmentation errors.
Full-field OCT	2002	No	5.6	1.7–2.4	40,000,000 (research)	Ocular surface conditions (dry eye disease, corneal inflammation).	Stable phase, no motion artifacts. Higher scanning power supported. Less sensitive to optical aberrations and signal loss.	Eye motion makes scanning difficult. Difficulties with optical path matching. Post-processing and image averaging necessary. Only select retinal layers visible.
Visible light OCT (Vis-OCT)	2002	No	1–1.4	4.6–10	30,000 (research)		Vastly improved axial resolution. Smaller bandwidth for same resolution. Higher image contrast. Oximetry and calculation of circulation metabolic parameters.	Slow imaging.
Adaptive optics OCT (AO-OCT)	2004	Yes	5–8	2–3	1,000,000 (research)		Vastly improved lateral resolution. Improvement of speckle width. Increased SNR. Visualization of single retinal cells and their function (phase-sensitive OCT). Improved lamina cribrosa visualization.	Slow imaging. Multiple scans required for registration. High cost. High complexity of devices. Limited scanning area. Large data size.
Handheld OCT (HH-OCT)	2007	Yes Yes	3–6	8–15	32,000 (clinical). 350,000 (research).	Pediatric conditions (congenital and pediatric glaucoma, macular edema, macular hole, epiretinal membrane, retinoschisis, retinal dystrophies). Intraoperative OCT (see below).	Imaging of challenging patient populations (bedridden and postoperative patients, children, remote access). Less expensive than benchtop OCT. Imaging of anterior and posterior segments in quick succession.	Probes still connected to bulky mobile carts.

(Continued)

TABLE 1 | (Continued)

OCT technology	Year introduced	Commercial availability	Axial resolution in tissue (μm)	Lateral resolution in tissue (μm)	Maximum scanning rates (A-scans per second)	Major clinical application(s)	Advantages	Disadvantages
Intraoperative OCT (I-OCT)						Glaucoma surgeries (trabeculectomies, drainage surgeries, canaloplasty, sclerectomy, and angle surgeries). Cornea surgeries (DALK, DSEK/DSAEK, DMEK). Cataract extraction surgeries. Retinal surgeries (ERM peeling, macular hole repair, gene therapies).	Live imaging feedback during surgery. Valuable information on diagnosis and surgery planning. Confirmation of optimal outcome. Assessment of intraoperative complications.	Technician often required. Pausing of surgery sometimes necessary.
Swept source OCT (SS-OCT)	2012	Yes	8–9	20	200,000 (clinical). 6,700,000 (research).	Most retinal pathologies.	Increased SNR. Improved scan quality. Improved imaging of deeper structures.	
Whole-eye OCT	2012	Yes	12.4–19	73	50,000–580,000 (clinical).	Biometry. Surgery planning (cataract extraction and refractive surgeries). Identification of high myopia causality.	Assessment of the entire ocular anatomy with a single scan in standard fields of view.	Time gap for switching scan configurations between anterior-posterior segment
OCT angiography (OCT-A)	2015	Yes	5	15–24 8–16 (ultra high-definition)	200,000 (clinical).	Conditions involving vasculature damage or neovascularization (glaucoma, AMD, DR, BRVO).	Lack of extrinsic dye. Vascular network imaging at different depths. Vascular biomarker identification.	No detection of vessel leakage. Imaging artifacts (projection and motion). Visibility of vessels dependent on flow. Low image contrast. Limited area of visualization.

in image quality. Combining OCT-A, as well as other OCT variations, with SLO (OCT-SLO) allows for the implementation of motion tracking to compensate for involuntary eye movements during imaging (474–477). Commercially available systems that already currently use integrated OCT-SLO technology include the Zeiss PLEX Elite, Heidelberg Spectralis, and Optos Silverstone. Handheld OCT-SLO devices have also been implemented and have expanded the accessibility of multimodal imaging for pediatric, bedridden, and immobilized patients (143, 144). Additionally, OCT-A devices can be combined with vis-OCT to establish a complementary endogenous contrast, which allows for blood oxygen saturation to be quantified and used as a biomarker for DR and AMD (96, 102, 105, 106, 478–482).

While no clinical system is commercially available, photoacoustic microscopy (PAM) is an imaging modality that can be used in ophthalmology to detect the distribution of emitted acoustic waves in vascular tissue, with the ability to map blood absorption without the use of exogenous contrast. Combining PAM with OCT imaging establishes complementary structural and vascular contrast, which has been used to capture neovascularization associated with DR and wet AMD in animal models (483–487). Nguyen et al. further demonstrated that the multimodal combination of PAM with OCT has utility in monitoring vascular and structural changes associated with vascular occlusion (488, 489). PAM has additionally been combined with Doppler OCT to measure retinal oxygen metabolism with the potential to aid in an earlier diagnosis of DR, AMD, and glaucoma (478, 490).

Other experimental imaging techniques that have begun to make headway in multimodal research include polarization-sensitive OCT, photothermal OCT, and optical coherence elastography, which, when combined with more standard techniques, have been shown to allow for the differentiation between depolarizing and birefringent tissue (491, 492), establishment of molecular contrast (493–496), and biomechanical assessment of tissue, respectively (497, 498).

CONCLUSION

The field of ocular imaging is rapidly advancing. The sheer number of imaging modalities that exist nowadays

provides physicians and researchers with a substantially high number to study eye conditions and gather information. This variety of available technologies (**Figure 9**) provides a multimodal approach to eye imaging, which will inevitably lead to optimization of imaging techniques for each condition individually.

Most innovations are centered around OCT, since it has become the gold standard of managing most retinal diseases; a summary of the OCT imaging modalities is displayed in **Table 1**. As hardware components and image processing improve, OCT is bound to be improved in multiple ways: faster and higher quality scanning, lower costs, and greater population coverage. These are applications that can be applied worldwide and elevate the standard, commercially available OCT scanner. Some of the new technologies described previously, such as AS-OCT, I-OCT, and HH-OCT, are beginning to be used more widely and are already making a significant impact on medical decisions. Others, like Vis-OCT, FF-OCT, and AO-OCT, that are still rapidly evolving, will undoubtedly be improved and optimized for routine clinical use.

The most exciting prospect of eye imaging is the incorporation of AI. AI is becoming more accessible and broadly studied, and ophthalmology provides the perfect foundation for its rapid evolution. As such, it is fairly safe to assume that ophthalmology will be among the first medical specialties to transition from a traditional, physician-only care approach to a collaboration between human and software decision-making. The ability to provide valuable data from simple images can help millions of people get eye care in the first place but also improve and optimize the way patients are managed and treated. There are still, though, issues to be considered before safely applying AI in the routine care; these range from mostly technical, namely, the issue of performing AI tasks in most imaging devices, to medical in order to ensure its efficacy and reliability, as well as ethical. Despite these hurdles, AI will be a huge step toward ultimately decreasing blindness and providing equal health care across the entire population.

In conclusion, the evolution of ocular imaging is truly fascinating. The next years will be critical in its evolution and will definitely contribute to the ultimate goals of minimizing blindness and ensuring optimal care for patients.

AUTHOR CONTRIBUTIONS

JS and PA contributed to conception and design of the study. JS, PA, and CM acquired the data and performed the analysis. PA and CM wrote the first draft of the manuscript. JS, PA, CM, and GW contributed to manuscript revision and approved the submitted version and took responsibility for the integrity of the data and the accuracy of the data analysis. All authors contributed to the article and approved the submitted version.

FUNDING

This study was supported by National Institutes of Health (Bethesda, MD, United States) R01-EY013178 (JS) and U01-EY033001 (JS). An unrestricted grant from Research to Prevent Blindness (New York, NY, United States) to the Department of Ophthalmology, NYU Langone Health, NYU Grossman School of Medicine, New York, NY, United States.

REFERENCES

1. Huang D, Swanson EA, Lin CP, Schuman JS, Stinson WG, Chang W, et al. Optical coherence tomography. *Science.* (1991) 254:1178–81. doi: 10.1126/science.1957169
2. Danielson BL, Boisrobert CY. Absolute optical ranging using low coherence interferometry. *Appl Opt.* (1991) 30:2975–9. doi: 10.1364/AO.30.002975
3. Qin J, An L. Optical coherence tomography for ophthalmology imaging. *Adv Exp Med Biol.* (2021) 3233:197–216. doi: 10.1007/978-981-15-7627-0_10
4. Fujimoto J, Swanson E. The development, commercialization, and impact of optical coherence tomography. *Invest Ophthalmol Vis Sci.* (2016) 57:Oct1–13. doi: 10.1167/iovs.16-19963
5. Geevarghese A, Wollstein G, Ishikawa H, Schuman JS. Optical coherence tomography and glaucoma. *Annu Rev Vis Sci.* (2021) 7:693–726. doi: 10.1146/annurev-vision-100419-111350
6. Leitgeb R, Hitzenberger C, Fercher A. Performance of fourier domain vs. time domain optical coherence tomography. *Opt Express.* (2003) 11:889–94. doi: 10.1364/OE.11.000889
7. Wojtkowski M, Leitgeb R, Kowalczyk A, Bajraszewski T, Fercher AF. In vivo human retinal imaging by Fourier domain optical coherence tomography. *J Biomed Opt.* (2002) 7:457–63. doi: 10.1117/1.1482379
8. Gabriele ML, Wollstein G, Ishikawa H, Xu J, Kim J, Kagemann L, et al. Three dimensional optical coherence tomography imaging: advantages and advances. *Prog Retin Eye Res.* (2010) 29:556–79. doi: 10.1016/j.preteyeres.2010.05.005
9. Jia Y, Tan O, Tokayer J, Potsaid B, Wang Y, Liu JJ, et al. Split-spectrum amplitude-decorrelation angiography with optical coherence tomography. *Opt Express.* (2012) 20:4710–25. doi: 10.1364/OE.20.004710
10. Freund KB, Gattoussi S, Leong BCS. Dense B-Scan optical coherence tomography angiography. *Am J Ophthalmol.* (2018) 190:78–88. doi: 10.1016/j.ajo.2018.03.029
11. Fang L, Li S, Nie Q, Izatt JA, Toth CA, Farsiu S, et al. Sparsity based denoising of spectral domain optical coherence tomography images. *Biomed Opt Express.* (2012) 3:927–42. doi: 10.1364/BOE.3.000927
12. Xu D, Huang Y, Kang JU. Volumetric (3D) compressive sensing spectral domain optical coherence tomography. *Biomed Opt Express.* (2014) 5:3921–34. doi: 10.1364/BOE.5.003921
13. Xu D, Vaswani N, Huang Y, Kang JU. Modified compressive sensing optical coherence tomography with noise reduction. *Opt Lett.* (2012) 37:4209–11. doi: 10.1364/OL.37.004209
14. Schwartz S, Liu C, Wong A, Clausi DA, Fieguth P, Bizheva K, et al. Energy-guided learning approach to compressive FD-OCT. *Opt Express.* (2013) 21:329–44. doi: 10.1364/OE.21.000329
15. Xu D, Huang Y, Kang JU. Compressive sensing with dispersion compensation on non-linear wavenumber sampled spectral domain optical coherence tomography. *Biomed Opt Express.* (2013) 4:1519–32. doi: 10.1364/BOE.4.001519
16. Xu D, Huang Y, Kang JU. Real-time compressive sensing spectral domain optical coherence tomography. *Opt Lett.* (2014) 39:76–9. doi: 10.1364/OL.39.000076
17. Xu D, Huang Y, Kang JU. Real-time dispersion-compensated image reconstruction for compressive sensing spectral domain optical coherence tomography. *J Opt Soc Am A Opt Image Sci Vis.* (2014) 31:2064–9. doi: 10.1364/JOSAA.31.002064
18. Yi L, Sun L. Full-depth compressive sensing spectral-domain optical coherence tomography based on a compressive dispersion encoding method. *Appl Opt.* (2018) 57:9316–21. doi: 10.1364/AO.57.009316

19. Yi L, Sun L, Zou M, Hou B. Dual-channel spectral domain optical coherence tomography based on a single spectrometer using compressive sensing. *Sensors (Basel).* (2019) 19:4006. doi: 10.3390/s19184006
20. Yi L, Guo X, Sun L, Hou B. Structural and functional sensing of biotissues based on compressive sensing spectral domain optical coherence tomography. *Sensors (Basel).* (2019) 19:4208. doi: 10.3390/s19194208
21. Tan B, Wong A, Bizheva K. Enhancement of morphological and vascular features in OCT images using a modified Bayesian residual transform. *Biomed Opt Express.* (2018) 9:2394–406. doi: 10.1364/BOE.9.002394
22. Anegondi N, Kshirsagar A, Mochi TB, Sinha Roy A. Quantitative comparison of retinal vascular features in optical coherence tomography angiography images from three different devices. *Ophthalmic Surg Lasers Imaging Retina.* (2018) 49:488–96. doi: 10.3928/23258160-20180628-04
23. Mochi T, Anegondi N, Girish M, Jayadev C, Sinha Roy A. Quantitative comparison between optical coherence tomography angiography and fundus fluorescein angiography images: effect of vessel enhancement. *Ophthalmic Surg Lasers Imaging Retina.* (2018) 49:e175–81. doi: 10.3928/23258160-20181101-15
24. Taibouni K, Chenoune Y, Miere A, Colantuono D, Souied E, Petit E, et al. Automated quantification of choroidal neovascularization on Optical Coherence Tomography Angiography images. *Comput Biol Med.* (2019) 114:103450. doi: 10.1016/j.compbiomed.2019.103450
25. Chua J, Tan B, Ang M, Nongpiur ME, Tan AC, Najjar RP, et al. Future clinical applicability of optical coherence tomography angiography. *Clin Exp Optom.* (2019) 102:260–9. doi: 10.1111/cxo.12854
26. Anvari P, Ashrafkhorasani M, Habibi A, Falavarjani KG. Artifacts in optical coherence tomography angiography. *J Ophthalmic Vis Res.* (2021) 16:271–86. doi: 10.18502/jovr.v16i2.9091
27. Tan B, Sim R, Chua J, Wong DWK, Yao X, Garhofer G, et al. Approaches to quantify optical coherence tomography angiography metrics. *Ann Transl Med.* (2020) 8:1205. doi: 10.21037/atm-20-3246
28. Ghassemi F, Berijani S, Babeli A, Faghihi H, Gholizadeh A, Sabour S, et al. The quantitative measurements of choroidal thickness and volume in diabetic retinopathy using optical coherence tomography and optical coherence tomography angiography; correlation with vision and foveal avascular zone. *BMC Ophthalmol.* (2022) 22:3. doi: 10.1186/s12886-021-02178-w
29. Xu B, Chen J, Zhang S, Shen S, Lan X, Chen Z, et al. Association between the severity of diabetic retinopathy and optical coherence tomography angiography metrics. *Front Endocrinol (Lausanne).* (2021) 12:777552. doi: 10.3389/fendo.2021.777552
30. Kalra G, Zarranz-Ventura J, Chahal R, Bernal-Morales C, Lupidi M, Chhablani J, et al. Optical coherence tomography (OCT) angiolytics: a review of OCT angiography quantitative biomarkers. *Surv Ophthalmol.* (2021) 67:1118–34. doi: 10.1016/j.survophthal.2021.11.002
31. Hsu CR, Lai TT, Hsieh YT, Ho TC, Yang CM, Yang CH, et al. Combined quantitative and qualitative optical coherence tomography angiography biomarkers for predicting active neovascular age-related macular degeneration. *Sci Rep.* (2021) 11:18068. doi: 10.1038/s41598-021-97652-2
32. Arrigo A, Perra C, Aragona E, Giusto D, Bandello F, Battaglia Parodi M, et al. Total flow intensity, active flow intensity and volume related flow intensity as new quantitative metrics in optical coherence tomography angiography. *Sci Rep.* (2021) 11:9094. doi: 10.1038/s41598-021-88681-y
33. Wang W, Lo ACY. Diabetic retinopathy: pathophysiology and treatments. *Int J Mol Sci.* (2018) 19:1816. doi: 10.3390/ijms19061816
34. Heng LZ, Comyn O, Peto T, Tadros C, Ng E, Sivaprasad S, et al. Diabetic retinopathy: pathogenesis, clinical grading, management and future developments. *Diabet Med.* (2013) 30:640–50. doi: 10.1111/dme.12089
35. Mohamed Q, Gillies MC, Wong TY. Management of diabetic retinopathy: a systematic review. *JAMA.* (2007) 298:902–16. doi: 10.1001/jama.298.8.902
36. Scarinci F, Nesper PL, Fawzi AA. Deep retinal capillary nonperfusion is associated with photoreceptor disruption in diabetic macular ischemia. *Am J Ophthalmol.* (2016) 168:129–38. doi: 10.1016/j.ajo.2016.05.002
37. Moore J, Bagley S, Ireland G, McLeod D, Boulton ME. Three dimensional analysis of microaneurysms in the human diabetic retina. *J Anat.* (1999) 194(Pt 1):89–100. doi: 10.1046/j.1469-7580.1999.19410089.x
38. Hasegawa N, Nozaki M, Takase N, Yoshida M, Ogura Y. New insights into microaneurysms in the deep capillary plexus detected by optical coherence tomography angiography in diabetic macular edema. *Invest Ophthalmol Vis Sci.* (2016) 57:OCT348–55. doi: 10.1167/iovs.15-18782
39. Carnevali A, Sacconi R, Corbelli E, Tomasso L, Querques L, Zerbini G, et al. Optical coherence tomography angiography analysis of retinal vascular plexuses and choriocapillaris in patients with type 1 diabetes without diabetic retinopathy. *Acta Diabetol.* (2017) 54:695–702. doi: 10.1007/s00592-017-0996-8
40. Onishi AC, Nesper PL, Roberts PK, Moharram GA, Chai H, Liu L, et al. Importance of considering the middle capillary plexus on OCT angiography in diabetic retinopathy. *Invest Ophthalmol Vis Sci.* (2018) 59:2167–76. doi: 10.1167/iovs.17-23304
41. Parravano M, De Geronimo D, Scarinci F, Querques L, Virgili G, Simonett JM, et al. Diabetic microaneurysms internal reflectivity on spectral-domain optical coherence tomography and optical coherence tomography angiography detection. *Am J Ophthalmol.* (2017) 179:90–6. doi: 10.1016/j.ajo.2017.04.021
42. Schreur V, Domanian A, Liefers B, Venhuizen FG, Klevering BJ, Hoyng CB, et al. Morphological and topographical appearance of microaneurysms on optical coherence tomography angiography. *Br J Ophthalmol.* (2018):bjohthalmol–2018–312258. [Online ahead of print], doi: 10.1136/bjophthalmol-2018-312258
43. Ishibazawa A, Nagaoka T, Yokota H, Takahashi A, Omae T, Song YS, et al. Characteristics of retinal neovascularization in proliferative diabetic retinopathy imaged by optical coherence tomography angiography. *Invest Ophthalmol Vis Sci.* (2016) 57:6247–55. doi: 10.1167/iovs.16-20210
44. Savastano MC, Federici M, Falsini B, Caporossi A, Minnella AM. Detecting papillary neovascularization in proliferative diabetic retinopathy using optical coherence tomography angiography. *Acta Ophthalmol.* (2018) 96:321–3. doi: 10.1111/aos.13166
45. Palma F, Camacho P. The role of optical coherence tomography angiography to detect early microvascular changes in diabetic retinopathy: a systematic review. *J Diabetes Metab Disord.* (2021) 20:1957–74. doi: 10.1007/s40200-021-00886-0
46. Ong JX, Fawzi AA. Perspectives on diabetic retinopathy from advanced retinal vascular imaging. *Eye (Lond).* (2022) 36:319–27. doi: 10.1038/s41433-021-01825-2
47. Russell JF, Han IC. Toward a new staging system for diabetic retinopathy using wide field swept-source optical coherence tomography angiography. *Curr Diab Rep.* (2021) 21:28. doi: 10.1007/s11892-021-01401-8
48. Cicinelli MV, Rabiolo A, Marchese A, de Vitis L, Carnevali A, Querques L, et al. Choroid morphometric analysis in non-neovascular age-related macular degeneration by means of optical coherence tomography angiography. *Br J Ophthalmol.* (2017) 101:1193–200. doi: 10.1136/bjophthalmol-2016-309481
49. Nesper PL, Soetikno BT, Fawzi AA. Choriocapillaris nonperfusion is associated with poor visual acuity in eyes with reticular pseudodrusen. *Am J Ophthalmol.* (2017) 174:42–55. doi: 10.1016/j.ajo.2016.10.005
50. Choi W, Moult EM, Waheed NK, Adhi M, Lee B, Lu CD, et al. Ultrahigh-speed, swept-source optical coherence tomography angiography in nonexudative age-related macular degeneration with geographic atrophy. *Ophthalmology.* (2015) 122:2532–44. doi: 10.1016/j.ophtha.2015.08.029
51. Sacconi R, Corbelli E, Carnevali A, Querques L, Bandello F, Querques G, et al. Optical coherence tomography angiography in geographic atrophy. *Retina.* (2018) 38:2350–5. doi: 10.1097/IAE.0000000000001873
52. Corbelli E, Sacconi R, Rabiolo A, Mercuri S, Carnevali A, Querques L, et al. Optical coherence tomography angiography in the evaluation of geographic atrophy area extension. *Invest Ophthalmol Vis Sci.* (2017) 58:5201–8. doi: 10.1167/iovs.17-22508
53. Jiang X, Shen M, Wang L, de Sisternes L, Durbin MK, Feuer W, et al. Validation of a novel automated algorithm to measure drusen volume and area using swept source optical coherence tomography angiography. *Transl Vis Sci Technol.* (2021) 10:11. doi: 10.1167/tvst.10.4.11
54. Kuehlewein L, Bansal M, Lenis TL, Iafe NA, Sadda SR, Bonini Filho MA, et al. Optical coherence tomography angiography of Type 1 neovascularization in age-related macular degeneration. *Am J Ophthalmol.* (2015) 160:739–48.e2. doi: 10.1016/j.ajo.2015.06.030
55. Kuehlewein L, Dansingani KK, de Carlo TE, Bonini Filho MA, Iafe NA, Lenis TL, et al. Optical coherence tomography angiography of Type 3

neovascularization secondary to age-related macular degeneration. *Retina.* (2015) 35:2229–35. doi: 10.1097/IAE.0000000000000835
56. Costanzo E, Miere A, Querques G, Capuano V, Jung C, Souied EH, et al. Type 1 choroidal neovascularization lesion size: indocyanine green angiography versus optical coherence tomography angiography. *Invest Ophthalmol Vis Sci.* (2016) 57:OCT307–13. doi: 10.1167/iovs.15-18830
57. Farecki ML, Gutfleisch M, Faatz H, Rothaus K, Heimes B, Spital G, et al. Characteristics of type 1 and 2 CNV in exudative AMD in OCT-Angiography. *Graefes Arch Clin Exp Ophthalmol.* (2017) 255:913–21. doi: 10.1007/s00417-017-3588-y
58. Phasukkijwatana N, Tan ACS, Chen X, Freund KB, Sarraf D. Optical coherence tomography angiography of type 3 neovascularisation in age-related macular degeneration after antiangiogenic therapy. *Br J Ophthalmol.* (2017) 101:597–602. doi: 10.1136/bjophthalmol-2016-308815
59. Schneider EW, Fowler SC. Optical coherence tomography angiography in the management of age-related macular degeneration. *Curr Opin Ophthalmol.* (2018) 29:217–25. doi: 10.1097/ICU.0000000000000469
60. Faridi A, Jia Y, Gao SS, Huang D, Bhavsar KV, Wilson DJ, et al. Sensitivity and specificity of OCT angiography to detect choroidal neovascularization. *Ophthalmol Retina.* (2017) 1:294–303. doi: 10.1016/j.oret.2017.02.007
61. Jia Y, Bailey ST, Wilson DJ, Tan O, Klein ML, Flaxel CJ, et al. Quantitative optical coherence tomography angiography of choroidal neovascularization in age-related macular degeneration. *Ophthalmology.* (2014) 121:1435–44. doi: 10.1016/j.ophtha.2014.01.034
62. Miere A, Querques G, Semoun O, Amoroso F, Zambrowski O, Chapron T, et al. Optical coherence tomography angiography changes in early Type 3 neovascularization after anti-vascular endothelial growth factor treatment. *Retina.* (2017) 37:1873–9. doi: 10.1097/IAE.0000000000001447
63. Miere A, Querques G, Semoun O, El Ameen A, Capuano V, Souied EH, et al. Optical coherence tomography angiography in early Type 3 neovascularization. *Retina.* (2015) 35:2236–41. doi: 10.1097/IAE.0000000000000834
64. Roisman L, Zhang Q, Wang RK, Gregori G, Zhang A, Chen CL, et al. Optical coherence tomography angiography of asymptomatic neovascularization in intermediate age-related macular degeneration. *Ophthalmology.* (2016) 123:1309–19. doi: 10.1016/j.ophtha.2016.01.044
65. Cherecheanu AP, Garhofer G, Schmidl D, Werkmeister R, Schmetterer L. Ocular perfusion pressure and ocular blood flow in glaucoma. *Curr Opin Pharmacol.* (2013) 13:36–42. doi: 10.1016/j.coph.2012.09.003
66. Nakazawa T. Ocular blood flow and influencing factors for glaucoma. *Asia Pac J Ophthalmol (Phila).* (2016) 5:38–44. doi: 10.1097/APO.0000000000000183
67. Geyman LS, Garg RA, Suwan Y, Trivedi V, Krawitz BD, Mo S, et al. Peripapillary perfused capillary density in primary open-angle glaucoma across disease stage: an optical coherence tomography angiography study. *Br J Ophthalmol.* (2017) 101:1261–8. doi: 10.1136/bjophthalmol-2016-309642
68. Chihara E, Dimitrova G, Amano H, Chihara T. Discriminatory power of superficial vessel density and prelaminar vascular flow index in eyes with glaucoma and ocular hypertension and normal eyes. *Invest Ophthalmol Vis Sci.* (2017) 58:690–7. doi: 10.1167/iovs.16-20709
69. Triolo G, Rabiolo A, Shemonski ND, Fard A, Di Matteo F, Sacconi R, et al. Optical coherence tomography angiography macular and peripapillary vessel perfusion density in healthy subjects, glaucoma suspects, and glaucoma patients. *Invest Ophthalmol Vis Sci.* (2017) 58:5713–22. doi: 10.1167/iovs.17-22865
70. Shoji T, Zangwill LM, Akagi T, Saunders LJ, Yarmohammadi A, Manalastas PIC, et al. Progressive macula vessel density loss in primary open-angle glaucoma: a longitudinal study. *Am J Ophthalmol.* (2017) 182:107–17. doi: 10.1016/j.ajo.2017.07.011
71. Wang X, Jiang C, Ko T, Kong X, Yu X, Min W, et al. Correlation between optic disc perfusion and glaucomatous severity in patients with open-angle glaucoma: an optical coherence tomography angiography study. *Graefes Arch Clin Exp Ophthalmol.* (2015) 253:1557–64. doi: 10.1007/s00417-015-3095-y
72. Rao HL, Pradhan ZS, Weinreb RN, Reddy HB, Riyazuddin M, Dasari S, et al. Regional comparisons of optical coherence tomography angiography vessel density in primary open-angle glaucoma. *Am J Ophthalmol.* (2016) 171:75–83. doi: 10.1016/j.ajo.2016.08.030
73. Nishida T, Moghimi S, Hou H, Proudfoot JA, Chang AC, David RCC, et al. Long-term reproducibility of optical coherence tomography angiography in healthy and stable glaucomatous eyes. *Br J Ophthalmol.* (2021):bjohthalmol–2021–320034. [Online ahead of print], doi: 10.1136/bjophthalmol-2021-320034
74. Lee JY, Shin JW, Song MK, Hong JW, Kook MS. Baseline vessel density parameters for predicting visual field progression in open-angle glaucoma eyes with central visual field damage. *Am J Ophthalmol.* (2021) 237:241–58. doi: 10.1016/j.ajo.2021.11.028
75. Shin JD, Wolf AT, Harris A, Verticchio Vercellin A, Siesky B, Rowe LW, et al. Vascular biomarkers from optical coherence tomography angiography and glaucoma: where do we stand in 2021? *Acta Ophthalmol.* (2022) 100:e377–85. doi: 10.1111/aos.14982
76. Zhu Q, Chen C, Yao J. Vessel density and retinal thickness from optical coherence tomography angiography as new indexes in adolescent myopia. *J Ophthalmol.* (2021) 2021:6069833. doi: 10.1155/2021/6069833
77. Kawai K, Murakami T, Sakaguchi S, Yamada T, Kadomoto S, Uji A, et al. Peripheral chorioretinal imaging through a front prism on optical coherence tomography angiography. *Transl Vis Sci Technol.* (2021) 10:36. doi: 10.1167/tvst.10.14.36
78. Kawai K, Uji A, Miyazawa T, Yamada T, Amano Y, Miyagi S, et al. Prevention of image quality degradation in wider field optical coherence tomography angiography images via image averaging. *Transl Vis Sci Technol.* (2021) 10:16. doi: 10.1167/tvst.10.13.16
79. Miao Y, Siadati M, Song J, Ma D, Jian Y, Beg MF, et al. Phase-corrected buffer averaging for enhanced OCT angiography using FDML laser. *Opt Lett.* (2021) 46:3833–6. doi: 10.1364/OL.430915
80. Nesper PL, Fawzi AA. New method for reducing artifactual flow deficits caused by compensation techniques in the choriocapillaris with optical coherence tomography angiography. *Retina.* (2022) 42:328–35. doi: 10.1097/IAE.0000000000003313
81. Wei W, Cogliati A, Canavesi C. Model-based optical coherence tomography angiography enables motion-insensitive vascular imaging. *Biomed Opt Express.* (2021) 12:2149–70. doi: 10.1364/BOE.420091
82. Zhang Q, Zhang A, Lee CS, Lee AY, Rezaei KA, Roisman L, et al. Projection artifact removal improves visualization and quantitation of macular neovascularization imaged by optical coherence tomography angiography. *Ophthalmol Retina.* (2017) 1:124–36. doi: 10.1016/j.oret.2016.08.005
83. Mehta N, Cheng Y, Alibhai AY, Duker JS, Wang RK, Waheed NK, et al. Optical coherence tomography angiography distortion correction in widefield montage images. *Quant Imaging Med Surg.* (2021) 11:928–38. doi: 10.21037/qims-20-791
84. Cheng Y, Chu Z, Wang RK. Robust three-dimensional registration on optical coherence tomography angiography for speckle reduction and visualization. *Quant Imaging Med Surg.* (2021) 11:879–94. doi: 10.21037/qims-20-751
85. Ploner SB, Kraus MF, Moult EM, Husvogt L, Schottenhamml J, Yasin Alibhai A, et al. Efficient and high accuracy 3-D OCT angiography motion correction in pathology. *Biomed Opt Express.* (2021) 12:125–46. doi: 10.1364/BOE.411117
86. Husvogt L, Ploner SB, Chen S, Stromer D, Schottenhamml J, Alibhai AY, et al. Maximum a posteriori signal recovery for optical coherence tomography angiography image generation and denoising. *Biomed Opt Express.* (2021) 12:55–68. doi: 10.1364/BOE.408903
87. Viekash VK, Jothi Balaji J, Lakshminarayanan V. FAZSeg: a new software for quantification of the foveal avascular zone. *Clin Ophthalmol.* (2021) 15:4817–27. doi: 10.2147/OPTH.S346145
88. Untracht GR, Matos RS, Dikaios N, Bapir M, Durrani AK, Butsabong T, et al. OCTAVA: an open-source toolbox for quantitative analysis of optical coherence tomography angiography images. *PLoS One.* (2021) 16:e0261052. doi: 10.1371/journal.pone.0261052
89. Zhang Y, Li H, Cao T, Chen R, Qiu H, Gu Y, et al. Automatic 3D adaptive vessel segmentation based on linear relationship between intensity and complex-decorrelation in optical coherence tomography angiography. *Quant Imaging Med Surg.* (2021) 11:895–906. doi: 10.21037/qims-20-868
90. Miguel A, Legeai J, Silva B. A software for quantification of vessel density in glaucoma: an OCT-angiography study. *J Fr Ophtalmol.* (2021) 44:376–81. doi: 10.1016/j.jfo.2020.06.038

91. Považay B, Apolonskiy A, Unterhuber A, Hermann B, Bizheva K, Sattmann H, et al. Visible light optical coherence tomography. *Proc SPIE.* (2002) 4619:90–4. doi: 10.1117/12.470466
92. Xu J, Song S, Wei W, Wang RK. Wide field and highly sensitive angiography based on optical coherence tomography with akinetic swept source. *Biomed Opt Express.* (2017) 8:420–35. doi: 10.1364/BOE.8.000420
93. Kolb JP, Klein T, Eibl M. *Megahertz FDML Laser with Up to 143nm Sweep Range for Ultrahigh Resolution OCT at 1050nm*. Bellingham, DC: SPIE (2016). doi: 10.1117/12.2214758
94. You Y-J, Wang C, Lin Y-L. Ultrahigh-resolution optical coherence tomography at 1.3μm central wavelength by using a supercontinuum source pumped by noise-like pulses. *Laser Phys Lett.* (2015) 13:025101. doi: 10.1088/1612-2011/13/2/025101
95. Werkmeister RM, Sapeta S, Schmidl D, Garhofer G, Schmidinger G, Aranha Dos Santos V, et al. Ultrahigh-resolution OCT imaging of the human cornea. *Biomed Opt Express.* (2017) 8:1221–39. doi: 10.1364/BOE.8.001221
96. Chong SP, Bernucci M, Radhakrishnan H, Srinivasan VJ. Structural and functional human retinal imaging with a fiber-based visible light OCT ophthalmoscope. *Biomed Opt Express.* (2017) 8:323–37. doi: 10.1364/BOE.8.000323
97. Shu X, Beckmann L, Zhang H. Visible-light optical coherence tomography: a review. *J Biomed Opt.* (2017) 22:1–14. doi: 10.1117/1.JBO.22.12.121707
98. Chong SP, Merkle CW, Leahy C, Srinivasan VJ. Cerebral metabolic rate of oxygen (CMRO2) assessed by combined Doppler and spectroscopic OCT. *Biomed Opt Express.* (2015) 6:3941–51. doi: 10.1364/BOE.6.003941
99. Yi J, Wei Q, Liu W, Backman V, Zhang HF. Visible-light optical coherence tomography for retinal oximetry. *Opt Lett.* (2013) 38:1796–8. doi: 10.1364/OL.38.001796
100. Yi J, Liu W, Chen S, Backman V, Sheibani N, Sorenson CM, et al. Visible light optical coherence tomography measures retinal oxygen metabolic response to systemic oxygenation. *Light Sci Appl.* (2015) 4:e334. doi: 10.1038/lsa.2015.107
101. Werkmeister RM, Schmidl D, Aschinger G, Doblhoff-Dier V, Palkovits S, Wirth M, et al. Retinal oxygen extraction in humans. *Sci Rep.* (2015) 5:15763. doi: 10.1038/srep15763
102. Chen S, Yi J, Zhang HF. Measuring oxygen saturation in retinal and choroidal circulations in rats using visible light optical coherence tomography angiography. *Biomed Opt Express.* (2015) 6:2840–53. doi: 10.1364/BOE.6.002840
103. Soetikno BT, Yi J, Shah R, Liu W, Purta P, Zhang HF, et al. Inner retinal oxygen metabolism in the 50/10 oxygen-induced retinopathy model. *Sci Rep.* (2015) 5:16752. doi: 10.1038/srep16752
104. Liu W, Wang S, Soetikno B, Yi J, Zhang K, Chen S, et al. Increased retinal oxygen metabolism precedes microvascular alterations in Type 1 diabetic mice. *Invest Ophthalmol Vis Sci.* (2017) 58:981–9. doi: 10.1167/iovs.16-20600
105. Nesper PL, Soetikno BT, Zhang HF, Fawzi AA. OCT angiography and visible-light OCT in diabetic retinopathy. *Vision Res.* (2017) 139:191–203. doi: 10.1016/j.visres.2017.05.006
106. Yi J, Chen S, Shu X, Fawzi AA, Zhang HF. Human retinal imaging using visible-light optical coherence tomography guided by scanning laser ophthalmoscopy. *Biomed Opt Express.* (2015) 6:3701–13. doi: 10.1364/BOE.6.003701
107. Shu X, Beckmann L, Wang Y, Rubinoff I, Lucy K, Ishikawa H, et al. Designing visible-light optical coherence tomography towards clinics. *Quant Imaging Med Surg.* (2019) 9:769–81. doi: 10.21037/qims.2019.05.01
108. Grannonico M, Miller DA, Liu M, Norat P, Deppmann CD, Netland PA, et al. Global and regional damages in retinal ganglion cell axon bundles monitored non-invasively by visible-light optical coherence tomography fibergraphy. *J Neurosci.* (2021) 41:10179–93. doi: 10.1523/JNEUROSCI.0844-21.2021
109. Miller DA, Grannonico M, Liu M, Kuranov RV, Netland PA, Liu X, et al. Visible-light optical coherence tomography fibergraphy for quantitative imaging of retinal ganglion cell axon bundles. *Transl Vis Sci Technol.* (2020) 9:11. doi: 10.1167/tvst.9.11.11
110. Pi S, Hormel TT, Wei X, Cepurna W, Morrison JC, Jia Y, et al. Imaging retinal structures at cellular-level resolution by visible-light optical coherence tomography. *Opt Lett.* (2020) 45:2107–10. doi: 10.1364/OL.386454
111. Zhang T, Kho AM, Srinivasan VJ. In vivo Morphometry of Inner Plexiform Layer (IPL) stratification in the human retina with visible light optical coherence tomography. *Front Cell Neurosci.* (2021) 15:655096. doi: 10.3389/fncel.2021.655096
112. Zhang T, Kho AM, Srinivasan VJ. Improving visible light OCT of the human retina with rapid spectral shaping and axial tracking. *Biomed Opt Express.* (2019) 10:2918–31. doi: 10.1364/BOE.10.002918
113. Ghassabi Z, Kuranov RV, Schuman JS, Zambrano R, Wu M, Liu M, et al. In vivo sublayer analysis of human retinal inner plexiform layer obtained by visible-light optical coherence tomography. *Invest Ophthalmol Vis Sci.* (2022) 63:18. doi: 10.1167/iovs.63.1.18
114. Zhang X, Beckmann L, Miller DA, Shao G, Cai Z, Sun C, et al. In Vivo imaging of Schlemm's canal and limbal vascular network in mouse using visible-light OCT. *Invest Ophthalmol Vis Sci.* (2020) 61:23. doi: 10.1167/iovs.61.2.23
115. Wang J, Baker A, Subramanian ML, Siegel NH, Chen X, Ness S, et al. Simultaneous visible light optical coherence tomography and near infrared OCT angiography in retinal pathologies: a case study. *Exp Biol Med (Maywood).* (2022) 247:377–84. doi: 10.1177/15353702211063839
116. Song W, Zhou L, Zhang S. Fiber-based visible and near infrared optical coherence tomography (vnOCT) enables quantitative elastic light scattering spectroscopy in human retina. *Biomed Opt Express.* (2018) 9:3464–80. doi: 10.1364/BOE.9.003464
117. Song W, Zhang S, Sadlak N. Visible and near-infrared optical coherence tomography (vnOCT) in glaucoma suspect, pre-perimetric, and perimetric glaucoma. *Invest Ophthalmol Vis Sci.* (2020) 61:2559–2559. doi: 10.1117/12.2578925
118. Song W, Shao W, Yi W, Liu R, Desai M, Ness S, et al. Visible light optical coherence tomography angiography (vis-OCTA) facilitates local microvascular oximetry in the human retina. *Biomed Opt Express.* (2020) 11:4037–51. doi: 10.1364/BOE.395843
119. Chen X, Tai V, McGeehan B, Ying GS, Viehland C, Imperio R, et al. Repeatability and reproducibility of axial and lateral measurements on handheld optical coherence tomography systems compared with tabletop system. *Transl Vis Sci Technol.* (2020) 9:25. doi: 10.1167/tvst.9.11.25
120. Scoville NM, Legocki AT, Touch P, Ding L, Moshiri Y, Bays-Muchmore C, et al. Vitreous opacities in infants born full-term and preterm by handheld swept-source optical coherence tomography. *J Am Assoc Pediatr Ophthalmol Strabismus.* (2022) 26:20.e1–7. doi: 10.1016/j.jaapos.2021.09.007
121. Patel PR, Imperio R, Viehland C, Tran-Viet D, Chiu SJ, Tai V, et al. Depth-resolved visualization of perifoveal retinal vasculature in preterm infants using handheld optical coherence tomography angiography. *Transl Vis Sci Technol.* (2021) 10:10. doi: 10.1167/tvst.10.9.10
122. Abdeen W, Esmael AF, Gawdat G, El-Fayoumi D. Anterior chamber angle features in primary congenital glaucoma infants using hand-held anterior segment-oct. *Eye (Lond).* (2021) 36:1238–45. doi: 10.1038/s41433-021-01583-1
123. Legocki AT, Moshiri Y, Zepeda EM, Gillette TB, Shariff A, Grant LE, et al. Dome-shaped macula in premature infants visualized by handheld spectral-domain optical coherence tomography. *J AAPOS.* (2021) 25:153.e1–6. doi: 10.1016/j.jaapos.2020.12.007
124. Edawaji BSA, Gottlob I, Proudlock FA. Anterior chamber measurements in healthy children: a cross-sectional study using optical coherence tomography. *Transl Vis Sci Technol.* (2021) 10:13. doi: 10.1167/tvst.10.6.13
125. Shah SD, Haq A, Toufeeq S, Tu Z, Edawaji B, Abbott J, et al. Reliability and recommended settings for pediatric circumpapillary retinal nerve fiber layer imaging using hand-held optical coherence tomography. *Transl Vis Sci Technol.* (2020) 9:43. doi: 10.1167/tvst.9.7.43
126. Nadiarnykh O, McNeill-Badalova NA, Gaillard MC, Bosscha MI, Fabius AWM, Verbraak FD, et al. Optical coherence tomography (OCT) to image active and inactive retinoblastomas as well as retinomas. *Acta Ophthalmol.* (2020) 98:158–65. doi: 10.1111/aos.14214
127. Lim ME, Jiramongkolchai K, Xu L, Freedman SF, Tai V, Toth CA, et al. Handheld optical coherence tomography normative inner retinal layer measurements for children <5 years of age. *Am J Ophthalmol.* (2019) 207:232–9. doi: 10.1016/j.ajo.2019.06.015
128. Pilat AV, Proudlock FA, Shah S, Sheth V, Purohit R, Abbot J, et al. Assessment of the anterior segment of patients with primary congenital glaucoma using handheld optical coherence tomography. *Eye (Lond).* (2019) 33:1232–9. doi: 10.1038/s41433-019-0369-3

129. Pilat AV, Shah S, Sheth V, Purohit R, Proudlock FA, Abbott J, et al. Detection and characterisation of optic nerve and retinal changes in primary congenital glaucoma using hand-held optical coherence tomography. *BMJ Open Ophthalmol.* (2019) 4:e000194. doi: 10.1136/bmjophth-2018-000194
130. Zepeda EM, Shariff A, Gillette TB, Grant L, Ding L, Tarczy-Hornoch K, et al. Vitreous bands identified by handheld spectral-domain optical coherence tomography among premature infants. *JAMA Ophthalmol.* (2018) 136:753–8. doi: 10.1001/jamaophthalmol.2018.1509
131. Ling KP, Mangalesh S, Tran-Viet D, Gunther R, Toth CA, Vajzovic L, et al. Handheld spectral domain optical coherence tomography findings of x-linked retinoschisis in early childhood. *Retina.* (2020) 40:1996–2003. doi: 10.1097/IAE.0000000000002688
132. Anwar S, Nath M, Patel A, Lee H, Brown S, Gottlob I, et al. Potential utility of foveal morphology in preterm infants measured using hand-held optical coherence tomography in retinopathy of prematurity screening. *Retina.* (2020) 40:1592–602. doi: 10.1097/IAE.0000000000002622
133. Chen X, Prakalapakorn SG, Freedman SF, Vajzovic L, Toth CA. Differentiating retinal detachment and retinoschisis using handheld optical coherence tomography in stage 4 retinopathy of prematurity. *JAMA Ophthalmol.* (2020) 138:81–5. doi: 10.1001/jamaophthalmol.2019.4796
134. Padhi TR, Anderson BJ, Abbey AM, Yonekawa Y, Stem M, Alam D, et al. Choroidal neovascular membrane in paediatric patients: clinical characteristics and outcomes. *Br J Ophthalmol.* (2018) 102:1232–7. doi: 10.1136/bjophthalmol-2017-310497
135. Agarwal K, Vinekar A, Chandra P, Padhi TR, Nayak S, Jayanna S, et al. Imaging the pediatric retina: an overview. *Indian J Ophthalmol.* (2021) 69:812–23. doi: 10.4103/ijo.IJO_1917_20
136. Moshiri Y, Legocki AT, Zhou K, Cabrera MT, Rezaei KA, Tarczy-Hornoch K, et al. Handheld swept-source optical coherence tomography with angiography in awake premature neonates. *Quant Imaging Med Surg.* (2019) 9:1495–502. doi: 10.21037/qims.2019.09.01
137. Shen LL, Mangalesh S, Michalak SM, McGeehan B, Sarin N, Finkle J, et al. Associations between systemic health and retinal nerve fibre layer thickness in preterm infants at 36 weeks postmenstrual age. *Br J Ophthalmol.* (2021):bjohthalmol–2021–319254. [Online ahead of print], doi: 10.1136/bjophthalmol-2021-319254
138. Heidelberg. (2021). Available online at: https://business-lounge.heidelbergengineering.com/gb/en/products/spectralis/flex-module/ (accessed June 16, 2022).
139. Leica. (2021). Available online at: https://www.leica-microsystems.com/products/surgical-microscopes/p/envisu-c2300/ (accessed June 16, 2022).
140. Shelton RL, Jung W, Sayegh SI, McCormick DT, Kim J, Boppart SA, et al. Optical coherence tomography for advanced screening in the primary care office. *J Biophotonics.* (2014) 7:525–33. doi: 10.1002/jbio.201200243
141. Song G, Chu KK, Kim S, Crose M, Cox B, Jelly ET, et al. First clinical application of low-cost OCT. *Transl Vis Sci Technol.* (2019) 8:61. doi: 10.1167/tvst.8.3.61
142. Malone JD, El-Haddad MT, Yerramreddy SS, Oguz I, Tao YK. Handheld spectrally encoded coherence tomography and reflectometry for motion-corrected ophthalmic optical coherence tomography and optical coherence tomography angiography. *Neurophotonics.* (2019) 6:041102. doi: 10.1117/1.NPh.6.4.041102
143. Larocca F, Nankivil D, Farsiu S, Izatt JA. Handheld simultaneous scanning laser ophthalmoscopy and optical coherence tomography system. *Biomed Opt Express.* (2013) 4:2307–21. doi: 10.1364/BOE.4.002307
144. LaRocca F, Nankivil D, DuBose T, Toth CA, Farsiu S, Izatt JA, et al. In vivo cellular-resolution retinal imaging in infants and children using an ultracompact handheld probe. *Nat Photonics.* (2016) 10:580–4. doi: 10.1038/nphoton.2016.141
145. Jung W, Kim J, Jeon M, Chaney EJ, Stewart CN, Boppart SA, et al. Handheld optical coherence tomography scanner for primary care diagnostics. *IEEE Trans Biomed Eng.* (2011) 58:741–4. doi: 10.1109/TBME.2010.2096816
146. Viehland C, Chen X, Tran-Viet D, Jackson-Atogi M, Ortiz P, Waterman G, et al. Ergonomic handheld OCT angiography probe optimized for pediatric and supine imaging. *Biomed Opt Express.* (2019) 10:2623–38. doi: 10.1364/BOE.10.002623
147. Cho NH, Park K, Wijesinghe RE, Shin YS, Jung W, Kim J, et al. Development of real-time dual-display handheld and bench-top hybrid-mode SD-OCTs. *Sensors (Basel).* (2014) 14:2171–81. doi: 10.3390/s140202171
148. Song S, Zhou K, Xu JJ, Zhang Q, Lyu S, Wang R, et al. Development of a clinical prototype of a miniature hand-held optical coherence tomography probe for prematurity and pediatric ophthalmic imaging. *Biomed Opt Express.* (2019) 10:2383–98. doi: 10.1364/BOE.10.002383
149. Lu CD, Kraus MF, Potsaid B, Liu JJ, Choi W, Jayaraman V, et al. Handheld ultrahigh speed swept source optical coherence tomography instrument using a MEMS scanning mirror. *Biomed Opt Express.* (2013) 5:293–311. doi: 10.1364/BOE.5.000293
150. Nankivil D, Waterman G, LaRocca F, Keller B, Kuo AN, Izatt JA, et al. Handheld, rapidly switchable, anterior/posterior segment swept source optical coherence tomography probe. *Biomed Opt Express.* (2015) 6:4516–28. doi: 10.1364/BOE.6.004516
151. Ni S, Wei X, Ng R, Ostmo S, Chiang MF, Huang D, et al. High-speed and widefield handheld swept-source OCT angiography with a VCSEL light source. *Biomed Opt Express.* (2021) 12:3553–70. doi: 10.1364/BOE.425411
152. Ni S, Nguyen TP, Ng R, Khan S, Ostmo S, Jia Y, et al. 105 degrees field of view non-contact handheld swept-source optical coherence tomography. *Opt Lett.* (2021) 46:5878–81. doi: 10.1364/OL.443672
153. Muijzer MB, Schellekens P, Beckers HJM, de Boer JH, Imhof SM, Wisse RPL, et al. Clinical applications for intraoperative optical coherence tomography: a systematic review. *Eye (Lond).* (2021) 36:379–91. doi: 10.1038/s41433-021-01686-9
154. Ehlers JP, Dupps WJ, Kaiser PK, Goshe J, Singh RP, Petkovsek D, et al. The Prospective Intraoperative and Perioperative Ophthalmic ImagiNg with Optical CoherEncE TomogRaphy (PIONEER) Study: 2-year results. *Am J Ophthalmol.* (2014) 158:999–1007. doi: 10.1016/j.ajo.2014.07.034
155. Ehlers JP, Srivastava SK, Feiler D, Noonan AI, Rollins AM, Tao YK, et al. Integrative advances for OCT-guided ophthalmic surgery and intraoperative OCT: microscope integration, surgical instrumentation, and heads-up display surgeon feedback. *PLoS One.* (2014) 9:e105224. doi: 10.1371/journal.pone.0105224
156. Mura M, Iannetta D, Nasini F, Barca F, Peiretti E, Engelbrecht L, et al. Use of a new intra-ocular spectral domain optical coherence tomography in vitreoretinal surgery. *Acta Ophthalmol.* (2016) 94:246–52. doi: 10.1111/aos.12961
157. Ehlers JP, Modi YS, Pecen PE, Goshe J, Dupps WJ, Rachitskaya A, et al. The DISCOVER study 3-year results: feasibility and usefulness of microscope-integrated intraoperative OCT during ophthalmic surgery. *Ophthalmology.* (2018) 125:1014–27. doi: 10.1016/j.ophtha.2017.12.037
158. Falkner-Radler CI, Glittenberg C, Gabriel M, Binder S. Intrasurgical microscope-integrated spectral domain optical coherence tomography-assisted membrane peeling. *Retina.* (2015) 35:2100–6. doi: 10.1097/IAE.0000000000000596
159. Leisser C, Hirnschall N, Palkovits S, Doeller B, Kefer K, Findl O, et al. Intraoperative optical coherence tomography-guided membrane peeling for surgery of macular pucker: advantages and limitations. *Ophthalmologica.* (2019) 241:234–40. doi: 10.1159/000493279
160. Leisser C, Hackl C, Hirnschall N, Luft N, Doller B, Draschl P, et al. Visualizing macular structures during membrane peeling surgery with an intraoperative spectral-domain optical coherence tomography device. *Ophthalmic Surg Lasers Imaging Retina.* (2016) 47:328–32. doi: 10.3928/23258160-20160324-04
161. Yee P, Sevgi DD, Abraham J, Srivastava SK, Le T, Uchida A, et al. iOCT-assisted macular hole surgery: outcomes and utility from the DISCOVER study. *Br J Ophthalmol.* (2021) 105:403–9. doi: 10.1136/bjophthalmol-2020-316045
162. Dayani PN, Maldonado R, Farsiu S, Toth CA. Intraoperative use of handheld spectral domain optical coherence tomography imaging in macular surgery. *Retina.* (2009) 29:1457–68. doi: 10.1097/IAE.0b013e3181b266bc
163. Hayashi A, Yagou T, Nakamura T, Fujita K, Oka M, Fuchizawa C, et al. Intraoperative changes in idiopathic macular holes by spectral-domain optical coherence tomography. *Case Rep Ophthalmol.* (2011) 2:149–54. doi: 10.1159/000328752
164. Bruyere E, Philippakis E, Dupas B, Nguyen-Kim P, Tadayoni R, Couturier A, et al. Benefit of intraoperative optical coherence tomography for

vitreomacular surgery in highly myopic eyes. *Retina.* (2018) 38:2035–44. doi: 10.1097/IAE.0000000000001827
165. Lytvynchuk LM, Falkner-Radler CI, Krepler K, Glittenberg CG, Ahmed D, Petrovski G, et al. Dynamic intraoperative optical coherence tomography for inverted internal limiting membrane flap technique in large macular hole surgery. *Graefes Arch Clin Exp Ophthalmol.* (2019) 257:1649–59. doi: 10.1007/s00417-019-04364-5
166. Kumar V, Yadav B. HOLE-DOOR SIGN: a novel intraoperative optical coherence tomography feature predicting macular hole closure. *Retina.* (2018) 38:2045–50. doi: 10.1097/IAE.0000000000001791
167. Cehajic-Kapetanovic J, Xue K, Edwards TL, Meenink TC, Beelen MJ, Naus GJ, et al. First-in-human robot-assisted subretinal drug delivery under local anaesthesia a randomised clinical trial. *Am J Ophthalmol.* (2021) 237:104–13. doi: 10.1016/j.ajo.2021.11.011
168. Vasconcelos HM Jr., Lujan BJ, Pennesi ME, Yang P, Lauer AK. Intraoperative optical coherence tomographic findings in patients undergoing subretinal gene therapy surgery. *Int J Retina Vitreous.* (2020) 6:13. doi: 10.1186/s40942-020-00216-1
169. Hussain RM, Tran KD, Maguire AM, Berrocal AM. Subretinal injection of voretigene Neparvovec-rzyl in a patient with RPE65-associated leber's congenital amaurosis. *Ophthalmic Surg Lasers Imaging Retina.* (2019) 50:661–3. doi: 10.3928/23258160-20191009-01
170. Au J, Goshe J, Dupps WJ Jr., Srivastava SK, Ehlers JP. Intraoperative optical coherence tomography for enhanced depth visualization in deep anterior lamellar keratoplasty from the PIONEER study. *Cornea.* (2015) 34:1039–43. doi: 10.1097/ICO.0000000000000508
171. Steven P, Le Blanc C, Lankenau E, Krug M, Oelckers S, Heindl LM, et al. Optimising deep anterior lamellar keratoplasty (DALK) using intraoperative online optical coherence tomography (iOCT). *Br J Ophthalmol.* (2014) 98:900–4. doi: 10.1136/bjophthalmol-2013-304585
172. De Benito-Llopis L, Mehta JS, Angunawela RI, Ang M, Tan DT. Intraoperative anterior segment optical coherence tomography: a novel assessment tool during deep anterior lamellar keratoplasty. *Am J Ophthalmol.* (2014) 157:334–341.e3. doi: 10.1016/j.ajo.2013.10.001
173. Santorum P, Yu AC, Bertelli E, Busin M. Microscope-integrated intraoperative optical coherence tomography-guided big-bubble deep anterior lamellar keratoplasty. *Cornea.* (2022) 41:125–9. doi: 10.1097/ICO.0000000000002826
174. Scorcia V, Busin M, Lucisano A, Beltz J, Carta A, Scorcia G, et al. Anterior segment optical coherence tomography-guided big-bubble technique. *Ophthalmology.* (2013) 120:471–6. doi: 10.1016/j.ophtha.2012.08.041
175. Guindolet D, Nguyen DT, Bergin C, Doan S, Cochereau I, Gabison EE, et al. Double-docking technique for femtosecond laser-assisted deep anterior lamellar keratoplasty. *Cornea.* (2018) 37:123–6. doi: 10.1097/ICO.0000000000001442
176. Cost B, Goshe JM, Srivastava S, Ehlers JP. Intraoperative optical coherence tomography-assisted descemet membrane endothelial keratoplasty in the DISCOVER study. *Am J Ophthalmol.* (2015) 160:430–7. doi: 10.1016/j.ajo.2015.05.020
177. Patel AS, Goshe JM, Srivastava SK, Ehlers JP. Intraoperative optical coherence tomography-assisted descemet membrane endothelial keratoplasty in the DISCOVER Study: first 100 cases. *Am J Ophthalmol.* (2020) 210:167–73. doi: 10.1016/j.ajo.2019.09.018
178. Sharma N, Sahay P, Maharana PK, Kumar P, Ahsan S, Titiyal JS, et al. Microscope integrated intraoperative optical coherence tomography-guided DMEK in corneas with poor visualization. *Clin Ophthalmol.* (2020) 14:643–51. doi: 10.2147/OPTH.S230195
179. Muijzer MB, Soeters N, Godefrooij DA, van Luijk CM, Wisse RPL. Intraoperative optical coherence tomography-assisted descemet membrane endothelial keratoplasty: toward more efficient. *Saf Surg Cornea.* (2020) 39:674–9. doi: 10.1097/ICO.0000000000002301
180. Steven P, Le Blanc C, Velten K, Lankenau E, Krug M, Oelckers S, et al. Optimizing descemet membrane endothelial keratoplasty using intraoperative optical coherence tomography. *JAMA Ophthalmol.* (2013) 131:1135–42. doi: 10.1001/jamaophthalmol.2013.4672
181. Saad A, Guilbert E, Grise-Dulac A, Sabatier P, Gatinel D. Intraoperative OCT-assisted DMEK: 14 consecutive cases. *Cornea.* (2015) 34:802–7. doi: 10.1097/ICO.0000000000000462
182. Miyakoshi A, Ozaki H, Otsuka M, Hayashi A. Efficacy of intraoperative anterior segment optical coherence tomography during descemet's stripping automated endothelial keratoplasty. *ISRN Ophthalmol.* (2014) 2014:562062. doi: 10.1155/2014/562062
183. Sng CC, Luengo Gimeno F, Mehta JS, Htoon HM, Tan DT. Intraoperative use of spectral-domain optical coherence tomography during Descemet's stripping automated endothelial keratoplasty. *Clin Ophthalmol.* (2012) 6:479–86. doi: 10.2147/OPTH.S28971
184. Steverink JG, Wisse RPL. Intraoperative optical coherence tomography in descemet stripping automated endothelial keratoplasty: pilot experiences. *Int Ophthalmol.* (2017) 37:939–44. doi: 10.1007/s10792-016-0338-9
185. Das S, Kummelil MK, Kharbanda V, Arora V, Nagappa S, Shetty R, et al. Microscope integrated intraoperative spectral domain optical coherence tomography for cataract surgery: uses and applications. *Curr Eye Res.* (2016) 41:643–52. doi: 10.3109/02713683.2015.1050742
186. Lytvynchuk LM, Glittenberg CG, Falkner-Radler CI, Neumaier-Ammerer B, Smretschnig E, Hagen S, et al. Evaluation of intraocular lens position during phacoemulsification using intraoperative spectral-domain optical coherence tomography. *J Cataract Refract Surg.* (2016) 42:694–702. doi: 10.1016/j.jcrs.2016.01.044
187. Hirnschall N, Farrokhi S, Amir-Asgari S, Hienert J, Findl O. Intraoperative optical coherence tomography measurements of aphakic eyes to predict postoperative position of 2 intraocular lens designs. *J Cataract Refract Surg.* (2018) 44:1310–6. doi: 10.1016/j.jcrs.2018.07.044
188. Rodriguez-Aramendia A, Diaz-Douton F, Fernandez-Trullas J, Falgueras P, Gonzalez L, Pujol J, et al. Whole anterior segment and retinal swept source OCT for comprehensive ocular screening. *Biomed Opt Express.* (2021) 12:1263–78. doi: 10.1364/BOE.414592
189. Grulkowski I, Manzanera S, Cwiklinski L, Sobczuk F, Karnowski K, Artal P, et al. Swept source optical coherence tomography and tunable lens technology for comprehensive imaging and biometry of the whole eye. *Optica.* (2018) 5:52–9. doi: 10.1364/OPTICA.5.000052
190. Jeong HW, Lee SW, Kim BM. Spectral-domain OCT with dual illumination and interlaced detection for simultaneous anterior segment and retina imaging. *Opt Express.* (2012) 20:19148–59. doi: 10.1364/OE.20.019148
191. Kim HJ, Kim PU, Hyeon MG, Choi Y, Kim J, Kim BM, et al. High-resolution, dual-depth spectral-domain optical coherence tomography with interlaced detection for whole-eye imaging. *Appl Opt.* (2016) 55:7212–7. doi: 10.1364/AO.55.007212
192. Luo M, Li Y, Zhuo Y. Advances and current clinical applications of anterior segment optical coherence tomography angiography. *Front Med (Lausanne).* (2021) 8:721442. doi: 10.3389/fmed.2021.721442
193. Fan S, Li L, Li Q, Dai C, Ren Q, Jiao S, et al. Dual band dual focus optical coherence tomography for imaging the whole eye segment. *Biomed Opt Express.* (2015) 6:2481–93. doi: 10.1364/BOE.6.002481
194. Jayaraman V, Cole GD, Robertson M, Uddin A, Cable A. High-sweep-rate 1310 nm MEMS-VCSEL with 150 nm continuous tuning range. *Electron Lett.* (2012) 48:867–9. doi: 10.1049/el.2012.1552
195. Grulkowski I, Liu JJ, Potsaid B, Jayaraman V, Lu CD, Jiang J, et al. Retinal, anterior segment and full eye imaging using ultrahigh speed swept source OCT with vertical-cavity surface emitting lasers. *Biomed Opt Express.* (2012) 3:2733–51. doi: 10.1364/BOE.3.002733
196. Grulkowski I, Liu JJ, Zhang JY, Potsaid B, Jayaraman V, Cable AE, et al. Reproducibility of a long-range swept-source optical coherence tomography ocular biometry system and comparison with clinical biometers. *Ophthalmology.* (2013) 120:2184–90. doi: 10.1016/j.ophtha.2013.04.007
197. Kim HJ, Kim M, Hyeon MG, Choi Y, Kim BM. Full ocular biometry through dual-depth whole-eye optical coherence tomography. *Biomed Opt Express.* (2018) 9:360–72. doi: 10.1364/BOE.9.000360
198. McNabb RP, Polans J, Keller B, Jackson-Atogi M, James CL, Vann RR, et al. Wide-field whole eye OCT system with demonstration of quantitative retinal curvature estimation. *Biomed Opt Express.* (2019) 10:338–55. doi: 10.1364/BOE.10.000338
199. Grulkowski I, Manzanera S, Cwiklinski L, Mompean J, de Castro A, Marin JM, et al. Volumetric macro- and micro-scale assessment of crystalline lens

opacities in cataract patients using long-depth-range swept source optical coherence tomography. *Biomed Opt Express.* (2018) 9:3821–33. doi: 10.1364/BOE.9.003821
200. de Castro A, Benito A, Manzanera S, Mompean J, Canizares B, Martinez D, et al. Three-dimensional cataract crystalline lens imaging with swept-source optical coherence tomography. *Invest Ophthalmol Vis Sci.* (2018) 59:897–903. doi: 10.1167/iovs.17-23596
201. Eugui P, Harper DJ, Kummer S, Lichtenegger A, Gesperger J, Himmel T, et al. Three-dimensional visualization of opacifications in the murine crystalline lens by in vivo optical coherence tomography. *Biomed Opt Express.* (2020) 11:2085–97. doi: 10.1364/BOE.387335
202. Pujari A, Yadav S, Sharma N, Khokhar S, Sinha R, Agarwal T, et al. Study 1: evaluation of the signs of deficient posterior capsule in posterior polar cataracts using anterior segment optical coherence tomography. *J Cataract Refract Surg.* (2020) 46:1260–5. doi: 10.1097/j.jcrs.0000000000000246
203. Martinez-Enriquez E, Perez-Merino P, Duran-Poveda S, Jimenez-Alfaro I, Marcos S. Estimation of intraocular lens position from full crystalline lens geometry: towards a new generation of intraocular lens power calculation formulas. *Sci Rep.* (2018) 8:9829. doi: 10.1038/s41598-018-28272-6
204. Kuo AN, McNabb RP, Izatt JA. Advances in whole-eye optical coherence tomography imaging. *Asia Pac J Ophthalmol (Phila).* (2019):10.22608/AO.201901. [Online ahead of print], doi: 10.22608/APO.201901
205. Begley CG, Chalmers RL, Abetz L, Venkataraman K, Mertzanis P, Caffery BA, et al. The relationship between habitual patient-reported symptoms and clinical signs among patients with dry eye of varying severity. *Invest Ophthalmol Vis Sci.* (2003) 44:4753–61. doi: 10.1167/iovs.03-0270
206. Schmidl D, Witkowska KJ, Kaya S, Baar C, Faatz H, Nepp J, et al. The association between subjective and objective parameters for the assessment of dry-eye syndrome. *Invest Ophthalmol Vis Sci.* (2015) 56:1467–72. doi: 10.1167/iovs.14-15814
207. Huang J, Hindman HB, Rolland JP. In vivo thickness dynamics measurement of tear film lipid and aqueous layers with optical coherence tomography and maximum-likelihood estimation. *Opt Lett.* (2016) 41:1981–4. doi: 10.1364/OL.41.001981
208. Dos Santos VA, Schmetterer L, Triggs GJ, Leitgeb RA, Groschl M, Messner A, et al. Super-resolved thickness maps of thin film phantoms and in vivo visualization of tear film lipid layer using OCT. *Biomed Opt Express.* (2016) 7:2650–70. doi: 10.1364/BOE.7.002650
209. Stegmann H, Aranha Dos Santos V, Messner A, Unterhuber A, Schmidl D, Garhofer G, et al. Automatic assessment of tear film and tear meniscus parameters in healthy subjects using ultrahigh-resolution optical coherence tomography. *Biomed Opt Express.* (2019) 10:2744–56. doi: 10.1364/BOE.10.002744
210. Ang M, Baskaran M, Werkmeister RM, Chua J, Schmidl D, Aranha Dos Santos V, et al. Anterior segment optical coherence tomography. *Prog Retin Eye Res.* (2018) 66:132–56. doi: 10.1016/j.preteyeres.2018.04.002
211. Carracedo G, Pastrana C, Serramito M, Rodriguez-Pomar C. Evaluation of tear meniscus by optical coherence tomography after different sodium hyaluronate eyedrops instillation. *Acta Ophthalmol.* (2019) 97:e162–9. doi: 10.1111/aos.13887
212. Wang Y, Zhuang H, Xu J, Wang X, Jiang C, Sun X, et al. Dynamic changes in the lower tear meniscus after instillation of artificial tears. *Cornea.* (2010) 29:404–8. doi: 10.1097/ICO.0b013e3181bd476c
213. Bujak MC, Yiu S, Zhang X, Li Y, Huang D. Serial measurement of tear meniscus by FD-OCT after instillation of artificial tears in patients with dry eyes. *Ophthalmic Surg Lasers Imaging.* (2011) 42:308–13. doi: 10.3928/15428877-20110603-02
214. Wang J, Cui L, Shen M, Perez VL, Wang MR. Ultra-high resolution optical coherence tomography for monitoring tear meniscus volume in dry eye after topical cyclosporine treatment. *Clin Ophthalmol.* (2012) 6:933–8. doi: 10.2147/OPTH.S32384
215. Sharma N, Singhal D, Maharana PK, Agarwal T, Sinha R, Satpathy G, et al. Spectral domain anterior segment optical coherence tomography in fungal keratitis. *Cornea.* (2018) 37:1388–94. doi: 10.1097/ICO.0000000000001715
216. Soliman W, Nassr MA, Abdelazeem K, Al-Hussaini AK. Appearance of herpes simplex keratitis on anterior segment optical coherence tomography. *Int Ophthalmol.* (2019) 39:2923–8. doi: 10.1007/s10792-019-01142-4
217. Oliveira MA, Rosa A, Soares M, Gil J, Costa E, Quadrado MJ, et al. Anterior segment optical coherence tomography in the early management of microbial keratitis: a cross-sectional study. *Acta Med Port.* (2020) 33:318–25. doi: 10.20344/amp.12663
218. Nanji AA, Sayyad FE, Galor A, Dubovy S, Karp CL. High-resolution optical coherence tomography as an adjunctive tool in the diagnosis of corneal and conjunctival pathology. *Ocul Surf.* (2015) 13:226–35. doi: 10.1016/j.jtos.2015.02.001
219. Konstantopoulos A, Kuo J, Anderson D, Hossain P. Assessment of the use of anterior segment optical coherence tomography in microbial keratitis. *Am J Ophthalmol.* (2008) 146:534–42. doi: 10.1016/j.ajo.2008.05.030
220. Fuentes E, Sandali O, El Sanharawi M, Basli E, Hamiche T, Goemaere I, et al. Anatomic predictive factors of acute corneal hydrops in keratoconus: an optical coherence tomography study. *Ophthalmology.* (2015) 122:1653–9. doi: 10.1016/j.ophtha.2015.04.031
221. Siebelmann S, Scholz P, Sonnenschein S, Bachmann B, Matthaei M, Cursiefen C, et al. Anterior segment optical coherence tomography for the diagnosis of corneal dystrophies according to the IC3D classification. *Surv Ophthalmol.* (2018) 63:365–80. doi: 10.1016/j.survophthal.2017.08.001
222. Mohammed ISK, Tran S, Toledo-Espiett LA, Munir WM. The detection of keratoconus using novel metrics derived by anterior segment optical coherence tomography. *Int Ophthalmol.* (2022): [Online ahead of print], doi: 10.1007/s10792-021-02210-4
223. Jin X, Jin H, Shi Y, Zhang N, Zhang H. Clinical observation of corneal endothelial plaques with fungal and bacterial keratitis by anterior segment optical coherence tomography and in vivo confocal microscopy. *Cornea.* (2021): [Online ahead of print], doi: 10.1097/ICO.0000000000002912
224. Wang F, Shi G, Li X, Lu J, Ding Z, Sun X, et al. Comparison of Schlemm's canal's biological parameters in primary open-angle glaucoma and normal human eyes with swept source optical. *J Biomed Opt.* (2012) 17:116008. doi: 10.1117/1.JBO.17.11.116008
225. Hong J, Xu J, Wei A, Wen W, Chen J, Yu X, et al. Spectral-domain optical coherence tomographic assessment of Schlemm's canal in Chinese subjects with primary open-angle glaucoma. *Ophthalmology.* (2013) 120:709–15. doi: 10.1016/j.ophtha.2012.10.008
226. Dada T, Sihota R, Gadia R, Aggarwal A, Mandal S, Gupta V, et al. Comparison of anterior segment optical coherence tomography and ultrasound biomicroscopy for assessment of the anterior segment. *J Cataract Refract Surg.* (2007) 33:837–40. doi: 10.1016/j.jcrs.2007.01.021
227. Console JW, Sakata LM, Aung T, Friedman DS, He M. Quantitative analysis of anterior segment optical coherence tomography images: the Zhongshan Angle Assessment Program. *Br J Ophthalmol.* (2008) 92:1612–6. doi: 10.1136/bjo.2007.129932
228. Baskaran M, Iyer JV, Narayanaswamy AK, He Y, Sakata LM, Wu R, et al. Anterior segment imaging predicts incident gonioscopic angle closure. *Ophthalmology.* (2015) 122:2380–4. doi: 10.1016/j.ophtha.2015.07.030
229. Nongpiur ME, He M, Amerasinghe N, Friedman DS, Tay WT, Baskaran M, et al. Lens vault, thickness, and position in Chinese subjects with angle closure. *Ophthalmology.* (2011) 118:474–9. doi: 10.1016/j.ophtha.2010.07.025
230. Nongpiur ME, Sakata LM, Friedman DS, He M, Chan YH, Lavanya R, et al. Novel association of smaller anterior chamber width with angle closure in Singaporeans. *Ophthalmology.* (2010) 117:1967–73. doi: 10.1016/j.ophtha.2010.02.007
231. Wang B, Sakata LM, Friedman DS, Chan YH, He M, Lavanya R, et al. Quantitative iris parameters and association with narrow angles. *Ophthalmology.* (2010) 117:11–7. doi: 10.1016/j.ophtha.2009.06.017
232. Li P, Reif R, Zhi Z, Martin E, Shen TT, Johnstone M, et al. Phase-sensitive optical coherence tomography characterization of pulse-induced trabecular meshwork displacement in ex vivo nonhuman primate eyes. *J Biomed Opt.* (2012) 17:076026. doi: 10.1117/1.JBO.17.7.076026
233. Huang AS, Belghith A, Dastiridou A, Chopra V, Zangwill LM, Weinreb RN, et al. Automated circumferential construction of first-order aqueous humor outflow pathways using spectral-domain optical coherence tomography. *J Biomed Opt.* (2017) 22:66010. doi: 10.1117/1.JBO.22.6.066010
234. Hong J, Yang Y, Wei A, Deng SX, Kong X, Chen J, et al. Schlemm's canal expands after trabeculectomy in patients with primary angle-closure

glaucoma. *Invest Ophthalmol Vis Sci.* (2014) 55:5637–42. doi: 10.1167/iovs.14-14712
235. Fuest M, Kuerten D, Koch E, Becker J, Hirsch T, Walter P, et al. Evaluation of early anatomical changes following canaloplasty with anterior segment spectral-domain optical coherence tomography and ultrasound biomicroscopy. *Acta Ophthalmol.* (2016) 94:e287–92. doi: 10.1111/aos.12917
236. Chen J, Huang H, Zhang S, Chen X, Sun X. Expansion of Schlemm's canal by travoprost in healthy subjects determined by Fourier-domain optical coherence tomography. *Invest Ophthalmol Vis Sci.* (2013) 54:1127–34. doi: 10.1167/iovs.12-10396
237. Skaat A, Rosman MS, Chien JL, Mogil RS, Ren R, Liebmann JM, et al. Effect of pilocarpine hydrochloride on the schlemm canal in healthy eyes and eyes with open-angle glaucoma. *JAMA Ophthalmol.* (2016) 134:976–81. doi: 10.1001/jamaophthalmol.2016.1881
238. Ruggeri M, Belloni G, Chang YC, Durkee H, Masetti E, Cabot F, et al. Combined anterior segment OCT and wavefront-based autorefractor using a shared beam. *Biomed Opt Express.* (2021) 12:6746–61. doi: 10.1364/BOE.435127
239. Huo T, Wang C, Zhang X, Chen T, Liao W, Zhang W, et al. Ultrahigh-speed optical coherence tomography utilizing all-optical 40 MHz swept-source. *J Biomed Opt.* (2015) 20:030503. doi: 10.1117/1.JBO.20.3.030503
240. Kolb JP, Klein T, Kufner CL, Wieser W, Neubauer AS, Huber R, et al. Ultra-widefield retinal MHz-OCT imaging with up to 100 degrees viewing angle. *Biomed Opt Express.* (2015) 6:1534–52. doi: 10.1364/BOE.6.001534
241. Zhi Z, Qin W, Wang J, Wei W, Wang RK. 4D optical coherence tomography-based micro-angiography achieved by 1.6-MHz FDML swept source. *Opt Lett.* (2015) 40:1779–82. doi: 10.1364/OL.40.001779
242. Gora M, Karnowski K, Szkulmowski M, Kaluzny BJ, Huber R, Kowalczyk A, et al. Ultra high-speed swept source OCT imaging of the anterior segment of human eye at 200 kHz with adjustable imaging range. *Opt Express.* (2009) 17:14880–94. doi: 10.1364/OE.17.014880
243. Ishida S, Nishizawa N. Quantitative comparison of contrast and imaging depth of ultrahigh-resolution optical coherence tomography images in 800-1700 nm wavelength region. *Biomed Opt Express.* (2012) 3:282–94. doi: 10.1364/BOE.3.000282
244. Lim H, Jiang Y, Wang Y, Huang YC, Chen Z, Wise FW, et al. Ultrahigh-resolution optical coherence tomography with a fiber laser source at 1 microm. *Opt Lett.* (2005) 30:1171–3. doi: 10.1364/OL.30.001171
245. Moon S, Kim DY. Ultra-high-speed optical coherence tomography with a stretched pulse supercontinuum source. *Opt Express.* (2006) 14:11575–84. doi: 10.1364/OE.14.011575
246. Nishizawa N, Chen Y, Hsiung P, Ippen EP, Fujimoto JG. Real-time, ultrahigh-resolution, optical coherence tomography with an all-fiber, femtosecond fiber laser continuum at 1.5 microm. *Opt Lett.* (2004) 29:2846–8. doi: 10.1364/OL.29.002846
247. Moutsouris K, Dapena I, Ham L, Balachandran C, Oellerich S, Melles GR, et al. Optical coherence tomography, Scheimpflug imaging, and slit-lamp biomicroscopy in the early detection of graft detachment after Descemet membrane endothelial keratoplasty. *Cornea.* (2011) 30:1369–75. doi: 10.1097/ICO.0b013e31820d86bd
248. Kagemann L, Wollstein G, Ishikawa H, Bilonick RA, Brennen PM, Folio LS, et al. Identification and assessment of Schlemm's canal by spectral-domain optical coherence tomography. *Invest Ophthalmol Vis Sci.* (2010) 51:4054–9. doi: 10.1167/iovs.09-4559
249. Leung CK, Li H, Weinreb RN, Liu J, Cheung CY, Lai RY, et al. Anterior chamber angle measurement with anterior segment optical coherence tomography: a comparison between slit lamp OCT and Visante OCT. *Invest Ophthalmol Vis Sci.* (2008) 49:3469–74. doi: 10.1167/iovs.07-1477
250. Werkmeister RM, Alex A, Kaya S, Unterhuber A, Hofer B, Riedl J, et al. Measurement of tear film thickness using ultrahigh-resolution optical coherence tomography. *Invest Ophthalmol Vis Sci.* (2013) 54:5578–83. doi: 10.1167/iovs.13-11920
251. Dubois A, Vabre L, Boccara AC, Beaurepaire E. High-resolution full-field optical coherence tomography with a Linnik microscope. *Appl Opt.* (2002) 41:805–12. doi: 10.1364/AO.41.000805
252. Auksorius E, Borycki D, Stremplewski P, Lizewski K, Tomczewski S, Niedzwiedziuk P, et al. In vivo imaging of the human cornea with high-speed and high-resolution Fourier-domain full-field optical coherence tomography. *Biomed Opt Express.* (2020) 11:2849–65. doi: 10.1364/BOE.393801
253. Hillmann D, Spahr H, Hain C, Sudkamp H, Franke G, Pfäffle C, et al. Aberration-free volumetric high-speed imaging of in vivo retina. *Sci Rep.* (2016) 6:35209.
254. Xiao P, Fink M, Boccara AC. Full-field spatially incoherent illumination interferometry: a spatial resolution almost insensitive to aberrations. *Opt Lett.* (2016) 41:3920–3. doi: 10.1364/OL.41.003920
255. Mazlin V, Xiao P, Dalimier E, Grieve K, Irsch K, Sahel JA, et al. In vivo high resolution human corneal imaging using full-field optical coherence tomography. *Biomed Opt Express.* (2018) 9:557–68. doi: 10.1364/BOE.9.000557
256. Mazlin V, Xiao P, Scholler J, Irsch K, Grieve K, Fink M, et al. Real-time non-contact cellular imaging and angiography of human cornea and limbus with common-path full-field/SD OCT. *Nat Commun.* (2020) 11:1868. doi: 10.1038/s41467-020-15792-x
257. Xiao P, Mazlin V, Grieve K. In vivo high-resolution human retinal imaging with wavefront-correctionless full-field OCT. *Optica.* (2018) 5:409–12. doi: 10.1364/OPTICA.5.000409
258. Mecê P, Groux K, Scholler J, Thouvenin O, Fink M, Grieve K, et al. Coherence gate shaping for wide field high-resolution in vivo retinal imaging with full-field OCT. *Biomed Opt Express.* (2020) 11:4928–41. doi: 10.1364/BOE.400522
259. von der Burchard C, Moltmann M, Tode J, Ehlken C, Sudkamp H, Theisen-Kunde D, et al. Self-examination low-cost full-field OCT (SELFF-OCT) for patients with various macular diseases. *Graefes Arch Clin Exp Ophthalmol.* (2021) 259:1503–11. doi: 10.1007/s00417-020-05035-6
260. Jayabalan GS, Bille JF. The development of adaptive optics and its application in ophthalmology. In: Bille JF editor. *High Resolution Imaging in Microscopy and Ophthalmology: New Frontiers in Biomedical Optics*. Cham: Springer (2019). doi: 10.1007/978-3-030-16638-0_16
261. Cense B, Gao W, Brown JM, Jones SM, Jonnal RS, Mujat M, et al. Retinal imaging with polarization-sensitive optical coherence tomography and adaptive optics. *Opt Express.* (2009) 17:21634–51. doi: 10.1364/OE.17.021634
262. Miller DT, Kurokawa K. Cellular-scale imaging of transparent retinal structures and processes using adaptive optics optical coherence tomography. *Annu Rev Vis Sci.* (2020) 6:115–48. doi: 10.1146/annurev-vision-030320-041255
263. Zhang Y, Cense B, Rha J, Jonnal RS, Gao W, Zawadzki RJ, et al. High-speed volumetric imaging of cone photoreceptors with adaptive optics spectral-domain optical coherence tomography. *Opt Express.* (2006) 14:4380–94. doi: 10.1364/OE.14.004380
264. Evans JW, Zawadzki RJ, Jones SM, Olivier SS, Werner JS. Error budget analysis for an adaptive optics optical coherence tomography system. *Opt Express.* (2009) 17:13768–84. doi: 10.1364/OE.17.013768
265. Hermann B, Fernandez EJ, Unterhuber A, Sattmann H, Fercher AF, Drexler W, et al. Adaptive-optics ultrahigh-resolution optical coherence tomography. *Opt Lett.* (2004) 29:2142–4. doi: 10.1364/OL.29.002142
266. Roorda A, Romero-Borja F, Donnelly Iii W, Queener H, Hebert T, Campbell M, et al. Adaptive optics scanning laser ophthalmoscopy. *Opt Express.* (2002) 10:405–12. doi: 10.1364/OE.10.000405
267. Jonnal RS, Kocaoglu OP, Zawadzki RJ, Liu Z, Miller DT, Werner JS, et al. A review of adaptive optics optical coherence tomography: technical advances, scientific applications, and the future. *Invest Ophthalmol Vis Sci.* (2016) 57:OCT51–68. doi: 10.1167/iovs.16-19103
268. Zhang Y, Rha J, Jonnal R, Miller D. Adaptive optics parallel spectral domain optical coherence tomography for imaging the living retina. *Opt Express.* (2005) 13:4792–811. doi: 10.1364/OPEX.13.004792
269. Kocaoglu OP, Cense B, Jonnal RS, Wang Q, Lee S, Gao W, et al. Imaging retinal nerve fiber bundles using optical coherence tomography with adaptive optics. *Vision Res.* (2011) 51:1835–44. doi: 10.1016/j.visres.2011.06.013
270. Zawadzki RJ, Choi SS, Jones SM, Oliver SS, Werner JS. Adaptive optics-optical coherence tomography: optimizing visualization of microscopic retinal structures in three dimensions. *J Opt Soc Am A Opt Image Sci Vis.* (2007) 24:1373–83. doi: 10.1364/JOSAA.24.001373
271. Cense B, Koperda E, Brown JM, Kocaoglu OP, Gao W, Jonnal RS, et al. Volumetric retinal imaging with ultrahigh-resolution spectral-domain

optical coherence tomography and adaptive optics using two broadband light sources. *Opt Express.* (2009) 17:4095–111. doi: 10.1364/OE.17.004095
272. Reumueller A, Wassermann L, Salas M, Schranz M, Hacker V, Mylonas G, et al. Three-dimensional composition of the photoreceptor cone layers in healthy eyes using adaptive-optics optical coherence tomography (AO-OCT). *PLoS One.* (2021) 16:e0245293. doi: 10.1371/journal.pone.0245293
273. Curcio CA, Sloan KR, Kalina RE, Hendrickson AE. Human photoreceptor topography. *J Comp Neurol.* (1990) 292:497–523. doi: 10.1002/cne.902920402
274. Li KY, Roorda A. Automated identification of cone photoreceptors in adaptive optics retinal images. *J Opt Soc Am A Opt Image Sci Vis.* (2007) 24:1358–63. doi: 10.1364/JOSAA.24.001358
275. Cooper RF, Wilk MA, Tarima S, Carroll J. Evaluating descriptive metrics of the human cone mosaic. *Invest Ophthalmol Vis Sci.* (2016) 57:2992–3001. doi: 10.1167/iovs.16-19072
276. Cooper RF, Lombardo M, Carroll J, Sloan KR, Lombardo G. Methods for investigating the local spatial anisotropy and the preferred orientation of cones in adaptive optics retinal images. *Vis Neurosci.* (2016) 33:E005. doi: 10.1017/S0952523816000018
277. Akyol E, Hagag AM, Sivaprasad S, Lotery AJ. Adaptive optics: principles and applications in ophthalmology. *Eye (Lond).* (2021) 35:244–64. doi: 10.1038/s41433-020-01286-z
278. Morgan JIW, Vergilio GK, Hsu J, Dubra A, Cooper RF. The reliability of cone density measurements in the presence of rods. *Transl Vis Sci Technol.* (2018) 7:21. doi: 10.1167/tvst.7.3.21
279. Pallikaris A, Williams DR, Hofer H. The reflectance of single cones in the living human eye. *Invest Ophthalmol Vis Sci.* (2003) 44:4580–92. doi: 10.1167/iovs.03-0094
280. Wynne N, Carroll J, Duncan JL. Promises and pitfalls of evaluating photoreceptor-based retinal disease with adaptive optics scanning light ophthalmoscopy (AOSLO). *Prog Retin Eye Res.* (2021) 83:100920. doi: 10.1016/j.preteyeres.2020.100920
281. Wells-Gray EM, Choi SS, Bries A, Doble N. Variation in rod and cone density from the fovea to the mid-periphery in healthy human retinas using adaptive optics scanning laser ophthalmoscopy. *Eye (Lond).* (2016) 30:1135–43. doi: 10.1038/eye.2016.107
282. Burns SA, Elsner AE, Sapoznik KA, Warner RL, Gast TJ. Adaptive optics imaging of the human retina. *Prog Retin Eye Res.* (2019) 68:1–30. doi: 10.1016/j.preteyeres.2018.08.002
283. Scoles D, Sulai YN, Dubra A. In vivo dark-field imaging of the retinal pigment epithelium cell mosaic. *Biomed Opt Express.* (2013) 4:1710–23. doi: 10.1364/BOE.4.001710
284. Rossi EA, Granger CE, Sharma R, Yang Q, Saito K, Schwarz C, et al. Imaging individual neurons in the retinal ganglion cell layer of the living eye. *Proc Natl Acad Sci U S A.* (2017) 114:586–91. doi: 10.1073/pnas.1613445114
285. Liu Z, Kurokawa K, Zhang F, Lee JJ, Miller DT. Imaging and quantifying ganglion cells and other transparent neurons in the living human retina. *Proc Natl Acad Sci U S A.* (2017) 114:12803–8. doi: 10.1073/pnas.1711734114
286. Querques G, Massamba N, Guigui B, Lea Q, Lamory B, Soubrane G, et al. In vivo evaluation of photoreceptor mosaic in early onset large colloid drusen using adaptive optics. *Acta Ophthalmol.* (2012) 90:e327–8. doi: 10.1111/j.1755-3768.2011.02228.x
287. Panorgias A, Zawadzki RJ, Capps AG, Hunter AA, Morse LS, Werner JS, et al. Multimodal assessment of microscopic morphology and retinal function in patients with geographic atrophy. *Invest Ophthalmol Vis Sci.* (2013) 54:4372–84. doi: 10.1167/iovs.12-11525
288. Godara P, Siebe C, Rha J, Michaelides M, Carroll J. Assessing the photoreceptor mosaic over drusen using adaptive optics and SD-OCT. *Ophthalmic Surg Lasers Imaging.* (2010) 41:S104–8. doi: 10.3928/15428877-20101031-07
289. Choi SS, Zawadzki RJ, Lim MC, Brandt JD, Keltner JL, Doble N, et al. Evidence of outer retinal changes in glaucoma patients as revealed by ultrahigh-resolution in vivo retinal imaging. *Br J Ophthalmol.* (2011) 95:131–41. doi: 10.1136/bjo.2010.183756
290. Werner JS, Keltner JL, Zawadzki RJ, Choi SS. Outer retinal abnormalities associated with inner retinal pathology in nonglaucomatous and glaucomatous optic neuropathies. *Eye (Lond).* (2011) 25:279–89. doi: 10.1038/eye.2010.218
291. Torti C, Povazay B, Hofer B, Unterhuber A, Carroll J, Ahnelt PK, et al. Adaptive optics optical coherence tomography at 120,000 depth scans/s for non-invasive cellular phenotyping of the living human retina. *Opt Express.* (2009) 17:19382–400. doi: 10.1364/OE.17.019382
292. Wang Q, Kocaoglu OP, Cense B, Bruestle J, Jonnal RS, Gao W, et al. Imaging retinal capillaries using ultrahigh-resolution optical coherence tomography and adaptive optics. *Invest Ophthalmol Vis Sci.* (2011) 52:6292–9. doi: 10.1167/iovs.10-6424
293. Kurokawa K, Sasaki K, Makita S, Hong YJ, Yasuno Y. Three-dimensional retinal and choroidal capillary imaging by power Doppler optical coherence angiography with adaptive optics. *Opt Express.* (2012) 20:22796–812. doi: 10.1364/OE.20.022796
294. Felberer F, Rechenmacher M, Haindl R, Baumann B, Hitzenberger CK, Pircher M, et al. Imaging of retinal vasculature using adaptive optics SLO/OCT. *Biomed Opt Express.* (2015) 6:1407–18. doi: 10.1364/BOE.6.001407
295. Tam J, Dhamdhere KP, Tiruveedhula P, Manzanera S, Barez S, Bearse MA Jr., et al. Disruption of the retinal parafoveal capillary network in type 2 diabetes before the onset of diabetic retinopathy. *Invest Ophthalmol Vis Sci.* (2011) 52:9257–66. doi: 10.1167/iovs.11-8481
296. Lombardo M, Parravano M, Lombardo G, Varano M, Boccassini B, Stirpe M, et al. Adaptive optics imaging of parafoveal cones in type 1 diabetes. *Retina.* (2014) 34:546–57. doi: 10.1097/IAE.0b013e3182a10850
297. Park SS, Bauer G, Abedi M, Pontow S, Panorgias A, Jonnal R, et al. Intravitreal autologous bone marrow CD34+ cell therapy for ischemic and degenerative retinal disorders: preliminary phase 1 clinical trial findings. *Invest Ophthalmol Vis Sci.* (2014) 56:81–9. doi: 10.1167/iovs.14-15415
298. Nakamura T, Ueda-Consolvo T, Oiwake T, Hayashi A. Correlation between outer retinal layer thickness and cone density in patients with resolved central serous chorioretinopathy. *Graefes Arch Clin Exp Ophthalmol.* (2016) 254:2347–54. doi: 10.1007/s00417-016-3403-1
299. Foote KG, Wong JJ, Boehm AE, Bensinger E, Porco TC, Roorda A, et al. Comparing cone structure and function in RHO- and RPGR-associated retinitis pigmentosa. *Invest Ophthalmol Vis Sci.* (2020) 61:42. doi: 10.1167/iovs.61.4.42
300. Foote KG, Loumou P, Griffin S, Qin J, Ratnam K, Porco TC, et al. Relationship between foveal cone structure and visual acuity measured with adaptive optics scanning laser ophthalmoscopy in retinal degeneration. *Invest Ophthalmol Vis Sci.* (2018) 59:3385–93. doi: 10.1167/iovs.17-23708
301. Thompson DA, Iannaccone A, Ali RR, Arshavsky VY, Audo I, Bainbridge JWB, et al. Advancing clinical trials for inherited retinal diseases: recommendations from the second monaciano symposium. *Transl Vis Sci Technol.* (2020) 9:2. doi: 10.1167/tvst.9.7.2
302. Reumueller A, Schmidt-Erfurth U, Salas M, Sacu S, Drexler W, Pircher M, et al. Three-dimensional adaptive optics-assisted visualization of photoreceptors in healthy and pathologically aged eyes. *Invest Ophthalmol Vis Sci.* (2019) 60:1144–55. doi: 10.1167/iovs.18-25702
303. Reumueller A, Wassermann L, Salas M, Karantonis MG, Sacu S, Georgopoulos M, et al. Morphologic and functional assessment of photoreceptors after macula-off retinal detachment with adaptive-optics OCT and microperimetry. *Am J Ophthalmol.* (2020) 214:72–85. doi: 10.1016/j.ajo.2019.12.015
304. Wong KS, Jian Y, Cua M, Bonora S, Zawadzki RJ, Sarunic MV, et al. In vivo imaging of human photoreceptor mosaic with wavefront sensorless adaptive optics optical coherence tomography. *Biomed Opt Express.* (2015) 6:580–90. doi: 10.1364/BOE.6.000580
305. South FA, Kurokawa K, Liu Z, Liu YZ, Miller DT, Boppart SA, et al. Combined hardware and computational optical wavefront correction. *Biomed Opt Express.* (2018) 9:2562–74. doi: 10.1364/BOE.9.002562
306. Kocaoglu OP, Lee S, Jonnal RS, Wang Q, Herde AE, Derby JC, et al. Imaging cone photoreceptors in three dimensions and in time using ultrahigh resolution optical coherence tomography with adaptive optics. *Biomed Opt Express.* (2011) 2:748–63. doi: 10.1364/BOE.2.000748
307. Lee SH, Werner JS, Zawadzki RJ. Improved visualization of outer retinal morphology with aberration cancelling reflective optical design for adaptive optics - optical coherence tomography. *Biomed Opt Express.* (2013) 4:2508–17. doi: 10.1364/BOE.4.002508

308. Kocaoglu OP, Turner TL, Liu Z, Miller DT. Adaptive optics optical coherence tomography at 1 MHz. *Biomed Opt Express.* (2014) 5:4186–200. doi: 10.1364/BOE.5.004186
309. Kocaoglu OP, Ferguson RD, Jonnal RS, Liu Z, Wang Q, Hammer DX, et al. Adaptive optics optical coherence tomography with dynamic retinal tracking. *Biomed Opt Express.* (2014) 5:2262–84. doi: 10.1364/BOE.5.002262
310. Pircher M, Zawadzki RJ, Evans JW, Werner JS, Hitzenberger CK. Simultaneous imaging of human cone mosaic with adaptive optics enhanced scanning laser ophthalmoscopy and high-speed transversal scanning optical coherence tomography. *Opt Lett.* (2008) 33:22–4. doi: 10.1364/OL.33.000022
311. Felberer F, Kroisamer JS, Baumann B, Zotter S, Schmidt-Erfurth U, Hitzenberger CK, et al. Adaptive optics SLO/OCT for 3D imaging of human photoreceptors in vivo. *Biomed Opt Express.* (2014) 5:439–56. doi: 10.1364/BOE.5.000439
312. Hillmann D, Spahr H, Hain C, Sudkamp H, Franke G, Pfaffle C, et al. Aberration-free volumetric high-speed imaging of in vivo retina. *Sci Rep.* (2016) 6:35209. doi: 10.1038/srep35209
313. Azimipour M, Jonnal RS, Werner JS, Zawadzki RJ. Coextensive synchronized SLO-OCT with adaptive optics for human retinal imaging. *Opt Lett.* (2019) 44:4219–22. doi: 10.1364/OL.44.004219
314. Azimipour M, Zawadzki RJ, Gorczynska I, Migacz J, Werner JS, Jonnal RS, et al. Intraframe motion correction for raster-scanned adaptive optics images using strip-based cross-correlation lag biases. *PLoS One.* (2018) 13:e0206052. doi: 10.1371/journal.pone.0206052
315. Liu Z, Kocaoglu OP, Miller DT. 3D Imaging of Retinal Pigment Epithelial Cells in the Living Human Retina. *Invest Ophthalmol Vis Sci.* (2016) 57:OCT533–43. doi: 10.1167/iovs.16-19106
316. Liu Z, Tam J, Saeedi O, Hammer DX. Trans-retinal cellular imaging with multimodal adaptive optics. *Biomed Opt Express.* (2018) 9:4246–62. doi: 10.1364/BOE.9.004246
317. Wells-Gray EM, Choi SS, Slabaugh M, Weber P, Doble N. Inner retinal changes in primary open-angle glaucoma revealed through adaptive optics-optical coherence tomography. *J Glaucoma.* (2018) 27:1025–8. doi: 10.1097/IJG.0000000000001039
318. Tanna H, Dubis AM, Ayub N, Tait DM, Rha J, Stepien KE, et al. Retinal imaging using commercial broadband optical coherence tomography. *Br J Ophthalmol.* (2010) 94:372–6. doi: 10.1136/bjo.2009.163501
319. Kurokawa K, Crowell JA, Zhang F, Miller DT. Suite of methods for assessing inner retinal temporal dynamics across spatial and temporal scales in the living human eye. *Neurophotonics.* (2020) 7:015013. doi: 10.1117/1.NPh.7.1.015013
320. Csaky K, Ferris F 3rd., Chew EY, Nair P, Cheetham JK, Duncan JL, et al. Report from the NEI/FDA endpoints workshop on age-related macular degeneration and inherited retinal diseases. *Invest Ophthalmol Vis Sci.* (2017) 58:3456–63. doi: 10.1167/iovs.17-22339
321. Pandiyan VP, Jiang X, Kuchenbecker JA, Sabesan R. Reflective mirror-based line-scan adaptive optics OCT for imaging retinal structure and function. *Biomed Opt Express.* (2021) 12:5865–80. doi: 10.1364/BOE.436337
322. Valente D, Vienola KV, Zawadzki RJ, Jonnal RS. Kilohertz retinal FF-SS-OCT and flood imaging with hardware-based adaptive optics. *Biomed Opt Express.* (2020) 11:5995–6011. doi: 10.1364/BOE.403509
323. Cooper RF, Tuten WS, Dubra A, Brainard DH, Morgan JIW. Non-invasive assessment of human cone photoreceptor function. *Biomed Opt Express.* (2017) 8:5098–112. doi: 10.1364/BOE.8.005098
324. Hüllmann D, Spahr H, Pfäffle C, Sudkamp H, Franke G, Hüttmann G, et al. In vivo optical imaging of physiological responses to photostimulation in human photoreceptors. *Proc Natl Acad Sci U S A.* (2016) 113:13138–43. doi: 10.1073/pnas.1606428113
325. Al-Aswad LA, Ramachandran R, Schuman JS. Artificial intelligence for glaucoma: creating and implementing AI for disease detection and progression. *Ophthalmol Glaucoma.* (2022):S2589–4196. [Online ahead of print], doi: 10.1016/j.ogla.2022.02.010
326. Blumenkranz MS, Tarver ME, Myung D, Eydelman MB. The collaborative community on ophthalmic imaging: accelerating global innovation and clinical utility. *Ophthalmology.* (2022) 129:e9–13. doi: 10.1016/j.ophtha.2021.10.001
327. Schuman JS, Ramos Cadena DLAM, McGee R, Al-Aswad LA, Medeiros FA. A case for the use of artificial intelligence in glaucoma assessment. *Ophthalmol Glaucoma.* (2021) 5:e3–13. doi: 10.1016/j.ogla.2021.12.003
328. Abramoff MD, Cunningham B, Patel B, Eydelman MB, Leng T, Sakamoto T, et al. Foundational considerations for artificial intelligence using ophthalmic images. *Ophthalmology.* (2022) 129:e14–32. doi: 10.1016/j.ophtha.2021.08.023
329. Fazal MI, Patel ME, Tye J, Gupta Y. The past, present and future role of artificial intelligence in imaging. *Eur J Radiol.* (2018) 105:246–50. doi: 10.1016/j.ejrad.2018.06.020
330. Benet D, Pellicer-Valero OJ. Artificial intelligence: the unstoppable revolution in ophthalmology. *Surv Ophthalmol.* (2022) 67:252–70. doi: 10.1016/j.survophthal.2021.03.003
331. Salazar H, Misra V, Swaminathan SS. Artificial intelligence and complex statistical modeling in glaucoma diagnosis and management. *Curr Opin Ophthalmol.* (2021) 32:105–17. doi: 10.1097/ICU.0000000000000741
332. Mirzania D, Thompson AC, Muir KW. Applications of deep learning in detection of glaucoma: a systematic review. *Eur J Ophthalmol.* (2021) 31:1618–42. doi: 10.1177/1120672120977346
333. Halupka KJ, Antony BJ, Lee MH, Lucy KA, Rai RS, Ishikawa H, et al. Retinal optical coherence tomography image enhancement via deep learning. *Biomed Opt Express.* (2018) 9:6205–21. doi: 10.1364/BOE.9.006205
334. Prabhakar B, Singh RK, Yadav KS. Artificial intelligence (AI) impacting diagnosis of glaucoma and understanding the regulatory aspects of AI-based software as medical device. *Comput Med Imaging Graph.* (2021) 87:101818. doi: 10.1016/j.compmedimag.2020.101818
335. Zheng C, Johnson TV, Garg A, Boland MV. Artificial intelligence in glaucoma. *Curr Opin Ophthalmol.* (2019) 30:97–103. doi: 10.1097/ICU.0000000000000552
336. Thompson AC, Jammal AA, Berchuck SI, Mariottoni EB, Medeiros FA. Assessment of a segmentation-free deep learning algorithm for diagnosing glaucoma from optical coherence tomography scans. *JAMA Ophthalmol.* (2020) 138:333–9. doi: 10.1001/jamaophthalmol.2019.5983
337. Raghavendra U, Gudigar A, Bhandary SV, Rao TN, Ciaccio EJ, Acharya UR, et al. A two layer sparse autoencoder for glaucoma identification with fundus images. *J Med Syst.* (2019) 43:299. doi: 10.1007/s10916-019-1427-x
338. Li Z, He Y, Keel S, Meng W, Chang RT, He M, et al. Efficacy of a deep learning system for detecting glaucomatous optic neuropathy based on color fundus photographs. *Ophthalmology.* (2018) 125:1199–206. doi: 10.1016/j.ophtha.2018.01.023
339. Liu H, Li L, Wormstone IM, Qiao C, Zhang C, Liu P, et al. Development and validation of a deep learning system to detect glaucomatous optic neuropathy using fundus photographs. *JAMA Ophthalmol.* (2019) 137:1353–60. doi: 10.1001/jamaophthalmol.2019.3501
340. Lee T, Jammal AA, Mariottoni EB, Medeiros FA. Predicting glaucoma development with longitudinal deep learning predictions from fundus photographs. *Am J Ophthalmol.* (2021) 225:86–94. doi: 10.1016/j.ajo.2020.12.031
341. Milea D, Najjar RP, Zhubo J, Ting D, Vasseneix C, Xu X, et al. Artificial intelligence to detect papilledema from ocular fundus photographs. *N Engl J Med.* (2020) 382:1687–95. doi: 10.1056/NEJMoa1917130
342. Liu TYA, Wei J, Zhu H, Subramanian PS, Myung D, Yi PH, et al. Detection of optic disc abnormalities in color fundus photographs using deep learning. *J Neuroophthalmol.* (2021) 41:368–74. doi: 10.1097/WNO.0000000000001358
343. Milea D, Singhal S, Najjar RP. Artificial intelligence for detection of optic disc abnormalities. *Curr Opin Neurol.* (2020) 33:106–10. doi: 10.1097/WCO.0000000000000773
344. Ran AR, Cheung CY, Wang X, Chen H, Luo LY, Chan PP, et al. Detection of glaucomatous optic neuropathy with spectral-domain optical coherence tomography: a retrospective training and validation deep-learning analysis. *Lancet Digit Health.* (2019) 1:e172–82. doi: 10.1016/S2589-7500(19)30085-8
345. Li L, Zhu H, Zhang Z, Zhao L, Xu L, Jonas RA, et al. Neural network-based retinal nerve fiber layer profile compensation for glaucoma diagnosis in myopia: model development and validation. *JMIR Med Inform.* (2021) 9:e22664. doi: 10.2196/22664

346. Porporato N, Tun TA, Baskaran M, Wong DWK, Husain R, Fu H, et al. Towards 'automated gonioscopy': a deep learning algorithm for 360° angle assessment by swept-source optical coherence tomography. *Br J Ophthalmol.* (2021):bjohthalmol–2020–318275. [Online ahead of print], doi: 10.1136/bjophthalmol-2020-318275
347. Devalla SK, Chin KS, Mari JM, Tun TA, Strouthidis NG, Aung T, et al. A deep learning approach to digitally stain optical coherence tomography images of the optic nerve head. *Invest Ophthalmol Vis Sci.* (2018) 59:63–74. doi: 10.1167/iovs.17-22617
348. Thompson AC, Jammal AA, Medeiros FA. A deep learning algorithm to quantify neuroretinal rim loss from optic disc photographs. *Am J Ophthalmol.* (2019) 201:9–18. doi: 10.1016/j.ajo.2019.01.011
349. Schottenhamml J, Würfl T, Mardin S, Ploner SB, Husvogt L, Hohberger B, et al. Glaucoma classification in 3 x 3 mm en face macular scans using deep learning in a different plexus. *Biomed Opt Express.* (2021) 12:7434–44. doi: 10.1364/BOE.439991
350. Bowd C, Belghith A, Zangwill LM, Christopher M, Goldbaum MH, Fan R, et al. Deep learning image analysis of optical coherence tomography angiography measured vessel density improves classification of healthy and glaucoma eyes. *Am J Ophthalmol.* (2021) 236:298–308. doi: 10.1016/j.ajo.2021.11.008
351. Mehta P, Petersen CA, Wen JC, Banitt MR, Chen PP, Bojikian KD, et al. Automated detection of glaucoma with interpretable machine learning using clinical data and multimodal retinal images. *Am J Ophthalmol.* (2021) 231:154–69. doi: 10.1016/j.ajo.2021.04.021
352. Sun S, Ha A, Kim YK, Yoo BW, Kim HC, Park KH, et al. Dual-input convolutional neural network for glaucoma diagnosis using spectral-domain optical coherence tomography. *Br J Ophthalmol.* (2021) 105:1555–60. doi: 10.1136/bjophthalmol-2020-316274
353. Panda SK, Cheong H, Tun TA, Devella SK, Senthil V, Krishnadas R, et al. Describing the structural phenotype of the glaucomatous optic nerve head using artificial intelligence. *Am J Ophthalmol.* (2021) 236:172–82. doi: 10.1016/j.ajo.2021.06.010
354. Andrade De Jesus D, Sánchez Brea L, Barbosa Breda J, Fokkinga E, Ederveen V, Borren N, et al. OCTA multilayer and multisector peripapillary microvascular modeling for diagnosing and staging of glaucoma. *Transl Vis Sci Technol.* (2020) 9:58. doi: 10.1167/tvst.9.2.58
355. Wu CW, Shen HL, Lu CJ, Chen SH, Chen HY. Comparison of different machine learning classifiers for glaucoma diagnosis based on spectralis OCT. *Diagnostics (Basel).* (2021) 11:1718. doi: 10.3390/diagnostics11091718
356. Shin Y, Cho H, Jeong HC, Seong M, Choi JW, Lee WJ, et al. Deep learning-based diagnosis of glaucoma using wide-field optical coherence tomography images. *J Glaucoma.* (2021) 30:803–12. doi: 10.1097/IJG.0000000000001885
357. Raja H, Hassan T, Akram MU, Werghi N. Clinically verified hybrid deep learning system for retinal ganglion cells aware grading of glaucomatous progression. *IEEE Trans Biomed Eng.* (2021) 68:2140–51. doi: 10.1109/TBME.2020.3030085
358. Wu JH, Nishida T, Weinreb RN, Lin JW. Performances of machine learning in detecting glaucoma using fundus and retinal optical coherence tomography images: a meta-analysis. *Am J Ophthalmol.* (2021) 237:1–12. doi: 10.1016/j.ajo.2021.12.008
359. Maetschke S, Antony B, Ishikawa H, Wollstein G, Schuman J, Garnavi R, et al. A feature agnostic approach for glaucoma detection in OCT volumes. *PLoS One.* (2019) 14:e0219126. doi: 10.1371/journal.pone.0219126
360. Kucur SS, Hollo G, Sznitman R. A deep learning approach to automatic detection of early glaucoma from visual fields. *PLoS One.* (2018) 13:e0206081. doi: 10.1371/journal.pone.0206081
361. Li F, Wang Z, Qu G, Song D, Yuan Y, Xu Y, et al. Automatic differentiation of Glaucoma visual field from non-glaucoma visual filed using deep convolutional neural network. *BMC Med Imaging.* (2018) 18:35. doi: 10.1186/s12880-018-0273-5
362. Devalla SK, Liang Z, Pham TH, Boote C, Strouthidis NG, Thiery AH, et al. Glaucoma management in the era of artificial intelligence. *Br J Ophthalmol.* (2020) 104:301–11. doi: 10.1136/bjophthalmol-2019-315016
363. Hashimoto Y, Asaoka R, Kiwaki T, Sugiura H, Asano S, Murata H, et al. Deep learning model to predict visual field in central 10° from optical coherence tomography measurement in glaucoma. *Br J Ophthalmol.* (2021) 105:507–13. doi: 10.1136/bjophthalmol-2019-315600
364. Hashimoto Y, Kiwaki T, Sugiura H, Asano S, Murata H, Fujino Y, et al. Predicting 10-2 visual field from optical coherence tomography in glaucoma using deep learning corrected with 24-2/30-2 visual field. *Transl Vis Sci Technol.* (2021) 10:28. doi: 10.1167/tvst.10.13.28
365. Yu HH, Maetschke SR, Antony BJ, Ishikawa H, Wollstein G, Schuman JS, et al. Estimating global visual field indices in glaucoma by combining macula and optic disc OCT scans using 3-dimensional convolutional neural networks. *Ophthalmol Glaucoma.* (2021) 4:102–12. doi: 10.1016/j.ogla.2020.07.002
366. Lazaridis G, Montesano G, Afgeh SS, Mohamed-Noriega J, Ourselin S, Lorenzi M, et al. Predicting visual fields from optical coherence tomography via an ensemble of deep representation learners. *Am J Ophthalmol.* (2022) 238:52–65. doi: 10.1016/j.ajo.2021.12.020
367. Christopher M, Bowd C, Proudfoot JA, Belghith A, Goldbaum MH, Rezapour J, et al. Deep learning estimation of 10-2 and 24-2 visual field metrics based on thickness maps from macula OCT. *Ophthalmology.* (2021) 128:1534–48. doi: 10.1016/j.ophtha.2021.04.022
368. Datta S, Mariottoni EB, Dov D, Jammal AA, Carin L, Medeiros FA, et al. RetiNerveNet: using recursive deep learning to estimate pointwise 24-2 visual field data based on retinal structure. *Sci Rep.* (2021) 11:12562. doi: 10.1038/s41598-021-91493-9
369. Christopher M, Bowd C, Belghith A, Goldbaum MH, Weinreb RN, Fazio MA, et al. Deep learning approaches predict glaucomatous visual field damage from OCT optic nerve head en face images and retinal nerve fiber layer thickness maps. *Ophthalmology.* (2020) 127:346–56. doi: 10.1016/j.ophtha.2019.09.036
370. Xiong J, Li F, Song D, Tang G, He J, Gao K, et al. Multimodal machine learning using visual fields and peripapillary circular OCT scans in detection of glaucomatous optic neuropathy. *Ophthalmology.* (2022) 129:171–80. doi: 10.1016/j.ophtha.2021.07.032
371. Li F, Yang Y, Sun X, Qiu Z, Zhang S, Tun TA, et al. Digital gonioscopy based on three-dimensional anterior-segment OCT: an international multicenter study. *Ophthalmology.* (2022) 129:45–53. doi: 10.1016/j.ophtha.2021.09.018
372. Fu H, Baskaran M, Xu Y, Lin S, Wong DWK, Liu J, et al. A deep learning system for automated angle-closure detection in anterior segment optical coherence tomography images. *Am J Ophthalmol.* (2019) 203:37–45. doi: 10.1016/j.ajo.2019.02.028
373. Randhawa J, Chiang M, Porporato N, Pardeshi AA, Dredge J, Apolo Aroca G, et al. Generalisability and performance of an OCT-based deep learning classifier for community-based and hospital-based detection of gonioscopic angle closure. *Br J Ophthalmol.* (2021) doi: 10.1136/bjophthalmol-2021-319470 [Epub ahead of print].
374. Li W, Chen Q, Jiang C, Shi G, Deng G, Sun X, et al. Automatic anterior chamber angle classification using deep learning system and anterior segment optical coherence tomography images. *Transl Vis Sci Technol.* (2021) 10:19. doi: 10.1167/tvst.10.6.19
375. Hao H, Zhao Y, Yan Q, Higashita R, Zhang J, Zhao Y, et al. Angle-closure assessment in anterior segment OCT images via deep learning. *Med Image Anal.* (2021) 69:101956. doi: 10.1016/j.media.2021.101956
376. Fu H, Xu Y, Lin S, Wong DWK, Baskaran M, Mahesh M, et al. Angle-closure detection in anterior segment OCT based on multilevel deep network. *IEEE Trans Cybern.* (2020) 50:3358–66. doi: 10.1109/TCYB.2019.2897162
377. Wen JC, Lee CS, Keane PA, Xiao S, Rokem AS, Chen PP, et al. Forecasting future Humphrey Visual Fields using deep learning. *PLoS One.* (2019) 14:e0214875. doi: 10.1371/journal.pone.0214875
378. Yousefi S, Kiwaki T, Zheng Y, Sugiura H, Asaoka R, Murata H, et al. Detection of longitudinal visual field progression in glaucoma using machine learning. *Am J Ophthalmol.* (2018) 193:71–9. doi: 10.1016/j.ajo.2018.06.007
379. Christopher M, Belghith A, Weinreb RN, Bowd C, Goldbaum MH, Saunders LJ, et al. Retinal nerve fiber layer features identified by unsupervised machine learning on optical coherence tomography scans predict glaucoma progression. *Invest Ophthalmol Vis Sci.* (2018) 59:2748–56. doi: 10.1167/iovs.17-23387
380. Sedai S, Antony B, Ishikawa H, Wollstein G, Schuman JS, Garnavi R, et al. Forecasting retinal nerve fiber layer thickness from multimodal temporal data incorporating OCT volumes. *Ophthalmol Glaucoma.* (2020) 3:14–24. doi: 10.1016/j.ogla.2019.11.001

381. Wong WL, Su X, Li X, Cheung CM, Klein R, Cheng CY, et al. Global prevalence of age-related macular degeneration and disease burden projection for 2020 and 2040: a systematic review and meta-analysis. *Lancet Glob Health.* (2014) 2:e106–16. doi: 10.1016/S2214-109X(13)70145-1
382. Neely DC, Bray KJ, Huisingh CE, Clark ME, McGwin G Jr., Owsley C, et al. Prevalence of undiagnosed age-related macular degeneration in primary eye care. *JAMA Ophthalmol.* (2017) 135:570–5. doi: 10.1001/jamaophthalmol.2017.0830
383. Burlina PM, Joshi N, Pekala M, Pacheco KD, Freund DE, Bressler NM, et al. Automated grading of age-related macular degeneration from color fundus images using deep convolutional neural networks. *JAMA Ophthalmol.* (2017) 135:1170–6. doi: 10.1001/jamaophthalmol.2017.3782
384. Dow ER, Keenan TDL, Lad EM, Lee AY, Lee CS, Lowenstein A, et al. From data to deployment: the Collaborative Communities on Ophthalmic Imaging roadmap for artificial intelligence in age-related macular degeneration. *Ophthalmology.* (2022) 129:e43–59. doi: 10.1016/j.ophtha.2022.01.002
385. Pandit RR, Wibbelsman TD, Considine SP, Jenkins TL, Xu D, Levin HJ, et al. Distribution and practice patterns of retina providers in the United States. *Ophthalmology.* (2020) 127:1580–1. doi: 10.1016/j.ophtha.2020.04.016
386. De Fauw J, Ledsam JR, Romera-Paredes B, Nikolov S, Tomasev N, Blackwell S, et al. Clinically applicable deep learning for diagnosis and referral in retinal disease. *Nat Med.* (2018) 24:1342–50. doi: 10.1038/s41591-018-0107-6
387. Kalra G, Kar SS, Sevgi DD, Madabhushi A, Srivastava SK, Ehlers JP, et al. Quantitative imaging biomarkers in age-related macular degeneration and diabetic eye disease: a step closer to precision medicine. *J Pers Med.* (2021) 11:1161. doi: 10.3390/jpm11111161
388. Saha S, Nassisi M, Wang M, Lindenberg S, Kanagasingam Y, Sadda S, et al. Automated detection and classification of early AMD biomarkers using deep learning. *Sci Rep.* (2019) 9:10990. doi: 10.1038/s41598-019-47390-3
389. Waldstein SM, Vogl WD, Bogunovic H, Sadeghipour A, Riedl S, Schmidt-Erfurth U, et al. Characterization of drusen and hyperreflective foci as biomarkers for disease progression in age-related macular degeneration using artificial intelligence in optical coherence tomography. *JAMA Ophthalmol.* (2020) 138:740–7. doi: 10.1001/jamaophthalmol.2020.1376
390. Schmitz-Valckenberg S, Gobel AP, Saur SC, Steinberg JS, Thiele S, Wojek C, et al. Automated retinal image analysis for evaluation of focal hyperpigmentary changes in intermediate age-related macular degeneration. *Transl Vis Sci Technol.* (2016) 5:3. doi: 10.1167/tvst.5.2.3
391. Wang J, Hormel TT, Gao L, Zang P, Guo Y, Wang X, et al. Automated diagnosis and segmentation of choroidal neovascularization in OCT angiography using deep learning. *Biomed Opt Express.* (2020) 11:927–44. doi: 10.1364/BOE.379977
392. Zhang G, Fu DJ, Liefers B, Faes L, Glinton S, Wagner S, et al. Clinically relevant deep learning for detection and quantification of geographic atrophy from optical coherence tomography: a model development and external validation study. *Lancet Digit Health.* (2021) 3:e665–75. doi: 10.1016/S2589-7500(21)00134-5
393. Yan Y, Jin K, Gao Z, Huang X, Wang F, Wang Y, et al. Attention-based deep learning system for automated diagnoses of age-related macular degeneration in optical coherence tomography images. *Med Phys.* (2021) 48:4926–34. doi: 10.1002/mp.15002
394. Keenan TDL, Clemons TE, Domalpally A, Elman MJ, Havilio M, Agrón E, et al. Retinal specialist versus artificial intelligence detection of retinal fluid from OCT: age-related eye disease study 2: 10-year follow-on study. *Ophthalmology.* (2021) 128:100–9. doi: 10.1016/j.ophtha.2020.06.038
395. Burlina PM, Joshi N, Pacheco KD, Freund DE, Kong J, Bressler NM, et al. Use of deep learning for detailed severity characterization and estimation of 5-year risk among patients with age-related macular degeneration. *JAMA Ophthalmol.* (2018) 136:1359–66. doi: 10.1001/jamaophthalmol.2018.4118
396. Peng Y, Keenan TD, Chen Q, Agron E, Allot A, Wong WT, et al. Predicting risk of late age-related macular degeneration using deep learning. *NPJ Digit Med.* (2020) 3:111. doi: 10.1038/s41746-020-00317-z
397. Peng Y, Dharssi S, Chen Q, Keenan TD, Agron E, Wong WT, et al. DeepSeeNet: a deep learning model for automated classification of patient-based age-related macular degeneration severity from color fundus photographs. *Ophthalmology.* (2019) 126:565–75. doi: 10.1016/j.ophtha.2018.11.015
398. Potapenko I, Kristensen M, Thiesson B, Ilginis T, Lykke Sørensen T, Nouri Hajari J, et al. Detection of oedema on optical coherence tomography images using deep learning model trained on noisy clinical data. *Acta Ophthalmol.* (2022) 100:103–10. doi: 10.1111/aos.14895
399. Sarici K, Abraham JR, Sevgi DD, Lunasco L, Srivastava SK, Whitney J, et al. Risk classification for progression to subfoveal geographic atrophy in dry age-related macular degeneration using machine learning-enabled outer retinal feature extraction. *Ophthalmic Surg Lasers Imaging Retina.* (2022) 53:31–9. doi: 10.3928/23258160-20211210-01
400. Abdelfattah NS, Zhang H, Boyer DS, Rosenfeld PJ, Feuer WJ, Gregori G, et al. Drusen volume as a predictor of disease progression in patients with late age-related macular degeneration in the fellow eye. *Invest Ophthalmol Vis Sci.* (2016) 57:1839–46. doi: 10.1167/iovs.15-18572
401. Zhao X, Zhang X, Lv B, Meng L, Zhang C, Liu Y, et al. Optical coherence tomography-based short-term effect prediction of anti-vascular endothelial growth factor treatment in neovascular age-related macular degeneration using sensitive structure guided network. *Graefes Arch Clin Exp Ophthalmol.* (2021) 259:3261–9. doi: 10.1007/s00417-021-05247-4
402. Romond K, Alam M, Kravets S, Sisternes L, Leng T, Lim JI, et al. Imaging and artificial intelligence for progression of age-related macular degeneration. *Exp Biol Med (Maywood).* (2021) 246:2159–69. doi: 10.1177/15353702211031547
403. Kashani AH, Zimmer-Galler IE, Shah SM, Dustin L, Do DV, Eliott D, et al. Retinal thickness analysis by race, gender, and age using Stratus OCT. *Am J Ophthalmol.* (2010) 149:496–502.e1. doi: 10.1016/j.ajo.2009.09.025
404. Alam M, Zhang Y, Lim JI, Chan RVP, Yang M, Yao X, et al. Quantitative optical coherence tomography angiography features for objective classification and staging of diabetic retinopathy. *Retina.* (2020) 40:322–32. doi: 10.1097/IAE.0000000000002373
405. Ting DSW, Cheung CY, Lim G, Tan GSW, Quang ND, Gan A, et al. Development and validation of a deep learning system for diabetic retinopathy and related eye diseases using retinal images from multiethnic populations with diabetes. *JAMA.* (2017) 318:2211–23. doi: 10.1001/jama.2017.18152
406. Walton OB, Garoon RB, Weng CY, Gross J, Young AK, Camero KA, et al. Evaluation of automated teleretinal screening program for diabetic retinopathy. *JAMA Ophthalmol.* (2016) 134:204–9. doi: 10.1001/jamaophthalmol.2015.5083
407. Arsalan M, Owais M, Mahmood T, Cho SW, Park KR. Aiding the diagnosis of diabetic and hypertensive retinopathy using artificial intelligence-based semantic segmentation. *J Clin Med.* (2019) 8:1446. doi: 10.3390/jcm8091446
408. Islam MM, Poly TN, Walther BA, Yang HC, Li YJ. Artificial intelligence in ophthalmology: a meta-analysis of deep learning models for retinal vessels segmentation. *J Clin Med.* (2020) 9:1018. doi: 10.3390/jcm9041018
409. Hassan B, Hassan T, Li B, Ahmed R, Hassan O. Deep ensemble learning based objective grading of macular edema by extracting clinically significant findings from fused retinal imaging modalities. *Sensors (Basel).* (2019) 19:2970. doi: 10.3390/s19132970
410. Verbraak FD, Abramoff MD, Bausch GCF, Klaver C, Nijpels G, Schlingemann RO, et al. Diagnostic accuracy of a device for the automated detection of diabetic retinopathy in a primary care setting. *Diabetes Care.* (2019) 42:651–6. doi: 10.2337/dc18-0148
411. Liu X, Ali TK, Singh P, Shah A, McKinney SM, Ruamviboonsuk P, et al. Deep learning to detect optical coherence tomography-derived diabetic macular edema from retinal photographs: a multicenter validation study. *Ophthalmol Retina.* (2022) 6:398–410. doi: 10.1016/j.oret.2021.12.021
412. Ipp E, Liljenquist D, Bode B, Shah VN, Silverstein S, Regillo CD, et al. Pivotal evaluation of an artificial intelligence system for autonomous detection of referrable and vision-threatening diabetic retinopathy. *JAMA Netw Open.* (2021) 4:e2134254. doi: 10.1001/jamanetworkopen.2021.34254
413. Nuzzi R, Boscia G, Marolo P, Ricardi F. The impact of artificial intelligence and deep learning in eye diseases: a review. *Front Med (Lausanne).* (2021) 8:710329. doi: 10.3389/fmed.2021.710329
414. Gulshan V, Peng L, Coram M, Stumpe MC, Wu D, Narayanaswamy A, et al. Development and validation of a deep learning algorithm for detection of diabetic retinopathy in retinal fundus photographs. *JAMA.* (2016) 316:2402–10. doi: 10.1001/jama.2016.17216

415. Gargeya R, Leng T. Automated identification of diabetic retinopathy using deep learning. *Ophthalmology.* (2017) 124:962–9. doi: 10.1016/j.ophtha.2017.02.008
416. Ardiyanto I, Nugroho HA, Buana RLB. Deep learning-based Diabetic Retinopathy assessment on embedded system. *Annu Int Conf IEEE Eng Med Biol Soc.* (2017) 2017:1760–3. doi: 10.1109/EMBC.2017.8037184
417. Ryu G, Lee K, Park D, Park SH, Sagong M. A deep learning model for identifying diabetic retinopathy using optical coherence tomography angiography. *Sci Rep.* (2021) 11:23024. doi: 10.1038/s41598-021-02479-6
418. Chen YM, Huang WT, Ho WH, Tsai JT. Classification of age-related macular degeneration using convolutional-neural-network-based transfer learning. *BMC Bioinformatics.* (2021) 22:99. doi: 10.1186/s12859-021-04001-1
419. Institute of Medicine (Us) Committee on Evaluating Clinical Applications of Telemedicine [IMCECAT]. *Telemedicine: A Guide to Assessing Telecommunications in Health Care*. Field MJ editor. Washington, DC: National Academies Press (1996).
420. Lord RK, Shah VA, San Filippo AN. Novel uses of smartphones in ophthalmology. *Ophthalmology.* (2010) 117:1274–1274.e3. doi: 10.1016/j.ophtha.2010.01.001
421. Pujari A, Saluja G, Agarwal D, Selvan H, Sharma N. Clinically useful smartphone ophthalmic imaging techniques. *Graefes Arch Clin Exp Ophthalmol.* (2021) 259:279–87. doi: 10.1007/s00417-020-04917-z
422. Kumar N, Bandello F, Sharma A. Smartphone-based gonio-imaging: a novel addition to glaucoma screening tools. *J Glaucoma.* (2019) 28:e149–50. doi: 10.1097/IJG.0000000000001306
423. Pujari A, Behera AK, Agarwal D, Sihota R, Dada T. A new technique of iPhone 11 Pro Max Smartphone-aided angle video and standstill image documentation. *J Glaucoma.* (2020) 29:e28–30. doi: 10.1097/IJG.0000000000001479
424. Pujari A, Selvan H, Asif MI, Gupta B, Dada T. Smartphone-aided quantification of iridocorneal angle. *J Glaucoma.* (2019) 28:e153–5. doi: 10.1097/IJG.0000000000001316
425. Pujari A, Mukhija R, Phuljhele S. Quantification of change in Iris Torsion using a smartphone. *Ophthalmology.* (2019) 126:126. doi: 10.1016/j.ophtha.2018.10.017
426. Pujari A, Phuljhele S, Sharma P. Quantification of Retinal Torsion in strabismus using a smartphone. *Ophthalmol Retina.* (2019) 3:379. doi: 10.1016/j.oret.2018.12.007
427. Sousa AI, Neves CM, Vieira P. Smartphone-based pupillometer with chromatic stimuli to screen neuro-ophthalmological diseases. In: Tiginyanu I, Sontea V, Railean S editors. *Proceeding of the 5th International Conference on Nanotechnologies and Biomedical Engineering*. Berlin: Springer International Publishing (2022). doi: 10.1007/978-3-030-92328-0_19
428. Chang LY, Turuwhenua J, Qu TY, Black JM, Acosta ML. Infrared video pupillography coupled with smart phone LED for measurement of pupillary light reflex. *Front Integr Neurosci.* (2017) 11:6. doi: 10.3389/fnint.2017.00006
429. McAnany JJ, Smith BM, Garland A, Kagen SL. iPhone-based Pupillometry: a novel approach for assessing the pupillary light reflex. *Optom Vis Sci.* (2018) 95:953–8. doi: 10.1097/OPX.0000000000001289
430. Pujari A, Kishore A, Makwana T, Sharma N. A simple tool to assess an implantable collamer lens vault. *J Cataract Refract Surg.* (2019) 45:883–4. doi: 10.1016/j.jcrs.2019.04.022
431. Pujari A, Yadav S, Mukhija R, Urkude J, Sharma N. Smartphone-aided technique to quantify toric intraocular lens alignment. *J Cataract Refract Surg.* (2019) 45:1833–4. doi: 10.1016/j.jcrs.2019.09.013
432. Pallas A, Yeo TK, Trevenen M, Barrett G. Evaluation of the accuracy of two marking methods and the novel toriCAM application for toric intraocular lens alignment. *J Refract Surg.* (2018) 34:150–5. doi: 10.3928/1081597X-20180115-03
433. Bastawrous A, Giardini ME, Bolster NM, Peto T, Shah N, Livingstone IA, et al. Clinical validation of a smartphone-based adapter for optic disc imaging in Kenya. *JAMA Ophthalmol.* (2016) 134:151–8. doi: 10.1001/jamaophthalmol.2015.4625
434. Russo A, Morescalchi F, Costagliola C, Delcassi L, Semeraro F. A novel device to exploit the smartphone camera for fundus photography. *J Ophthalmol.* (2015) 2015:823139. doi: 10.1155/2015/823139
435. Nazari Khanamiri H, Nakatsuka A, El-Annan J. Smartphone fundus photography. *J Vis Exp.* (2017) 125:55958. doi: 10.3791/55958 [Epub ahead of print].
436. Pujari A, Mukhija R, Chawla R, Phuljhele S, Saxena R, Sharma P, et al. Smartphone-based evaluation of the optic nerve head. *Indian J Ophthalmol.* (2018) 66:1617–8. doi: 10.4103/ijo.IJO_394_18
437. Suto S, Hiraoka T, Oshika T. Fluorescein fundus angiography with smartphone. *Retina.* (2014) 34:203–5. doi: 10.1097/IAE.0000000000000041
438. Sivaraman A, Nagarajan S, Vadivel S, Dutt S, Tiwari P, Narayana S, et al. A novel, smartphone-based, teleophthalmology-enabled, widefield fundus imaging device with an autocapture algorithm. *Transl Vis Sci Technol.* (2021) 10:21. doi: 10.1167/tvst.10.12.21
439. Bilong Y, Domngang CN, Nwanlih Gimma G, Katte JC, Afetane TE, Kagmeni G, et al. Smartphone-assisted glaucoma screening in patients with Type 2 diabetes: a pilot study. *Med Hypothesis Discov Innov Ophthalmol.* (2020) 9:61–5.
440. Alawa KA, Nolan RP, Han E, Arboleda A, Durkee H, Sayed MS, et al. Low-cost, smartphone-based frequency doubling technology visual field testing using a head-mounted display. *Br J Ophthalmol.* (2021) 105:440–4. doi: 10.1136/bjophthalmol-2019-314031
441. Rathi S, Tsui E, Mehta N, Zahid S, Schuman JS. The current state of teleophthalmology in the United States. *Ophthalmology.* (2017) 124:1729–34. doi: 10.1016/j.ophtha.2017.05.026
442. Bergua A, Mardin CY, Horn FK. Tele-transmission of stereoscopic images of the optic nerve head in glaucoma via Internet. *Telemed J E Health.* (2009) 15:439–44. doi: 10.1089/tmj.2008.0162
443. Kiage D, Kherani IN, Gichuhi S, Damji KF, Nyenze M. The muranga teleophthalmology study: comparison of virtual (Teleglaucoma) with in-person clinical assessment to diagnose glaucoma. *Middle East Afr J Ophthalmol.* (2013) 20:150–7. doi: 10.4103/0974-9233.110604
444. Sakamoto M, Kanamori A, Fujihara M, Yamada Y, Nakamura M, Negi A, et al. Assessment of IcareONE rebound tonometer for self-measuring intraocular pressure. *Acta Ophthalmol.* (2014) 92:243–8. doi: 10.1111/aos.12108
445. Mansouri K, Medeiros FA, Tafreshi A, Weinreb RN. Continuous 24-hour monitoring of intraocular pressure patterns with a contact lens sensor: safety, tolerability, and reproducibility in patients with glaucoma. *Arch Ophthalmol.* (2012) 130:1534–9. doi: 10.1001/archophthalmol.2012.2280
446. Li B, Powell AM, Hooper PL, Sheidow TG. Prospective evaluation of teleophthalmology in screening and recurrence monitoring of neovascular age-related macular degeneration: a randomized clinical trial. *JAMA Ophthalmol.* (2015) 133:276–82. doi: 10.1001/jamaophthalmol.2014.5014
447. Chew EY, Clemons TE, Bressler SB, Elman MJ, Danis RP, Domalpally A, et al. Randomized trial of a home monitoring system for early detection of choroidal neovascularization home monitoring of the Eye (HOME) study. *Ophthalmology.* (2014) 121:535–44. doi: 10.1016/j.ophtha.2013.10.027
448. Tan CH, Kyaw BM, Smith H, Tan CS, Tudor Car L. Use of smartphones to detect diabetic retinopathy: scoping review and meta-analysis of diagnostic test accuracy studies. *J Med Internet Res.* (2020) 22:e16658. doi: 10.2196/16658
449. Kirkizlar E, Serban N, Sisson JA, Swann JL, Barnes CS, Williams MD, et al. Evaluation of telemedicine for screening of diabetic retinopathy in the Veterans Health Administration. *Ophthalmology.* (2013) 120:2604–10. doi: 10.1016/j.ophtha.2013.06.029
450. Silva PS, Horton MB, Clary D, Lewis DG, Sun JK, Cavallerano JD, et al. Identification of diabetic retinopathy and ungradable image rate with ultrawide field imaging in a national teleophthalmology program. *Ophthalmology.* (2016) 123:1360–7. doi: 10.1016/j.ophtha.2016.01.043
451. Pujari A, Saluja G, Agarwal D, Sinha A, Ananya PR, Kumar A, et al. Clinical role of smartphone fundus imaging in diabetic retinopathy and other neuro-retinal diseases. *Curr Eye Res.* (2021) 46:1605–13. doi: 10.1080/02713683.2021.1958347
452. Rajalakshmi R, Subashini R, Anjana RM, Mohan V. Automated diabetic retinopathy detection in smartphone-based fundus photography using artificial intelligence. *Eye (Lond).* (2018) 32:1138–44. doi: 10.1038/s41433-018-0064-9

453. Sheikh A, Bhatti A, Adeyemi O, Raja M, Sheikh I. The utility of smartphone-based artificial intelligence approaches for diabetic retinopathy: a literature review and meta-analysis. *J Curr Ophthalmol.* (2021) 33:219–26. doi: 10.4103/2452-2325.329064
454. Bernstein PS, Sauer L. Fluorescence lifetime imaging ophthalmoscopy: a new era of autofluorescence imaging of the human retina. *Retina.* (2019) 39:817–9. doi: 10.1097/IAE.0000000000002517
455. Bernstein P, Dysli C, Fischer J, Hammer M, Katayama Y, Sauer L, et al. Fluorescence Lifetime Imaging Ophthalmoscopy (FLIO). In: Bille JF editor. *High Resolution Imaging in Microscopy and Ophthalmology: New Frontiers in Biomedical Optics*. Cham: Springer (2019). doi: 10.1007/978-3-030-16638-0_10
456. Li DQ, Choudhry N. The future of retinal imaging. *Curr Opin Ophthalmol.* (2020) 31:199–206. doi: 10.1097/ICU.0000000000000653
457. Dysli C, Wolf S, Berezin MY. Fluorescence lifetime imaging ophthalmoscopy. *Prog Retin Eye Res.* (2017) 60:120–43. doi: 10.1016/j.preteyeres.2017.06.005
458. Klemm M, Dietzel A, Haueisen J, Nagel E, Hammer M, Schweitzer D, et al. Repeatability of autofluorescence lifetime imaging at the human fundus in healthy volunteers. *Curr Eye Res.* (2013) 38:793–801. doi: 10.3109/02713683.2013.779723
459. Dysli C, Quellec G, Abegg M, Menke MN, Wolf-Schnurrbusch U, Kowal J, et al. Quantitative analysis of fluorescence lifetime measurements of the macula using the fluorescence lifetime imaging ophthalmoscope in healthy subjects. *Invest Ophthalmol Vis Sci.* (2014) 55:2106–13. doi: 10.1167/iovs.13-13627
460. Kwon S, Borrelli E, Fan W, Ebraheem A, Marion KM, Sadda SR, et al. Repeatability of fluorescence lifetime imaging ophthalmoscopy in normal subjects with mydriasis. *Transl Vis Sci Technol.* (2019) 8:15. doi: 10.1167/tvst.8.3.15
461. Sauer L, Gensure RH, Andersen KM, Kreilkamp L, Hageman GS, Hammer M, et al. Patterns of fundus autofluorescence lifetimes in eyes of individuals with nonexudative age-related macular degeneration. *Invest Ophthalmol Vis Sci.* (2018) 59:AMD65–77. doi: 10.1167/iovs.17-23764
462. Dysli C, Fink R, Wolf S, Zinkernagel MS. Fluorescence lifetimes of drusen in age-related macular degeneration. *Invest Ophthalmol Vis Sci.* (2017) 58:4856–62. doi: 10.1167/iovs.17-22184
463. Sauer L, Vitale AS, Modersitzki NK, Bernstein PS. Fluorescence lifetime imaging ophthalmoscopy: autofluorescence imaging and beyond. *Eye (Lond).* (2021) 35:93–109. doi: 10.1038/s41433-020-01287-y
464. Dysli C, Wolf S, Hatz K, Zinkernagel MS. Fluorescence lifetime imaging in stargardt disease: potential marker for disease progression. *Invest Ophthalmol Vis Sci.* (2016) 57:832–41. doi: 10.1167/iovs.15-18033
465. Sauer L, Calvo CM, Vitale AS, Henrie N, Milliken CM, Bernstein PS, et al. Imaging of hydroxychloroquine toxicity with fluorescence lifetime imaging ophthalmoscopy. *Ophthalmol Retina.* (2019) 3:814–25. doi: 10.1016/j.oret.2019.04.025
466. Solberg Y, Dysli C, Moller B, Wolf S, Zinkernagel MS. Fluorescence lifetimes in patients with hydroxychloroquine retinopathy. *Invest Ophthalmol Vis Sci.* (2019) 60:2165–72. doi: 10.1167/iovs.18-26079
467. Schweitzer D, Deutsch L, Klemm M, Jentsch S, Hammer M, Peters S, et al. Fluorescence lifetime imaging ophthalmoscopy in type 2 diabetic patients who have no signs of diabetic retinopathy. *J Biomed Opt.* (2015) 20:61106. doi: 10.1117/1.JBO.20.6.061106
468. Schweitzer D, Quick S, Klemm M, Hammer M, Jentsch S, Dawczynski J, et al. [Time-resolved autofluorescence in retinal vascular occlusions]. *Ophthalmologe.* (2010) 107:1145–52. doi: 10.1007/s00347-010-2195-7
469. Dysli C, Berger L, Wolf S, Zinkernagel MS. Fundus autofluorescence lifetimes and central serous chorioretinopathy. *Retina.* (2017) 37:2151–61. doi: 10.1097/IAE.0000000000001452
470. Sauer L, Gensure RH, Hammer M, Bernstein PS. Fluorescence lifetime imaging ophthalmoscopy: a novel way to assess macular telangiectasia Type 2. *Ophthalmol Retina.* (2018) 2:587–98. doi: 10.1016/j.oret.2017.10.008
471. Vitale AS, Sauer L, Modersitzki NK, Bernstein PS. Fluorescence Lifetime Imaging Ophthalmoscopy (FLIO) in patients with choroideremia. *Transl Vis Sci Technol.* (2020) 9:33. doi: 10.1167/tvst.9.10.33
472. Dysli C, Schuerch K, Escher P, Wolf S, Zinkernagel MS. Fundus autofluorescence lifetime patterns in retinitis pigmentosa. *Invest Ophthalmol Vis Sci.* (2018) 59:1769–78. doi: 10.1167/iovs.17-23336
473. Sauer L, Peters S, Schmidt J, Schweitzer D, Klemm M, Ramm L, et al. Monitoring macular pigment changes in macular holes using fluorescence lifetime imaging ophthalmoscopy. *Acta Ophthalmol.* (2017) 95:481–92. doi: 10.1111/aos.13269
474. Vienola KV, Braaf B, Sheehy CK. Real-time eye motion compensation for OCT imaging with tracking SLO. *Biomed Opt Express.* (2012) 3:2950–63. doi: 10.1364/BOE.3.002950
475. Schwarzhans F, Desissaire S, Steiner S. Generating large field of view en-face projection images from intra-acquisition motion compensated volumetric optical coherence tomography data. *Biomed Opt Express.* (2020) 11:6881–904. doi: 10.1364/BOE.404738
476. Pircher M, Götzinger E, Sattmann H, Leitgeb RA, Hitzenberger CK. In vivo investigation of human cone photoreceptors with SLO/OCT in combination with 3D motion correction on a cellular level. *Opt Express.* (2010) 18:13935–44. doi: 10.1364/OE.18.013935
477. Pircher M, Baumann B, Götzinger E. Simultaneous SLO/OCT imaging of the human retina with axial eye motion correction. *Opt Express.* (2007) 15:16922–32. doi: 10.1364/OE.15.016922
478. Yu DY, Cringle SJ. Retinal degeneration and local oxygen metabolism. *Exp Eye Res.* (2005) 80:745–51. doi: 10.1016/j.exer.2005.01.018
479. Pi S, Camino A, Zhang M, Cepurna W, Liu G, Huang D, et al. Angiographic and structural imaging using high axial resolution fiber-based visible-light OCT. *Biomed Opt Express.* (2017) 8:4595–608. doi: 10.1364/BOE.8.004595
480. Pi S, Camino A, Wei X, Simonett J, Cepurna W, Huang D, et al. Rodent retinal circulation organization and oxygen metabolism revealed by visible-light optical coherence tomography. *Biomed Opt Express.* (2018) 9:5851–62. doi: 10.1364/BOE.9.005851
481. Pi S, Hormel TT, Wei X, Cepurna W, Wang B, Morrison JC, et al. Retinal capillary oximetry with visible light optical coherence tomography. *Proc Natl Acad Sci U S A.* (2020) 117:11658–66. doi: 10.1073/pnas.1918546117
482. Chen S, Shu X, Nesper PL. Retinal oximetry in humans using visible-light optical coherence tomography [Invited]. *Biomed Opt Express.* (2017) 8:1415–29. doi: 10.1364/BOE.8.001415
483. Jiao S, Jiang M, Hu J, Fawzi A, Zhou Q, Shung KK, et al. Photoacoustic ophthalmoscopy for in vivo retinal imaging. *Opt Express.* (2010) 18:3967–72. doi: 10.1364/OE.18.003967
484. Penn JS, Madan A, Caldwell RB, Bartoli M, Caldwell RW, Hartnett ME, et al. Vascular endothelial growth factor in eye disease. *Prog Retin Eye Res.* (2008) 27:331–71. doi: 10.1016/j.preteyeres.2008.05.001
485. Zhang W, Li Y, Nguyen VP. High-resolution, in vivo multimodal photoacoustic microscopy, optical coherence tomography, and fluorescence microscopy imaging of rabbit retinal neovascularization. *Light: Sci Appl.* (2018) 7:103. doi: 10.1038/s41377-018-0093-y
486. Nguyen VP, Li Y, Aaberg M. In Vivo 3D Imaging of Retinal Neovascularization Using Multimodal Photoacoustic Microscopy and Optical Coherence Tomography Imaging. *J Imaging.* (2018) 4:150. doi: 10.3390/jimaging4120150
487. Li Y, Zhang W, Nguyen VP, Rosen R, Wang X, Xia X, et al. Real-time OCT guidance and multimodal imaging monitoring of subretinal injection induced choroidal neovascularization in rabbit eyes. *Exp Eye Res.* (2019) 186:107714–107714. doi: 10.1016/j.exer.2019.107714
488. Nguyen VP, Li Y, Zhang W, Wang X, Paulus YM. High-resolution multimodal photoacoustic microscopy and optical coherence tomography image-guided laser induced branch retinal vein occlusion in living rabbits. *Sci Rep.* (2019) 9:10560. doi: 10.1038/s41598-019-47062-2
489. Nguyen VP, Li Y, Henry J, Zhang W, Wang X, Paulus YM, et al. High resolution multimodal photoacoustic microscopy and optical coherence tomography visualization of choroidal vascular occlusion. *Int J Mol Sci.* (2020) 21:6508. doi: 10.3390/ijms21186508
490. Song W, Wei Q, Liu W. A combined method to quantify the retinal metabolic rate of oxygen using photoacoustic ophthalmoscopy and optical coherence tomography. *Sci Rep.* (2014) 4:6525. doi: 10.1038/srep06525
491. Braaf B, Donner S, Nam AS, Bouma BE, Vakoc BJ. Complex differential variance angiography with noise-bias correction for optical coherence tomography of the retina. *Biomed Opt Express.* (2018) 9:486–506. doi: 10.1364/BOE.9.000486

492. Gong P, Li Q, Wang Q, Karnowski K, Sampson DD. Jones matrix-based speckle-decorrelation angiography using polarization-sensitive optical coherence tomography. *J Biophotonics.* (2020) 13:e202000007. doi: 10.1002/jbio.202000007
493. Gordon AY, Lapierre-Landry M, Skala MC. Photothermal optical coherence tomography of anti-angiogenic treatment in the mouse retina using gold nanorods as contrast agents. *Transl Vis Sci Technol.* (2019) 8:18–18. doi: 10.1167/tvst.8.3.18
494. Adler DC, Huang S-W, Huber R, Fujimoto JG. Photothermal detection of gold nanoparticles using phase-sensitive optical coherence tomography. *Opt Express.* (2008) 16:4376–93. doi: 10.1364/OE.16.004376
495. Lapierre-Landry M, Gordon AY, Penn JS. In vivo photothermal optical coherence tomography of endogenous and exogenous contrast agents in the eye. *Sci Rep.* (2017) 7:9228. doi: 10.1038/s41598-017-10050-5
496. Lapierre-Landry M, Huckenpahler AL, Link BA, Collery RF, Carroll J, Skala MC, et al. Imaging melanin distribution in the zebrafish retina using photothermal optical coherence tomography. *Transl Vis Sci Technol.* (2018) 7:4–4. doi: 10.1167/tvst.7.5.4
497. Kennedy BF, Kennedy KM, Sampson DDA. Review of optical coherence elastography: fundamentals, techniques and prospects. *IEEE J Selected Topics Quantum Electron.* (2014) 20:272–88. doi: 10.1109/JSTQE.2013.2291445
498. Ramier A, Eltony AM, Chen Y, Clouser F, Birkenfeld JS, Watts A, et al. In vivo measurement of shear modulus of the human cornea using optical coherence elastography. *Sci Rep.* (2020) 10:17366. doi: 10.1038/s41598-020-74383-4
499. Li XX, Wu W, Zhou H, Deng JJ, Zhao MY, Qian TW, et al. A quantitative comparison of five optical coherence tomography angiography systems in clinical performance. *Int J Ophthalmol.* (2018) 11:1784–95.
500. Jung W, Kim J, Jeon M, Chaney EJ, Stewart CN, Boppart SA, et al. Handheld optical coherence tomography scanner for primary care diagnostics. *IEEE Trans Biomed Eng.* (2010) 58:741–4. doi: 10.1109/TBME.2010.2096816
501. Hahn P, Migacz J, O'Connell R, Maldonado RS, Izatt JA, Toth CA, et al. The use of optical coherence tomography in intraoperative ophthalmic imaging. *Ophthalmic Surg Lasers Imaging.* (2011) 42:S85–94. doi: 10.3928/15428877-20110627-08
502. Izatt JA, Hee MR, Swanson EA, Lin CP, Huang D, Schuman JS, et al. Micrometer-scale resolution imaging of the anterior eye in vivo with optical coherence tomography. *Arch Ophthalmol.* (1994) 112:1584–9. doi: 10.1001/archopht.1994.01090240090031
503. Považay B, Apolonskiy A, Unterhuber A. Visible light optical coherence tomography. *Proc SPIE.* (2002) 4619:90–4.
504. Zhang T, Kho AM, Yiu G. Visible Light Optical Coherence Tomography (OCT) quantifies subcellular contributions to outer retinal band 4. *Transl Vis Sci Technol.* (2021) 10:30–30. doi: 10.1167/tvst.10.3.30
505. Chong SP, Zhang T, Kho A, Bernucci MT, Dubra A, Srinivasan VJ, et al. Ultrahigh resolution retinal imaging by visible light OCT with longitudinal achromatization. *Biomed Opt Express.* (2018) 9:1477–91. doi: 10.1364/BOE.9.001477
506. Klein T, Wieser W, Reznicek L, Neubauer A, Kampik A, Huber R, et al. Multi-MHz retinal OCT. *Biomed Opt Express.* (2013) 4:1890–908. doi: 10.1364/BOE.4.001890
507. de Carlo TE, Romano A, Waheed NK, Duker JS. A review of optical coherence tomography angiography (OCTA). *Int J Retina Vitreous.* (2015) 1:5. doi: 10.1186/s40942-015-0005-8
508. Heisler M, Ju MJ, Bhalla M, Schuck N, Athwal A, Navajas EV, et al. Automated identification of cone photoreceptors in adaptive optics optical coherence tomography images using transfer learning. *Biomed Opt Express.* (2018) 9:5353–67. doi: 10.1364/BOE.9.005353

Conflict of Interest: JS: Aerie Pharmaceuticals, Inc. and Opticient: consultant/advisor and equity owner. BrightFocus Foundation and National Eye Institute: grant support. Boehringer Ingelheim, Perfuse, Inc., Regeneron, Inc., and SLACK Incorporated: consultant/advisor. Carl Zeiss Meditec: patents/royalty/consultant/advisor. Massachusetts Eye and Ear Infirmary and Massachusetts Institute of Technology, New York University, Tufts University, and University of Pittsburgh: intellectual property. Ocugenix: equity owner, and patents/royalty. Ocular Therapeutix, Inc.: consultant/advisor and equity owner.

The remaining authors declare that the research was conducted in the absence of any commercial or financial relationships that could be construed as a potential conflict of interest.

Publisher's Note: All claims expressed in this article are solely those of the authors and do not necessarily represent those of their affiliated organizations, or those of the publisher, the editors and the reviewers. Any product that may be evaluated in this article, or claim that may be made by its manufacturer, is not guaranteed or endorsed by the publisher.